

# **Resistance Spot Welding of Al to Mg with Different Interlayers**

by

Pavlo Penner

A thesis  
presented to the University of Waterloo  
in fulfillment of the  
thesis requirement for the degree of  
Master of Applied Science  
in  
Mechanical Engineering

Waterloo, Ontario, Canada, 2013

©Pavlo Penner 2013

## **Author's Declaration**

I hereby declare that I am the sole author of this thesis. This is a true copy of the thesis, including any required final revisions, as accepted by my examiners.

I understand that my thesis may be made electronically available to the public.

Pavlo Penner

## **Abstract**

In order to meet the increasing fuel efficiency requirements, the automotive industry has strived for component weight reduction in order to improve the performance of automotive vehicles through the use of light Al and Mg alloys. Resistance spot welding (RSW) currently is the primary joining method in the manufacturing of automotive assemblies. With the increased use of Al and Mg, there is a pressing need for a technology to produce dissimilar Al/Mg joints, and preferably by RSW since this technology is already prevalent in the industry. Direct welding of Al to Mg usually results in formation of hard and brittle intermetallic compounds and poor quality of the welds. Employing an interlayer is a promising approach to overcome this problem. Current literature, however, does not consider the effects of different interlayers on RSW of Al to Mg. This thesis examines effects of different interlayers on microstructure and mechanical properties of Al/Mg joints made by RSW. Effects of three types of interlayers, specifically pure Ni foil, Au-coated Ni foil and Zn-coated were investigated in details. While only brief investigation of joints made with Sn-coated steel, Zn foil, and Cu foil interlayers was conducted.

No joints were achieved with a bare Ni interlayer during Al to Mg alloy resistance spot welding, as coupons separated without applying any force. The Ni interlayer remained intact and Al-Mg intermetallic compounds did not form. Addition of Au coating on Ni surface greatly contributed to the metallurgical bonding at the interfaces and welds easily met requirements of the AWS D17.2 standard. Average lap-shear strength reached 90% of that in similar AZ31B resistance spot welds.

Acceptable welds were also produced using galvanised Zn-coated steel interlayer, which easily met strength requirements of the AWS D17.2 standard. Average failure load reached 74% of same size similar AZ31B joints. The steel interlayer was not melted which prevented mixing of Al and Mg. The Zn coating on the steel interlayer was melted and squeezed to the nugget periphery, providing a clean steel surface for welding-brazing in the center and acting as a solder metal at the periphery.

A feasibility study of Al/Mg RSW with Sn-coated steel, Zn foil and Cu foil interlayers was also conducted. Mechanical properties of welds made with Sn-coated steel interlayer were very similar to those made with Zn-coated steel interlayer. While welds made with only a Zn foil interlayer were much weaker. The Zn foil completely melted during the welding which resulted in

formation of brittle Al-Mg-Zn phases. None of the welds made with Zn foil interlayer met requirements of the AWS D17.2 standard. RSW of Al to Mg with Cu foil interlayer also could not produce welds with acceptable strength.

## **Acknowledgements**

I wish to thank my supervisors Dr. Norman Zhou and Dr. Adrian Gerlich for their support, guidelines and assistance. I also want to express special thanks to Dr. Lei Liu for help I received from him during my first days in University of Waterloo. In addition I want to acknowledge Ali Nasiri, Dr. Sashank Nayak, Tirdad Niknejad and all the rest of Centre for Advanced Materials Joining members for help and assistance I received from them.

I am truly thankful to all of my Canadian relatives who provided me with guidelines, room, board and supported me in everything during two years of my studying. Moreover, I want to acknowledge my family and friends in Ukraine who supported me in my decisions and helped me to accomplish my goals.

This research was financially supported by Automotive Partnership Canada within the scope of Magnesium Front End Research and Development (MFERD) project. In-kind support was also provided by Huys and POSCO, I would not be able to finish this work without their help.

## Table of Contents

Author's Declaration.....	ii
Abstract.....	iii
Acknowledgements.....	v
Table of Contents.....	vi
List of Figures .....	viii
List of Tables .....	xii
Chapter 1 : Introduction.....	1
1.1 Background .....	1
1.2 Resistance Spot Welding.....	1
1.3 Mg and Al Alloys.....	2
1.4 Joining of Al to Mg .....	3
1.5 Interlayers Used .....	4
1.6 Motivation .....	4
1.7 Objectives.....	4
1.8 Thesis Outline .....	5
Chapter 2 : Literature Review.....	6
2.1 Resistance Spot Welding.....	6
2.1.1 Principals of RSW .....	6
2.1.2 RSW Parameters .....	7
2.1.3 RSW of Light Alloys .....	9
2.1.4 RSW of Dissimilar Materials .....	10
2.1.5 Weld Quality.....	10
2.2 Mg and Al Alloys.....	11
2.3 Welding of Al to Mg .....	13
2.3.1 Direct Welding.....	13
2.3.2 Welding with Interlayers .....	19
2.4 Selection of Interlayers for RSW of Al to Mg .....	21
2.5 Summary .....	22
Chapter 3 : Experimental Apparatus and Methods .....	23
3.1 Material Selection .....	23
3.1.1 Welding Coupons.....	23

3.1.2 Interlayers .....	23
3.2 Welding Equipment .....	25
3.3 Mechanical Testing.....	27
3.4 Metallographic Analysis .....	29
Chapter 4 : Resistance Spot Welding of Al to Mg with Ni-based Interlayers .....	30
4.1 Experiments with Bare Ni Interlayer.....	30
4.1.1 Mechanical Properties.....	30
4.1.2 Fracture Surface Examination .....	31
4.2 Experiments with Au-coated Ni Interlayer .....	34
4.2.1 Mechanical Properties.....	34
4.2.2 Interfacial Microstructure Examination.....	38
4.2.3 Fracture Surface Examination .....	43
4.3 Summary .....	49
Chapter 5 : Resistance Spot Welding of Al to Mg with Zn-coated Steel Interlayer .....	50
5.1 Experiments with Zn-coated Steel Interlayer.....	50
5.1.1 Mechanical Properties.....	50
5.1.2 Interfacial Microstructure Examination.....	52
5.1.3 Fracture Surface Examination .....	63
5.2 Summary .....	69
Chapter 6 : Conclusions.....	71
6.1 RSW of Al to Mg with Ni-based Interlayers .....	71
6.2 RSW of Al to Mg with Zn-coated Steel Interlayer .....	72
Appendix A :RSW of Al to Mg with Sn-coated Steel, Zn foil and Cu foil Interlayers .....	73
Appendix B : Direct RSW, Weld Bonding and Adhesive Bonding of Al to Mg .....	84
Appendix C : RSW of Mg to Steel .....	88
Appendix D : RSW of Mg Alloys .....	90
Appendix E : RSW of Unequal Thickness AZ31B Sheets.....	94
References .....	95

## List of Figures

Figure 1.1: Schematic sketch of RSW of two sheets [1] (reprinted with permission of ASM International) .....	2
Figure 2.1: Temperature distribution during RSW [2].....	7
Figure 2.2: RSW of unequal thickness sheets with different upper and bottom electrodes [1] (reprinted with permission of ASM International) .....	9
Figure 2.3: Some applications of Mg and Al alloys into automotive and achieved weight reduction [27] .....	12
Figure 2.4: Al-Mg binary phase diagram [42] (reprinted with permission of ASM International) .	15
Figure 2.5: Microhardness profile of direct Al/Mg resistance spot welds made with welding currents of 22-33 kA [4].....	16
Figure 2.6: Fracture surface of direct Al/Mg resistance spot weld on Mg side [4] .....	16
Figure 2.7: Interfacial microstructure and Material flow in different zones of dissimilar Al/Mg butt friction stir weld [10] .....	18
Figure 2.8: Sketch of Al/Mg joint made by laser-TIG welding with Fe foil interlayer [37] .....	21
Figure 3.1: Interface between steel and Zn coating in HSLA hot-dip galvanised steel. a SEM micrograph; b Fe, Al and Zn element distribution maps of area marked in a .....	25
Figure 3.2: RSW machine and a schematic of the welding coupons being joined .....	26
Figure 3.3: Full welding schedule used in the current study .....	27
Figure 3.4: Test coupon geometry and tensile shear test set-up .....	28
Figure 3.5: Cross-sectioned weld and hardness traverse .....	29
Figure 4.1: Surface of the Al and Mg sheets after welding with bare Ni interlayer and 24 kA welding current.....	30
Figure 4.2: Correlation between melted zone size on both Al and Mg side and welding current during RSW with bare Ni interlayer .....	31
Figure 4.3: Fracture surface of the bare Ni interlayer at Al side (produced in a weld made using 24 kA). a overview; b details of region A in a.....	32
Figure 4.4: Al/Ni weld (without Mg). a SEM micrograph; b EDX line scan across Al/Ni interface marked in a .....	33
Figure 4.5: XRD analysis of the bare Ni interlayer fracture surface on both Al and Mg side. a Al side; b Mg side.....	34

Figure 4.6: Correlation between nugget size on both Al and Mg side and welding current during RSW with Au-coated Ni interlayer .....	35
Figure 4.7: Correlation between peak load and welding current during RSW of Al to Mg with Au-coated Ni interlayer .....	37
Figure 4.8: Hardness distribution across Al/Mg weld made with Au-coated Ni interlayer and 24 kA welding current .....	37
Figure 4.9: Typical Al/Mg weld made with Au-coated Ni interlayer and 24kA welding current....	38
Figure 4.10: Location of the zones which exhibit differ rent interfacial microstructure in Al/Mg weld made with Au-coated Ni interlayer and 24kA welding current.....	39
Figure 4.11: Al/Ni interface of the weld made with Au-coated Ni interlayer and 24 kA welding current, which corresponds to interfaces noted in Figure 4.10. a zone AI; b zone AII; c zone AIII; d details of the region C from b .....	40
Figure 4.12: Mg/Ni interfaces in the weld made with Au-coated Ni interlayer and 24 kA welding current, which corresponds to interfaces noted in Figure 4.10. a and b zone MI; c zone MII; d zone MIII; e zones MIV and MV .....	42
Figure 4.13: Au-Mg binary phase diagram [42] (reprinted with permission of ASM International) .....	43
Figure 4.14: Fracture surface of the Au coated Ni interlayer at Al side (produced in a weld made using 24 kA). a overview; b zone D from a; c details of the zone E from a .....	45
Figure 4.15: XRD analysis of the Au-coated Ni interlayer fracture surface on both Al and Mg side. a Al side; b Mg side .....	46
Figure 4.16: Fracture surface of the Au coated Ni interlayer at Mg side (produced in a weld made using 24 kA). a overview; b details of zone MI from a; c details of zone MII from a; d details of zone MIII from a; e details of zones MIV and MV from a .....	48
Figure 5.1: Correlation between nugget size on both Al and Mg side and welding current during RSW with Zn-coated steel interlayer .....	50
Figure 5.2: Correlation between peak load and welding current during RSW of Al to Mg with Zn-coated steel interlayer .....	51
Figure 5.3: Hardness distribution across Al/Mg weld made with Zn-coated steel interlayer and 28 kA welding current.....	52
Figure 5.4: Typical Al/Mg weld made with Zn-coated steel interlayer and 28 kA welding current .....	52

Figure 5.5: Location of the zones which exhibit different interfacial microstructure in Al/Mg weld made with Zn-coated steel interlayer and 28 kA welding current.....	53
Figure 5.6: Al/steel interface of zone AS-I from Figure 5.5. a center of AS-I; b details of F from a; c details of G from a; d zone AS-I close to the boundary with AS-II.....	55
Figure 5.7: Characterisation of interfacial microstructure of Al/steel RSW joint by Qiu <i>et al.</i> [57]. a bright field image of the reaction layer; b distribution chart of the reaction layer thickness at the welding interface; c SEM images of the weld cross section at the Al/steel interface.....	56
Figure 5.8: Schematic representation of the phases formed at the interface between molten Al and solid Fe [71] .....	56
Figure 5.9: Al/steel interface beyond the fusion nugget, which corresponds to interfaces noted in Figure 5.5. a zone AS-II; b zone AS-III; c region beyond AS-III .....	58
Figure 5.10: Center of Mg/steel interface of the weld made with Zn-coated steel interlayer and 28 kA welding current. a SEM micrograph; b element distribution map of region H from a .....	60
Figure 5.11 – Mg/steel interface beyond the fusion zone. a zones MS-II and MS-III; b zone MS-II close to the fusion nugget; c details of I from a; d details of J from a; e region beyond zone MS-III .....	62
Figure 5.12 - Fracture surface of the Zn-coated steel interlayer at Al side (produced in a weld made using 28 kA). a overview; b details of region L from a; c details of region M from a; d details of zone AS-II from a; e details of zone AS-III from a; f region beyond zone AS-III.....	65
Figure 5.13: XRD analysis of the Zn-coated steel interlayer fracture surface on Al side .....	66
Figure 5.14: Fracture surface morphology of the Mg/steel interface at steel side (produced in a weld made using 28 kA). a overview; b details of region N from a; c details of region O from a; d details of zone MS-II from a; e details of zone MS-III from a; f region beyond MS-III zone .....	68
Figure 5.15: XRD analysis of the Zn-coated steel interlayer fracture surface on Mg side .....	69

## List of Tables

Table 1.1: List of materials used as interlayers for RSW of Al/Mg in the current study .....	4
Table 2.1: Maximum tensile shear strength of Al/Mg welds produced by different welding techniques (modified from Patel <i>et al.</i> [16]) .....	14
Table 2.2: List of interlayers and techniques used by other researchers to weld Al to Mg .....	20
Table 3.1: Chemical composition of Al and Mg alloys used in this study in wt.% [60] .....	23
Table 3.2: Basic properties of Al and Mg alloys used in this study [60, 61].....	23
Table 3.3: Chemical composition of the hot-dip Zn-coated steel used as an interlayer (wt.%)... <td>24</td>	24
Table 3.4: Welding parameters used for RSW of Al to Mg with interlayers .....	27
Table 4.1: EDX quantification (in wt.%) of different areas in Figure 4.3b .....	32
Table 4.2: EDX quantification (in wt.%) of different areas in Figure 4.11 .....	40
Table 4.3: EDX quantification (in wt.%) of different areas in Figure 4.12 .....	43
Table 4.4: EDX quantification (in wt.%) of different areas in Figure 4.14 .....	45
Table 4.5: EDX quantification (in wt.%) of different areas in Figure 4.16 .....	49
Table 5.1: EDX quantification (in wt.%) of different areas in Figure 5.6 .....	55
Table 5.2: EDX quantification (in wt.%) of different areas in Figure 5.9 .....	58
Table 5.3: EDX quantification (in wt.%) of different areas in Figure 5.11 .....	63
Table 5.4: EDX quantification (in wt.%) of different areas in Figure 5.12 .....	66
Table 5.5: EDX quantification (in wt.%) of different areas in Figure 5.14 .....	69

# **Chapter 1: Introduction**

## **1.1 Background**

The automotive industry is continually struggling to improve fuel efficiency by employing lightweight materials such as Al and Mg alloys, since reducing vehicle weight can greatly lower fuel consumption. With the increased use of Al and Mg, there is a pressing need for a technology to produce dissimilar Al/Mg joints, and preferably by RSW since this technology is currently predominant in the industry. To-date the problem of joining Al and Mg remains open. The major difficulty in welding of Al to Mg is formation of hard and brittle intermetallic compounds which have a detrimental effect on the joints strength. Currently, the most promising approach to solve this problem is employing interlayers which can improve microstructure and mechanical performance of Al/Mg welds. Very limited information on RSW of Al to Mg is available in the literature while there is no any information on RSW of Al to Mg with an interlayer. Therefore, it is essential to explore effects of different interlayers on dissimilar Al/Mg resistance spot welds to fill the gap between RSW and other joining techniques in amount of information available on the subject and promote farther implementation of light alloys in the automotive industry.

## **1.2 Resistance Spot Welding**

RSW is a welding technique in which the faying sheets of metal are joined in a spot by the heat produced due to resistance to the electric current which passes through coupons squeezed from top and bottom by electrodes. The basic RSW process involves a few consecutive steps: clamping electrodes to tightly press welding coupons together; applying welding force which is significantly higher than initial squeezing force; applying welding current which leads to melting of coupons in weld zone; holding coupons with certain force while fusion zone solidifies; unclamping of the electrodes. A schematic sketch of RSW of two sheets is shown on Figure 1.1.

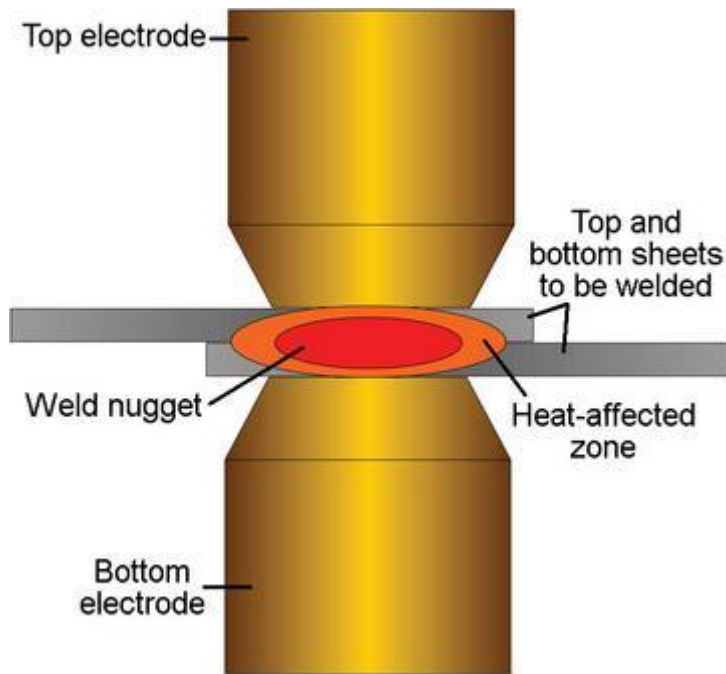


**Figure 1.1: Schematic sketch of RSW of two sheets [1] (reprinted with permission of ASM International)**

RSW is the primary joining technique for many sheet metal applications. Employing this welding technique is cost-effective, fast and can be easily automated. Sheets with thicknesses up to 3.2 mm can be joined by this technique, which suits most applications since the majority of commercial assemblies involves sheets with thicknesses less than 3 mm. RSW also allows one to produce spot joints of multiple sheets stacks, where the quantity of sheets in the stack is usually less or equal to five. The major limitation of RSW is that only joints in overlap configuration can be produced by this technique. However, sheet metal joining in overlap configuration is required for many applications in variety of industries [2, 3]. For example 5,000 resistance spot welds performed in manufacturing an automobile [4].

### 1.3 Mg and Al Alloys

The automotive industry is continually struggling to improve fuel efficiency by employing lightweight materials such as Al and Mg alloys, since reducing vehicle weight can greatly lower fuel consumption. It was reported that 100 kg of reduced vehicle weight saves about 0.3 L of fuel per 100 km [5]. Although some Al-based frame structures have been already produced,

utilization of these alloys has generally been incremental and resulted in designs which employ multiple materials, which often need to be joined in dissimilar combinations.

#### **1.4 Joining of Al to Mg**

Since, Al and Mg alloys can both be potentially used in the same structure the problem of joining these two materials must be addressed. Numerous studies regarding dissimilar joining of Al to Mg by different techniques can be found in the literature. The common problem with all fusion-based dissimilar metal joining techniques of Al to Mg is the formation of hard and brittle intermetallic compounds [6, 7]. Solid state processes which involve comparatively low temperatures such as diffusion bonding [8, 9], butt friction stir welding (FSW) [10-12] and some others can achieve relatively high strength, however even in this case formation of brittle Al-Mg intermetallic compounds cannot be completely avoided. In addition solid state welding techniques such as friction stir welding have significant limitations and were not widely adopted by automotive and other mass production industries.

To mitigate the formation of undesirable intermetallics, some work has been done to explore the effect of different interlayers on the properties of Al/Mg joints. A variety of interlayers such as Zn [13], Ce [14], Ag [15], Sn [16], Ti [17], Cu [18], Ni [12, 19] and others were incorporated with different solid- and non-solid state welding processes. In general, employing interlayers reduced fraction of Al-Mg intermetallics and improved mechanical properties of the joints.

RSW of Al to Mg is particularly interesting since it is the predominant joining technique in the automotive industry. Nevertheless, only one detailed study on RSW of Al to Mg is available in the literature [4]. The strength of the welds achieved in this study was negatively influenced by formation of brittle intermetallic compounds. In addition this study considered commercially pure Al, which inevitably would result in low strength joints due to fracture propagation through the soft base metal as well. Therefore, a suitable technology for achieving high strength Al/Mg welds by RSW has yet to be developed.

Considering information available in the literature, employing an interlayer during welding of Al to Mg might be a feasible approach to eliminate intermetallics and improve mechanical properties of the joints during RSW.

## **1.5 Interlayers Used**

RSW of Al to Mg with six different interlayers was performed in the current study. As can be seen from Table 1.1 welds made with three different interlayers met requirements of AWS D17.2 standard. Ni-based interlayers and Zn-coated steel were chosen to be analysed in details in the current study. Brief information on RSW with other interlayers summarised in the appendices. Despite the fact that welds made with Sn-coated steel interlayer also met requirements of the standard, it was concluded that Zn-coated steel is more important to analyse, since it is much more common material and much lower cost than Au-coated Ni.

**Table 1.1: List of materials used as interlayers for RSW of Al/Mg in the current study**

Interlayer	Lap shear strength met requirement of AWS D17.2 standard [20]
Au-coated Ni	Yes
Ni foil	No
Sn-coated steel	Yes
Zn-coated steel	Yes
Zn foil	No
Cu foil	No

## **1.6 Motivation**

Technology of producing high strength Al/Mg RSW has not been developed yet. Employing an interlayer is the most promising approach in dissimilar welding of Al to Mg. However, there is a scarcity of literature on RSW of Al to Mg with different interlayers. Understanding the metallurgical aspects of welding Al to Mg with different interlayers is essential in order to promote utilization of these alloys in the automotive industry.

## **1.7 Objectives**

The objective of this thesis is to study feasibility of achieving high strength Al/Mg resistance spot welds by means of interlayer. The specific objectives are summarised as follows:

1. Achieve high strength Al/Mg resistance spot welds by means of interlayer
2. Investigate the role of different interlayers on the microstructure and mechanical properties of Al/Mg resistance spot welds
3. Characterise the bonding mechanism which took place during welding of Al to Mg with Au-coated Ni and Zn-coated steel interlayers

## 1.8 Thesis Outline

This thesis consists of six chapters and five appendices. Chapter 2 reviews literature on subjects related to RSW of Al to Mg. Chapter 3 details experimental apparatus and methods. In Chapter 4 microstructure and mechanical properties of Al/Mg resistance spot welds made with Ni-based interlayers, including Au-coated and bare Ni foils are examined. Chapter 5 explores mechanical and microstructural properties of Al/Mg welds made by RSW with Zn-coated steel interlayer. Key results attained in this work summarised in Chapter 6. A summary of data on RSW of Al to Mg with Sn-coated steel, Zn foil and Cu foil interlayers is shown in Appendix A. Appendices B to E summarise results of the feasibility tests of similar and dissimilar RSW of Mg-based alloys. Some information used in this thesis was already summarised and published in a form of a journal article [21].

## Chapter 2: Literature Review

### 2.1 Resistance Spot Welding

#### 2.1.1 Principles of RSW

As was briefly explained in the introduction chapter, a resistance spot weld is made by heat generated due to resistance to the electrical current which passes through welding coupons squeezed by electrodes.

The heat generated in the resistance is given by:

$$Q = I^2 R t \quad (2.1)$$

Where  $I$  is the current,  $R$  is the total resistance and  $t$  is the welding time. Amount of heat generated can be changed by changing any or all of the three factors mentioned above.  $I$  and  $t$  can be easily altered by regulating welding control while  $R$  depends on the resistance of the welding specimens. Two kinds of resistance can be found in the secondary circuit of RSW machine: bulk resistance of the material and contact resistance of the faying surfaces. Bulk resistance attributed to all materials and depends on the material composition and temperature. Bulk resistance is measured experimentally for standard volume of the material at known temperature, while contact resistance is the resistance to the flow of electrical current across the faying surfaces of two materials. Contact resistance greatly depends on the type of the material, condition of the surfaces, area of the contact and pressure. For metals with clean surfaces contact resistance usually follows bulk resistivity of the metals involved [1, 2].

Figure 2.1 shows all the resistances (marked as 1-7) involved in the RSW process. Since all the resistances are in series and the same current passing through each resistance, heat produced at each location would be proportional to the resistance at the location. Therefore, it is very important to minimize resistance at all the locations except faying surfaces of the welding coupons. In practise resistance at electrode/workpiece interfaces (2 and 6 on Figure 2.1) minimised by using copper electrodes with very low electrical resistivity. In addition dissipation of heat at the electrode/workpiece interfaces is much higher due to continuous water cooling.

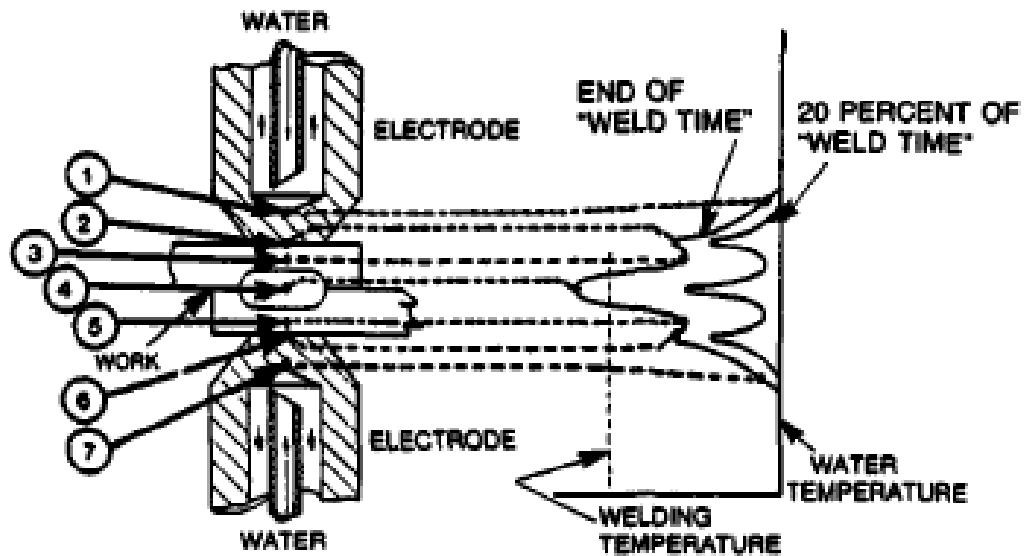


**Figure 2.1: Temperature distribution during RSW [2]**

### 2.1.2 RSW Parameters

The basic RSW parameters include welding current, welding time, electrode force and electrode geometry.

#### 2.1.2.1 Welding Current and Welding Time

Precise control of the heat input required in order to achieve high quality weld. If heat input is too low, weak and undersized nuggets might be produced. Usually minimum weld-nugget size can be determined using following equation [2, 22]:

$$MWS = 4\sqrt{t} \quad (2.2)$$

Where  $MWS$  is minimum weld-nugget size,  $t$  is the average sheet thickness in mm. On the other hand, excessive heat input will result in severe expulsion which is undesirable since it can cause cavities inside the fusion nugget. Welding current and time are the only parameters which regulate the heat input directly. As can be seen from the equation (2.1) a change in welding current has greater effect on the heat input than welding time since the factor  $I$  is squared. Although, heat input can be regulated by means of both parameters, generally welding

time kept as short as possible. In this situation, less heat is dissipated through conduction to the electrodes and colder areas of the workpieces. In addition, excessive welding time can result in increased wear of the electrodes and indentation on the workpieces [23]. However, in specific cases increased welding time can be required. For example, Dickenson *et al.* showed that up to 100% increase in welding time requires during welding of Zn coated steels to melt Zn coating and displace it out of the nugget [24].

#### 2.1.2.2 Welding Force

The basic RSW process employ two welding forces: initial squeeze force to clamp workpieces together and actual welding force which is usually a few times higher than initial squeeze force. Welding force can influence heat generation through change in contact resistance. Higher electrode force results in better contact at the interfaces and therefore decreases contact resistance [25]. Lower contact resistance usually leads to lower heat generation which might have to be compensated by increased welding current or welding time.

#### 2.1.2.3 Electrodes Type

Electrodes pass the current through the workpieces, apply the force and cool the welding pool after the welding. Therefore electrodes shape, size and material have a vital effect on the RSW process. Practically, all the electrodes made from Cu-based alloys. Cu has very low electrical resistance which minimises contact resistance at the electrode/workpiece interface. The electrode shape and diameter has great effect on the current density and therefore on the heat generation and location of the nugget. Usually the contact radius of curvature of the electrodes is selected according to the thickness of the sheets to be welded. In certain cases different top and bottom electrodes can be used in order to maintain heat balance, for example during welding of unequal thickness sheets or dissimilar metals with different bulk resistivity. Figure 2.2 shows RSW of unequal thickness specimens, electrode with smaller diameter was used at the bottom to concentrate heat generation closer to the thinner sheet.

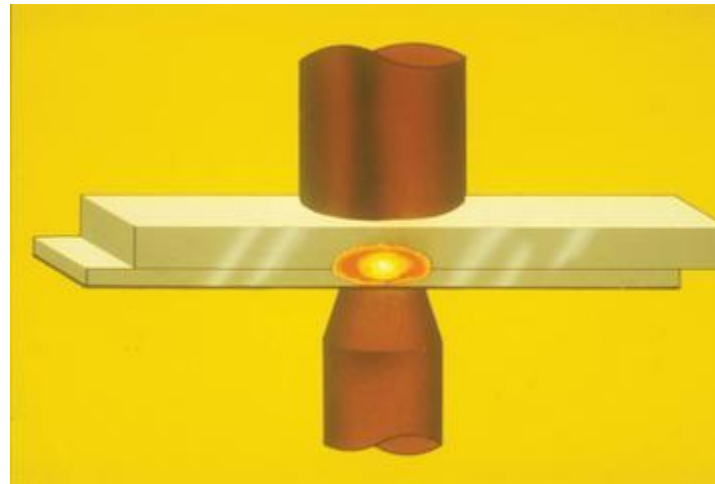


**Figure 2.2: RSW of unequal thickness sheets with different upper and bottom electrodes [1] (reprinted with permission of ASM International)**

### 2.1.3 RSW of Light Alloys

RSW of Al alloys significantly differs from traditional RSW of steels. Al alloys have very high thermal and electrical conductivity which brings certain specifics to the RSW of these materials. Up to three times higher welding current and four times shorter welding time requires for welding of Al alloys compared to welding of steels. If welding time is too long, heat generated at the faying surfaces will be conducted away through the rest of Al workpiece and no fusion nugget will be formed. Another specific of Al alloys is a narrow plastic range ( $95\text{-}205^\circ\text{C}$ ) [26], which is difference between melting and softening temperatures. Due to such a narrow plastic range, electrode force, welding time and current have to be controlled very carefully to avoid excessive expulsion and indentation of the electrodes into workpiece. Finally, surface condition of the workpieces play a very important role in RSW of Al alloys. To ensure uniform heat generation and distribution, surface of the workpieces has to be extremely clean. Chemical cleaning is one of the most common methods it consists of: degreasing and acid pickling of the surfaces.

RSW of Mg alloys is similar to RSW of Al alloys. Mg alloys have slightly lower electrical and thermal conductivity, but high welding currents and short welding times are still required for resistance welding of these alloys. Common practise shows that equipment used for RSW of Al alloys can be successfully used for RSW of Mg alloys, since requirements to the welding

parameters are similar [2]. Although, there is much in common between Al and Mg alloys, Mg alloys have some unique characteristics as well, such as small difference between melting and boiling points. The boiling point of Mg is 1091 °C which is just 440 °C higher than the melting point, this inevitably leads to a problem of Mg evaporation. Therefore, very precise control of the welding time and current required to manage the heat generation and avoid boiling of Mg during RSW.

#### **2.1.4 RSW of Dissimilar Materials**

There are two important concerns in RSW of dissimilar materials: heat distribution in the weld, and metallurgy of the alloy produced by mixing of these materials. Heat distribution in the weld largely depends on the difference in thermo-physical properties of the materials involved. If one of the materials have significantly larger electrical resistivity, there is a risk that fusion nugget will form inside the sheet of this material and not at the interface. The heat balance can be maintained by using dissimilar top and bottom electrodes. For example, larger diameter electrode can be used at the less conductive material side to dissipate the current. A similar approach commonly used in case of welding unequal thickness specimens, such as shown on Figure 2.2.

Another concern in RSW of dissimilar metals is microstructural and mechanical properties of the alloy produced by mixing of different metals. This problem is usually difficult to overcome since there are no general rules to follow and each materials combination has to be considered individually. It is important to predict type of the intermetallics and/or solid solutions which will be produced. Welding parameters can be used to adjust heat generation and distribution in order to achieve more desirable phases. Filler metals and interlayers also commonly used in dissimilar metals welding, since addition of third materials often can improve properties of the phases produced. Usually, practices developed for other fusion welding techniques can be applied in RSW. However, specifics in heat distribution in RSW have to be considered, since it has great effect on metallurgy and differs from other welding techniques.

#### **2.1.5 Weld Quality**

For most industrial applications the overlap shear strength of a resistance spot weld reflects the weld quality. Strength is usually specified in kN or pounds-force and results from a

variety of factors such as nugget size, fusion penetration, microhardness, amount of defects, or different microstructural features etc. Strength can be evaluated by variety of tests such as tension-shear test, cross-tension test, mechanised peel test etc. Overlap tension-shear testing is by far most common strength evaluation test for RSW due to its simple set-up. Minimum tension-shear strength requirements in kN or pounds-force specified by different standards such as AWS, ISO and SAE. The requirements of the standards are based on the strength of the materials and thickness of the sheets to be welded.

Microstructural properties often have a great impact on the strength of resistance spot welds. For optimisation of the weld strength it is important to analyse interfacial microstructure and fracture surface of the welds in details to determine which phases are more preferable. Some cracks, pores and cavities are usually present in commercial welds. These defects do not necessarily have significant effect on the weld strength [2], since it largely depends on the location of the defects and overall nugget geometry.

## 2.2 Mg and Al Alloys

Most of the metal parts in automotive industry were traditionally manufactured from steels and cast irons. In order to meet new emission and fuel consumption standards, auto manufacturing first turned into using Al alloys, which provides great weight savings compare to steels and cast irons. However as a demand for light weight automotive structures is increasing day by day, manufacturers started to look for material lighter than Al and began to invest into Mg, since it is the lightest commercially available structural metal. Density of Mg is just 1.74 g/cm<sup>3</sup>, while densities of Al and Fe are 2.7 g/cm<sup>3</sup> and 7.86 g/cm<sup>3</sup> respectively, which makes Mg 35% lighter than Al and at least four times lighter than steels. Beside lightness, Mg also has higher specific strength (tensile strength/density) than Al or Fe which makes it even more attractive for automotive industry [27].

Applications of Mg and Al in auto industry are similar. Some of the components which manufactured or can be manufactured from Al and Mg are shown on Figure 2.3, among them: engine and transmission parts, interior parts, chassis components and body components. Weight saving obtained by using Al and Mg parts instead of steel and cast iron parts are also mentioned on Figure 2.3. It should be noted that not all the applications of Al and Mg alloys in automotive industry are the same, there are certain applications for which one of the metals is

more suitable than another due to advantage in a specific property, such as damping capacity for Mg and creep resistance for Al. Therefore both materials are expected to be used in the automotive industry in the future. Combining Al and Mg in one hybrid structure would make possible to use these alloys for even more applications which will result in desirable weight saving.

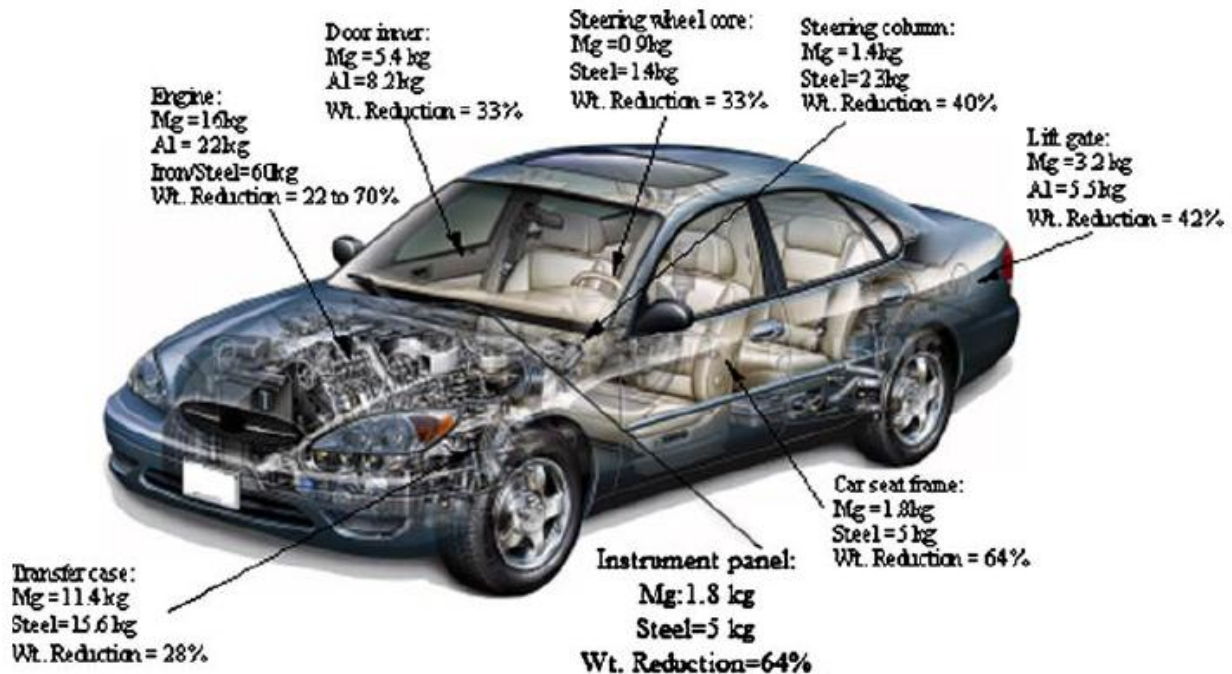


**Figure 2.3: Some applications of Mg and Al alloys into automotive and achieved weight reduction [27]**

Increase in amount of Al and Mg alloys in automotive industry predicted by many sources [27-30]. For example, Shultz *et al.* [29] reported amount of Mg and Al used in North American auto production in 2007 and predicted usage of these materials in 2015. According to the study conducted by Shultz *et al.* average amount of Mg used in a vehicle supposed to reach 10 kg by 2015 which is three times more than in 2007. Amount of Al will also significantly increase, reaching 169 kg in 2015 which is about 20 kg more than in 2007. United States Council for Automotive Research also made positive predictions regarding usage of Mg in auto industry, setting a goal to substitute 290 kg of steel and Al parts with 155 kg of Mg components per vehicle by 2020 [30].

Due to continuously increasing usage of Al and Mg in automotive industry and the large amount of potential applications of Al/Mg hybrid structures, problem of joining these materials has to be addressed. RSW of Al to Mg is particularly interesting since this is the lowest cost and most widely used automotive welding technique.

## **2.3 Welding of Al to Mg**

### **2.3.1 Direct Welding**

Direct welding of Al to Mg by different welding techniques is studied fairly well at the current moment. Table 2.1 summarises maximum shear strengths achieved by different welding techniques based on the information available in the literature. It should be noted that studies examining joining of Al to Mg by spot welding techniques usually report strength as maximum failure load in kN which make them not directly comparable. Nevertheless, Patel *et al.*[16] made an attempt to compare lap-shear strength of Al/Mg dissimilar welds made by different spot welding techniques. Data reported by Patel *et al.* is also included in Table 2.1. A few rough approximations were made by Patel *et al.*: nugget diameter for RSW, area of welding tip for ultrasonic spot welding (USW), and shoulder diameter for friction stir spot welding (FSSW) were used as nominal bonding area to calculate peak load strength. In addition variation in thickness of the samples and type of alloys used was neglected in the study.

**Table 2.1: Maximum tensile shear strength of Al/Mg welds produced by different welding techniques (modified from Patel *et al.* [16])**

Technique	Maximum Shear Strength for type of welding, MPa	References
Diffusion bonding	57	[8, 31-34]
Explosive Welding	70	[35]
Friction Stir Welding (butt configuration)	189	[10-12]
Laser	48	[36]
Laser-TIG Welding	36	[14, 37]
Electromagnetic Impact Welding	185	[38]
Friction Stir Welding (lap configuration)	13	[16, 39]
Friction Stir Spot Welding	27	[16, 40]
Resistance Spot Welding	36	[4, 16]
Ultrasonic Spot Welding	35	[16]

Although significant assumptions were made, Table 2.1 still reflects general situation in dissimilar Al/Mg welding and can be used as reference. It was noted that fusion welding techniques including RSW yielded strengths lower than most solid state welding techniques. The mutual problem of all fusion-based welding techniques [4, 7, 36, 37, 41] is inevitable formation of very hard and brittle intermetallics, specifically  $\text{Al}_3\text{Mg}_2$  and  $\text{Al}_{12}\text{Mg}_{17}$  (Figure 2.4), which results in low strength of the welds. For example, Liu *et al.* [7] who employed Nd:YAG laser to weld Al and Mg together reported that both  $\text{Al}_3\text{Mg}_2$  and  $\text{Al}_{12}\text{Mg}_{17}$  intermetallics formed at the fusion zone, which had harmful effect on the welds strength. Similarly, Qi *et al.* [37] reported that they could not avoid formation of brittle Al-Mg intermetallics in case of direct Al/Mg laser-TIG welding and therefore weak joints with maximum tensile shear strength of 26 MPa were produced. The only detailed study on Al/Mg RSW [4] also reported that formation of Al-Mg intermetallic compounds was inevitable and harmful for the joints strength. Figure 2.5 and Figure 2.6 show microhardness profile and fracture surface of direct Al/Mg resistance spot welds. It can be seen that there is a vast increase in hardness in the fusion zone due to

formation of very hard  $\text{Al}_3\text{Mg}_2$  and  $\text{Al}_{12}\text{Mg}_{17}$ . Fracture surface of the welds also exhibits brittle morphology and as expected, strength of the joints was far from ideal.

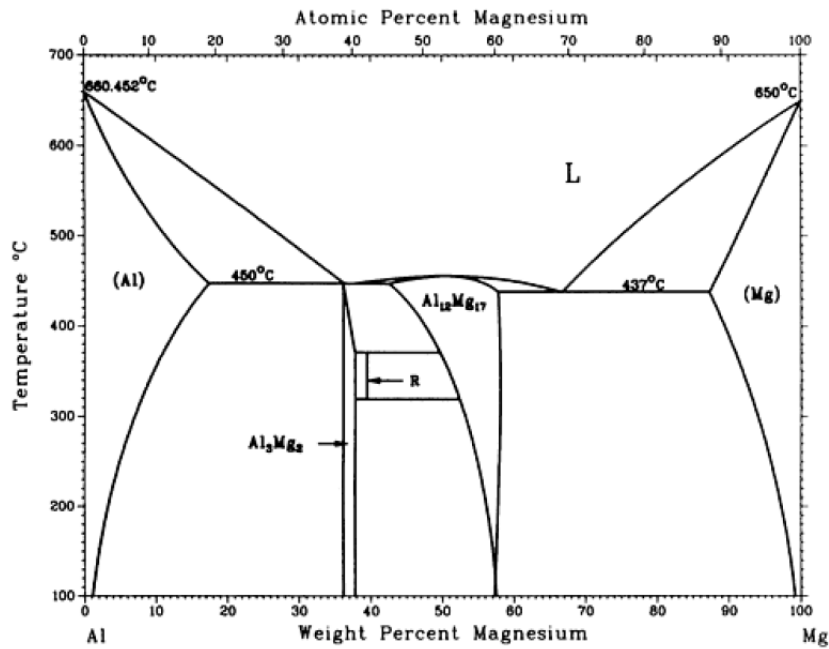


**Figure 2.4: Al-Mg binary phase diagram [42] (reprinted with permission of ASM International)**

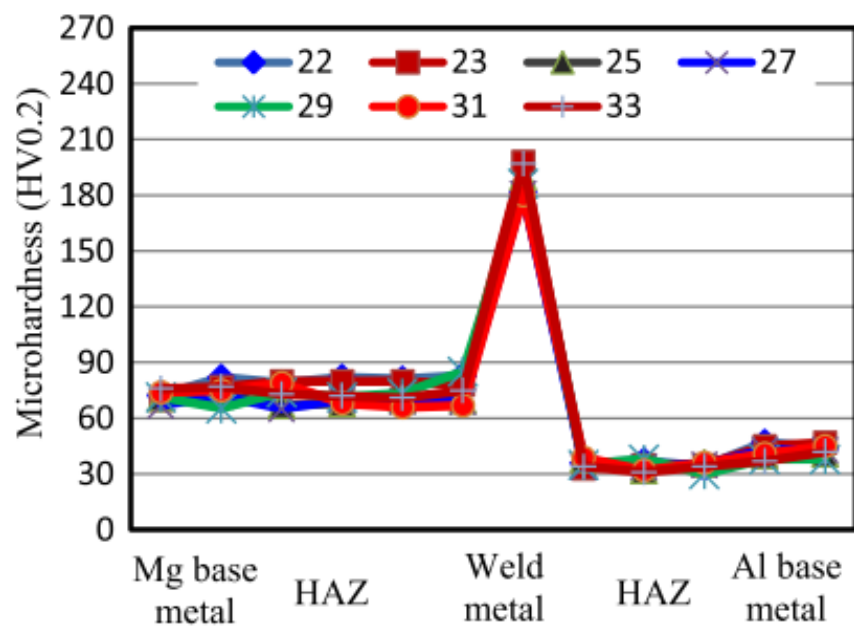


**Figure 2.5: Microhardness profile of direct Al/Mg resistance spot welds made with welding currents of 22-33 kA [4]**

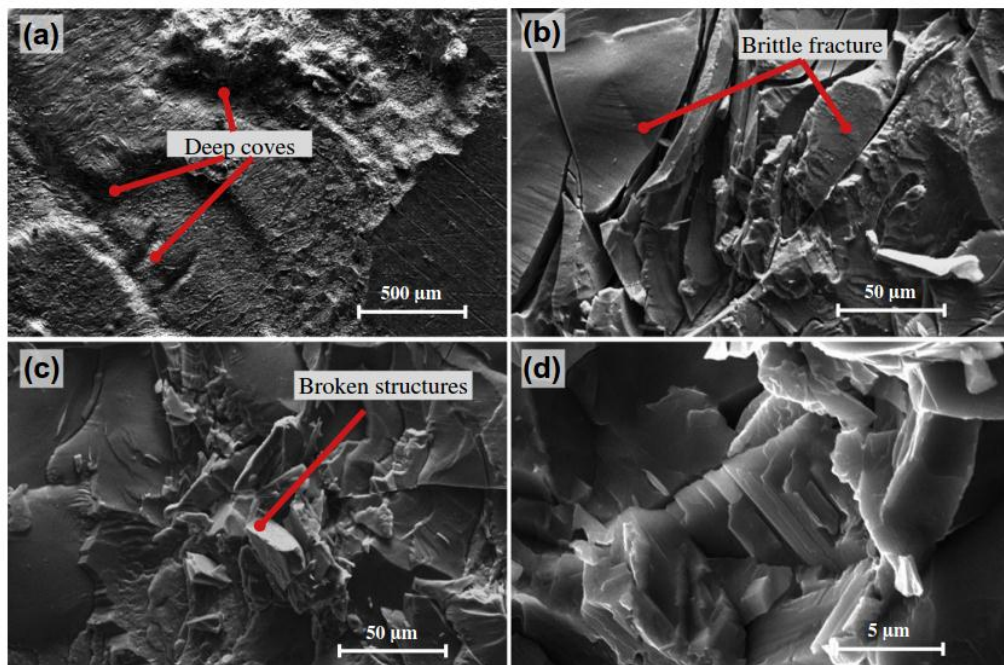


**Figure 2.6: Fracture surface of direct Al/Mg resistance spot weld on Mg side [4]**

Most of the solid state welding techniques showed better results in Al/Mg dissimilar welding than fusion-based techniques. In the case of diffusion bonding [8, 31-34] slightly higher strength was achieved compare to fusion welding techniques due to more precise control over the intermetallic formation which let to create intermetallic layer with optimal thickness. Friction stir spot welding [40, 43] and friction welding in lap configuration [39, 44] also could not produce high strength welds due to fracture propagation through layer of hard and brittle intermetallics which formed between upper and bottom sheets. Friction stir welding in butt configuration [10-12] could not completely avoid formation of brittle intermetallics as well. However, the strongest Al/Mg joints were produced by this technique. Recent study conducted by Venkateswaran *et al.* [45] showed that welds produced by this technique have high strength due to large length and complexity of the interface which creates more self-clamping effect and longer fracture path. Typical Al/Mg friction stir butt weld is shown on Figure 2.7. It also should be noted that friction stir welding involves formation of a thinner intermetallic compound layer than fusion welding techniques, due to much lower heat input. The highest strength of Al/Mg joints produced by butt friction stir welding was reported as 189 MPa [10].

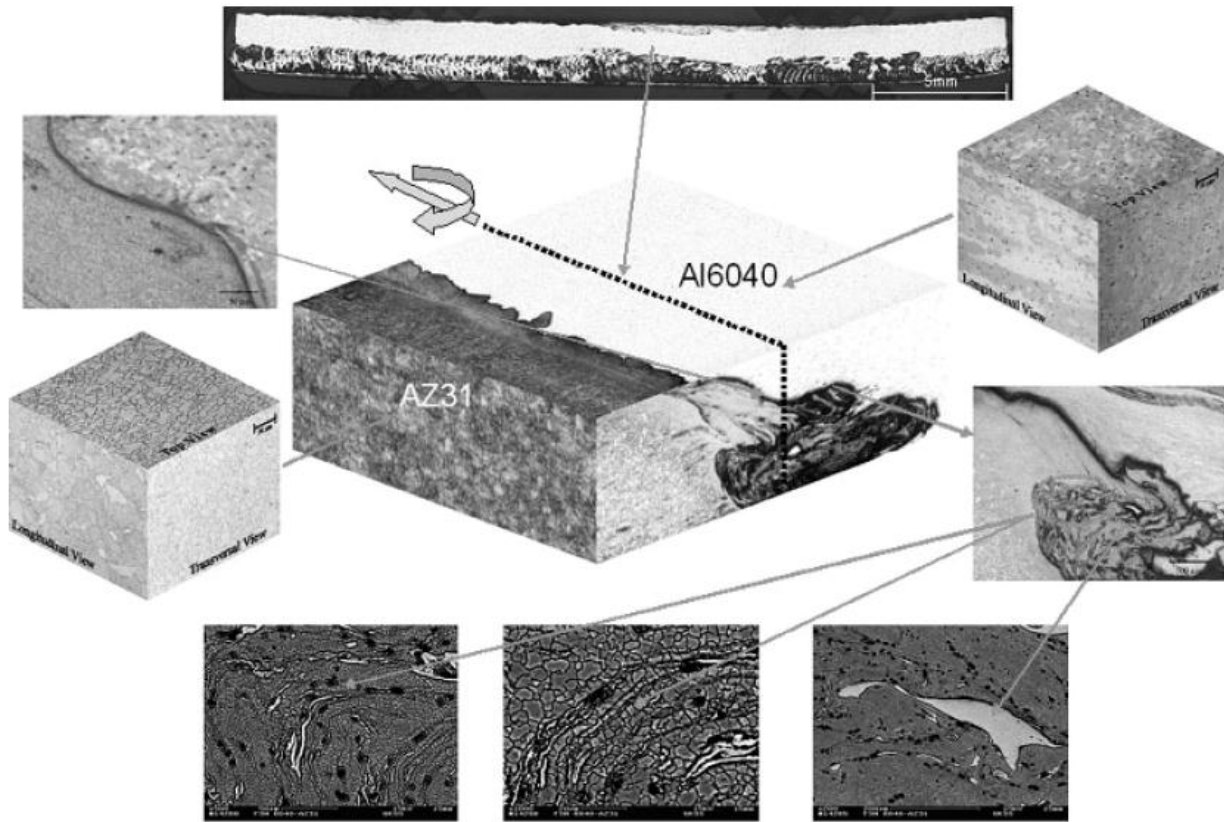


**Figure 2.7: Interfacial microstructure and Material flow in different zones of dissimilar Al/Mg butt friction stir weld [10]**

Although high strength welds were achieved by friction stir welding in butt configuration, this technique has many limitations and therefore was not widely adopted in automotive and other industries. Among limitations of butt friction stir welding are: high cost, limited weld geometry, low speed, and requirement of heavy fixtures. Therefore, further improvement of fusion welding of Al to Mg should be done. Employing of different interlayers currently is the most promising approach in dissimilar Al/Mg welding. Effects of different interlayers on microstructure and mechanical properties of Al/Mg welds made by different welding techniques are analysed in next section.

### **2.3.2 Welding with Interlayers**

Employing an interlayer or a filler metal is a common approach in dissimilar materials joining. Numerous studies investigating Al/Mg joints made with different interlayers and welding techniques can be found in the literature. The highest strength achieved in each study as well as type of interlayers and employed welding techniques are listed in Table 2.2. All of the studies reported that addition of an interlayer improved the strength of the joints. Interlayer material usually reacted with Al and Mg, forming more preferable intermetallics than  $\text{Al}_3\text{Mg}_2$  and  $\text{Al}_{12}\text{Mg}_{17}$ , which led to the increase in strength. In some cases interlayer formed common fusion zone of Al, Mg and interlayer and in some cases addition of interlayer completely prevented interaction between Al and Mg. It was noted that usually better results were achieved when interaction between Al and Mg was completely prevented. For example during diffusion bonding of Al to Mg with Zn foil interlayer, Liu *et. al.* [46] found that better results can be obtained with shorter holding times when diffusion is not significant enough to let Mg and Al interact. While with longer holding times diffusion of Al and Mg atoms was more intense and formation of Al-Mg intermetallics occurred which had a negative effect on weld strength.

**Table 2.2: List of interlayers and techniques used by other researchers to weld Al to Mg**

Interlayer Type	Welding Technique	Shear Strength Reported, MPa	References
Ag-based	Diffusion bonding	15	[15]
Ce-based	Laser-TIG	56	[14]
Cu-based	Cold Metal Transfer	35	[18]
Fe-based	Laser-TIG	100	[37]
Ni-based	Diffusion Bonding	Not reported	[19]
	Hybrid Laser-FSW (butt conf.)	169	[12]
Ti-based	Laser	78	[17]
Sn-based	TIG	Not reported	[47]
	Ultrasonic Spot Welding	42	[16]
Zn-based	Diffusion Bonding	86	[13, 46, 48]
	Laser	80	[49]
	MIG	64	[50]

It can be seen from Table 2.2 that the highest strength of Al/Mg interlayer added joints was achieved by hybrid laser-FSW in butt configuration [12]. Cheng *et al.* who conducted this study, reported that Al-Mg compounds were not completely eliminated, but addition of Ni foil interlayer still improved the strength of the welds due to presence of less brittle Ni-based phases instead of  $\text{Al}_{12}\text{Mg}_{17}$ . Second highest strength was achieved by Qi *et al.* using laser-TIG welding with Fe foil interlayer [37]. Qi *et al.* reported that under optimal parameters of welding Fe foil interlayer reacted with Al sheet forming continuous layer of Fe-Al intermetallic compounds, as shown on Figure 2.8. Formation of the Fe-Al intermetallics prevented direct contact between Mg and Al and therefore no brittle Al-Mg compounds were formed which resulted in significant improvement in tensile-shear strength of the joints compared to direct welding.

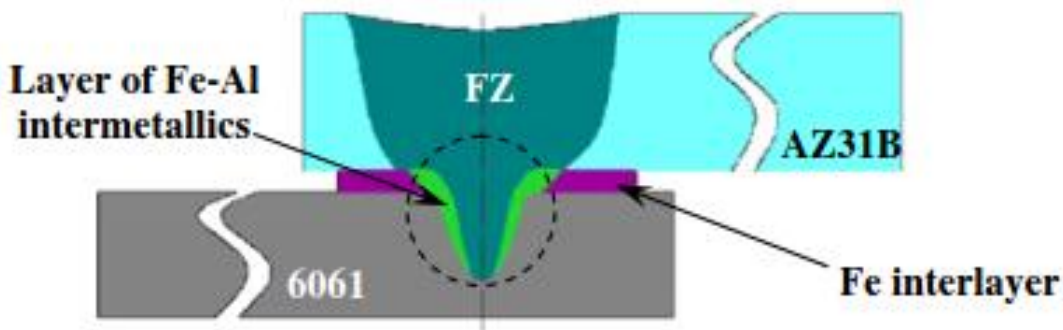


**Figure 2.8: Sketch of Al/Mg joint made by laser-TIG welding with Fe foil interlayer [37]**

## 2.4 Selection of Interlayers for RSW of Al to Mg

Based on the information available in the literature RSW of Al to Mg might be feasible with right interlayer. As was noted in previous section it is better to completely avoid interaction between Al and Mg. Employing an interlayer with a high melting point which will remain intact during RSW should entirely prevent formation of Al/Mg intermetallics. Ni-based foils are strong interlayer candidates, since high melting point of Ni ( $1455^{\circ}\text{C}$ ) compared to Mg ( $650^{\circ}\text{C}$ ) and Al ( $660\text{-}42^{\circ}\text{C}$ ) will prevent mixing of Al and Mg during RSW. Also, the literature suggests that Al-Ni and Mg-Ni intermetallics are less brittle and therefore more preferable than Al-Mg intermetallics [12, 51]. Therefore it was decided to investigate effects of the Ni and Au-coated Ni foils on RSW of Al to Mg in this thesis.

Another strong candidate to the interlayer for Al/Mg RSW is hot-dip galvanised Zn-coated steel. As it was evident in the literature all commercially available hot-dip galvanised steels have nanoscale layer of  $\text{Fe}_2\text{Al}_5$  intermetallic compound [52-54]. About 0.18 wt.% Al is always present in the galvanising Zn bath, specifically to form nanoscale layer of  $\text{Fe}_2\text{Al}_5$  which inhibits formation of brittle Fe-Zn intermetallics and improves adhesion of Zn coating on steel surface. A recent study on RSW of Mg to galvanised Zn-coated steel conducted by Liu *et al.* [55], showed that despite of immiscibility between Mg and Fe, Mg still can be successfully joined to steel if nanoscale layer of  $\text{Fe}_2\text{Al}_5$  is present. The strength of the Mg/Steel joints produced by Liu *et al.* [55, 56] reached 95% of same size optimised Mg/Mg joint. Based on the literature, Al also can be successfully joined to steel by RSW. During RSW Fe and Al form mutual reaction layer and if this reaction layer kept thin by proper selection of the parameters it does not reduce strength of the joints [57-59]. Therefore it was concluded that Zn-coated steel is also a strong

candidate to the interlayer and its effects on dissimilar Al/Mg resistance spot welds, should be studied in this thesis.

## 2.5 Summary

Al and Mg alloys are desirable in modern automotive manufacturing due to their high specific strengths. To enhance utilization of these materials in auto manufacturing, technology for joining these materials should be developed. RSW of Al to Mg is especially interesting, since it is predominant joining technique in automotive industry.

Direct joining of Al to Mg cannot be currently accomplished by any of fusion welding techniques due to inevitable formation of brittle Al-Mg intermetallics which have detrimental effect on the welds quality. Literature suggests that employing of interlayers during Al/Mg welding is a promising approach to improve microstructure and strength of the welds. Multiple studies on joining Al to Mg with different interlayers can be found in the literature. However, none of the studies employ RSW.

This thesis examines effects of different interlayers on mechanical and microstructural properties of Al/Mg resistance spot welds. Detailed analysis of fracture surfaces and interfacial microstructures was carried out in order to determine bonding mechanism in different areas of the welds.

## **Chapter 3: Experimental Apparatus and Methods**

### **3.1 Material Selection**

#### **3.1.1 Welding Coupons**

Welding specimens used in this study were commercially available sheets of Mg alloy AZ31B-H24 and Al alloy 5754-0. Dimensions of the Al and Mg alloy welding coupons were 100 mm x 35 mm x 2 mm. Nominal composition and basic mechanical and physical properties of both alloys used in the study are summarised in Table 3.1 and Table 3.2 respectively. The surface of the Mg sheets was treated with solution of 2.5 g chromic oxide and 100 mL water prior to welding, and the Al coupons were ultrasonically cleaned in ethanol for 10 minutes and treated with solution of 1.2 mL HF, 67.5 mL HNO<sub>3</sub> and 100 mL water.

**Table 3.1: Chemical composition of Al and Mg alloys used in this study in wt.% [60]**

	Al	Mg	Si	Fe	Mn	Zn	Cr
Mg AZ31B	3	Bal.	0.1	-	0.2	1	-
Al 5754	Bal.	3	0.4	0.4	0.5	0.2	0.3

**Table 3.2: Basic properties of Al and Mg alloys used in this study [60, 61]**

	Ultimate Tensile Strength, MPa	Electrical Resistivity, nΩ·m	Thermal Conductivity, W·m <sup>-1</sup> ·K <sup>-1</sup>
Mg AZ31B-H24	285	92	96
Al 5754-0	215	49	147

#### **3.1.2 Interlayers**

##### **3.1.2.1 Ni-based Interlayers**

Pure Ni foil was used as an interlayer in this study, in either an uncoated condition or with an electrolytic Au plating typically 4 to 6 µm in thickness. Dimensions of the Ni-based interlayers were 10 mm x 10 mm x 0.2 mm. Bare Ni interlayers were ultrasonically cleaned in acetone for 10 minutes prior the welding while Au-coated Ni was used in as-received condition.

### 3.1.2.2 Zn-coated Steel Interlayer

Another type of interlayer which was used in this study is hot-dip galvanised HSLA steel. Composition of the steel is summarised in Table 3.3. Thickness of Zn coating was approximately 10 µm on both sides. Zn-coated steel interlayers were larger than Ni-based interlayers, exact dimensions are: 20 mm x 20 mm x 0.7 mm. Before, the welding Zn-coated steel was ultrasonically cleaned in acetone for 5 min.

**Table 3.3: Chemical composition of the hot-dip Zn-coated steel used as an interlayer (wt.%)**

C	Mn	Si	Al	Cr	Ni	Cu	Nb
0.06	0.62	0.23	0.04	0.04	0.01	0.04	0.02

As evident in literature [52-54] and was described in section 2.4 of this thesis, all hot-dip galvanised steels have nanoscale layer of Fe-Al intermetallic between Zn coating and steel surface. Figure 3.1 shows Zn/steel interface of the interlayer used in this study. Increase of Al content between Zn and steel proves that nanoscale layer of Fe-Al intermetallic, was also present in the steel used in the current study.

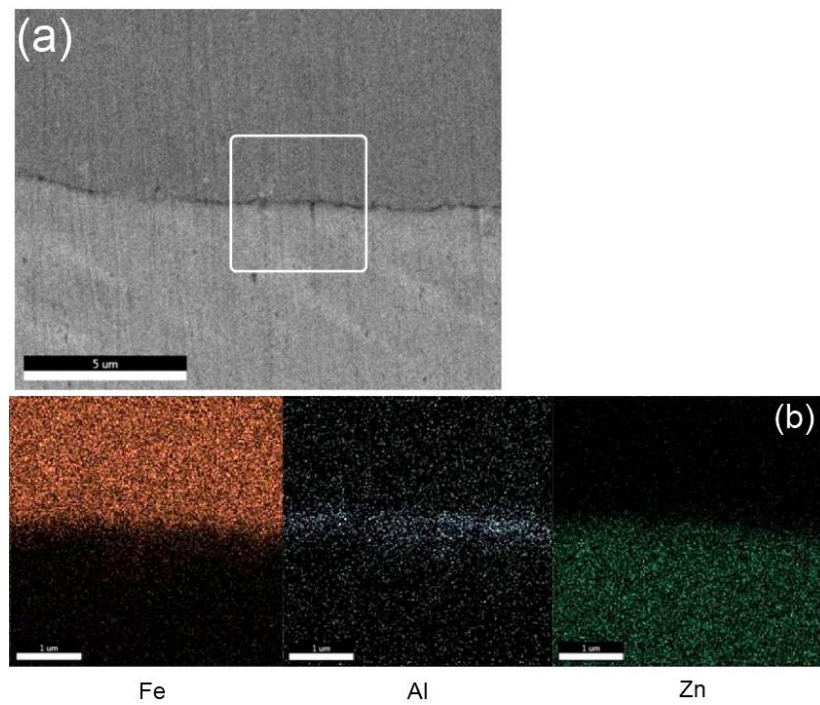


**Figure 3.1: Interface between steel and Zn coating in HSLA hot-dip galvanised steel. a SEM micrograph; b Fe, Al and Zn element distribution maps of area marked in a**

### 3.2 Welding Equipment

The RSW equipment used in this study was a mid-frequency direct current resistance spot welder (custom edition built by Centerline Ltd. for University of Waterloo). Figure 3.2 shows photo of the RSW machine and a schematic of the welding coupons being joined. The MFDC RSW machine was equipped with a precise data acquisition system, which is able to record load, current and voltage simultaneously.

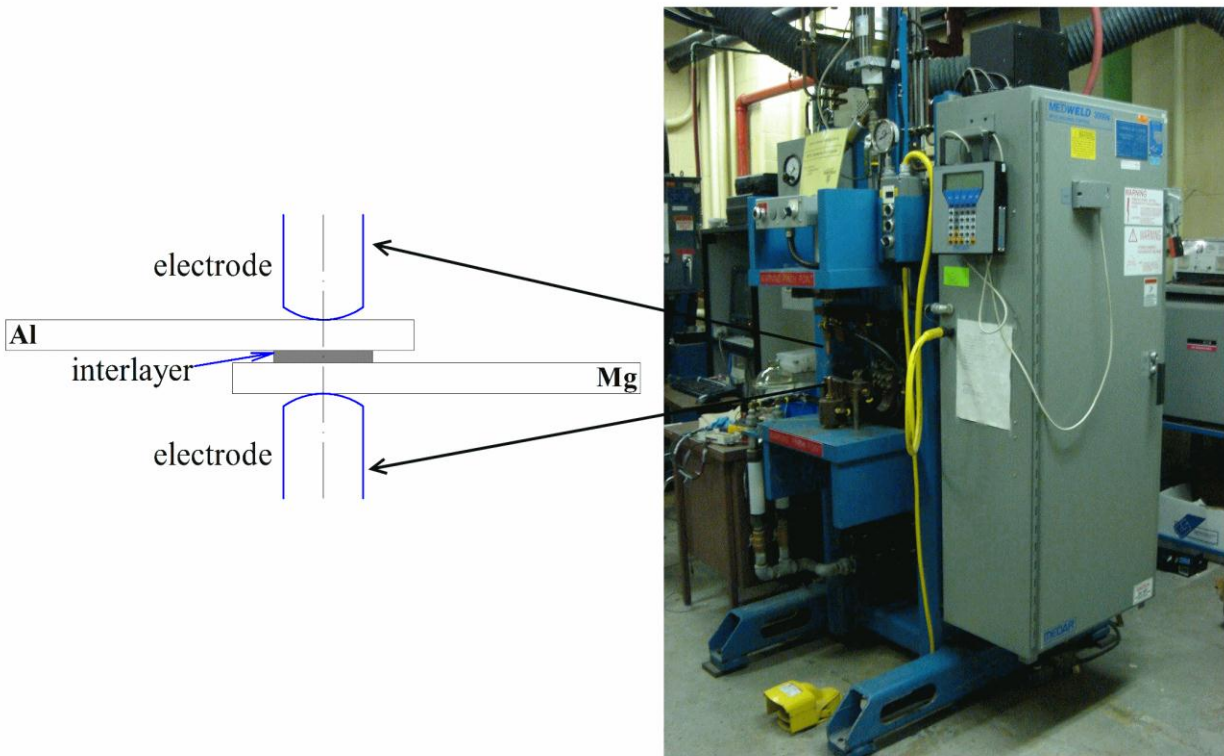


**Figure 3.2: RSW machine and a schematic of the welding coupons being joined**

Welding parameters used in the study are summarised in Table 3.4. Electrode caps type FF25 were used and had a spherical radius of 50.8 mm and face diameter of 16 mm, manufactured from Cu–Cr–Zr alloy. It should be noted that welding current was the only variable welding parameter in this study and it ranged from 16 to 24 kA for Ni-based interlayers and from 16 to 32 kA for Zn-coated steel interlayers. Welding currents higher than 24 kA were not tested for Ni-based interlayers, due to small size of the Au-coated Ni sheets available for the experiments. Schematic of the typical welding schedule used in this study is shown on Figure 3.3.

**Table 3.4: Welding parameters used for RSW of Al to Mg with interlayers**

Squeeze Force, kN	Squeeze Time	Welding Force, kN	Welding Force Time	Welding Current, kA	Welding Time	Hold Time
2	30 cycles (0.5s)	4	30 cycles (0.5s)	16; 20; 24; 28; 32	5 cycles (1/12s)	30 cycles (0.5s)

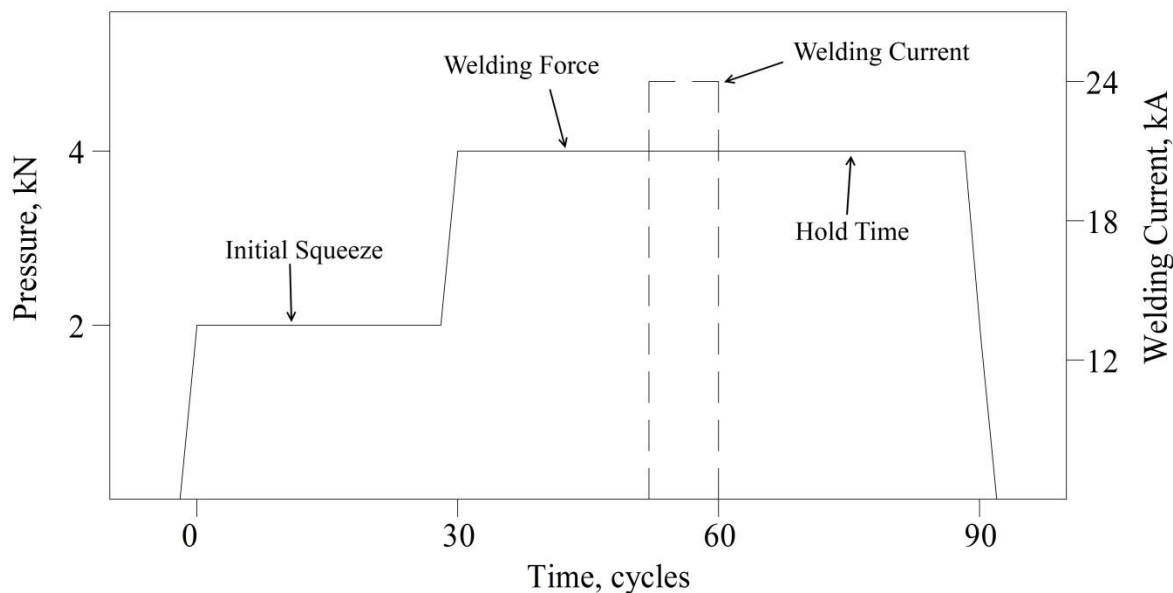


**Figure 3.3: Full welding schedule used in the current study**

### 3.3 Mechanical Testing

Three samples per condition were tested via tensile shear loading with welding currents 16 and 20 kA while six samples tested with welding currents of 24, 28 and 32 kA. An Instron 4206 (Norwood, MA) tensile test machine was used in this study, where specimens were strained to failure with a cross head speed of 1 mm/min. The geometry of the welding coupons for tensile shear test as well as the test set-up are shown on Figure 3.4. Alignment spacer sheets were used to grip the samples during overlap shear testing to minimize the bending or misalignment effects.

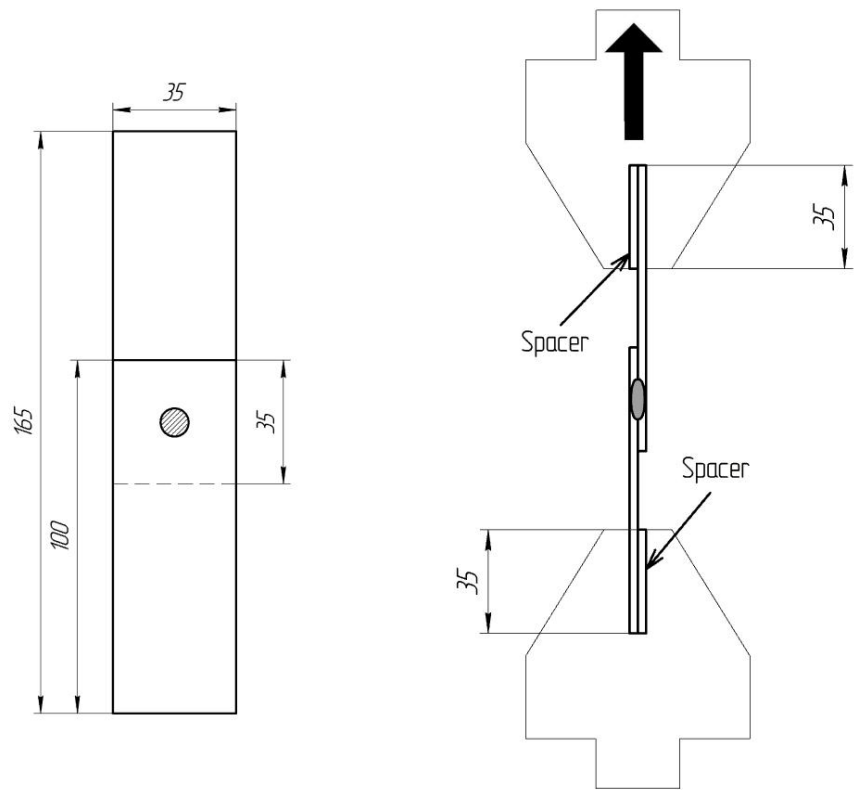


**Figure 3.4: Test coupon geometry and tensile shear test set-up**

Leco MHT series 200 Vickers microhardness tester was used for microhardness evaluation. Test was performed along diagonal across the weld from top coupon to bottom coupon (Figure 3.5), such as prescribed by AWS D8.9 standard. Each indent was made with a 100 g load and 15 sec indentation time. Distance between each measurement was equal to 0.254 mm (1/10") which was always larger than three times the average of any two adjacent indents.

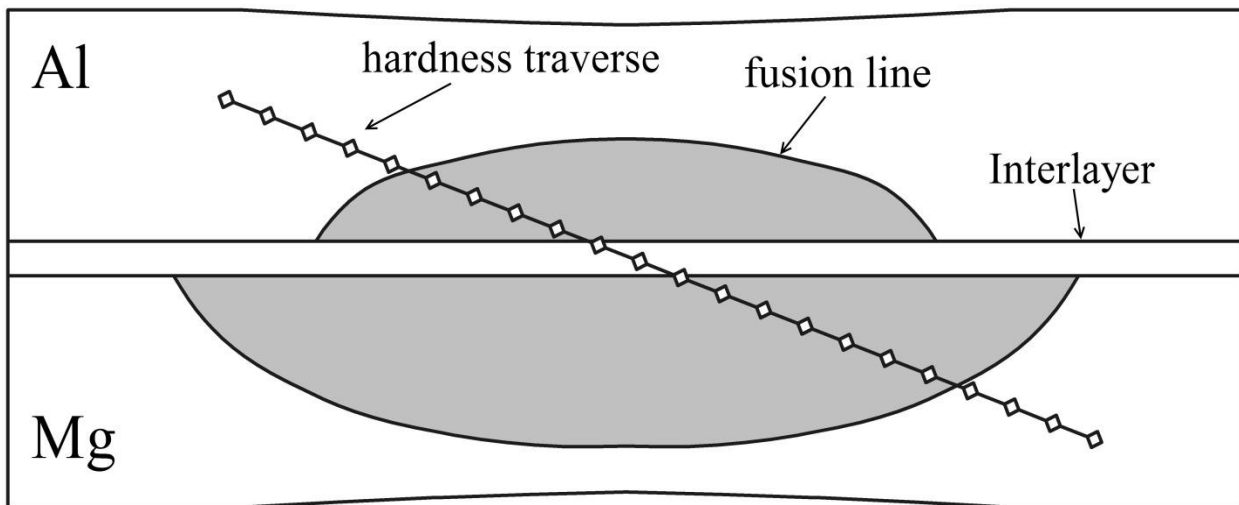


**Figure 3.5: Cross-sectioned weld and hardness traverse**

### 3.4 Metallographic Analysis

Metallographic weld specimens were cut, mounted, polished and examined by optical and scanning electron microscopy (SEM). SEM microscope used was a JEOL JSM-6460 equipped with Oxford Instruments INCA-350 energy-dispersive spectroscopy system.

The size of the fusion nugget diameter was measured from the cross-sections on both the Al and Mg side of the transverse weld sections, with a minimum of three samples per condition for nugget size measurement. Acetic-Picral etching solution (acetic acid – 20 mL; picric acid – 3 g; ethanol – 50 mL; water – 20 mL) was used for etching of the Mg alloy while the Al alloy was etched with 2% hydrofluoric acid. The fracture surfaces of the samples were examined by SEM and X-Ray diffraction techniques (XRD) using a Rigaku Ultima IV with a Co K-alpha source after tensile shear testing.

## Chapter 4: Resistance Spot Welding of Al to Mg with Ni-based Interlayers

### 4.1 Experiments with Bare Ni Interlayer

#### 4.1.1 Mechanical Properties

RSW of Al to Mg with bare Ni interlayer was studied first. No joints were produced with a bare Ni interlayer in a range of currents from 16 to 24 kA. Coupons separated without applying any force immediately after welding. Figure 4.1 shows a photo of Al and Mg sheets after welding. It was noted that when welding currents of 20 and 24 kA were employed, the Al sheet always separated from Ni interlayer suggesting that some bonding occurred between Mg and the bare Ni interlayer.

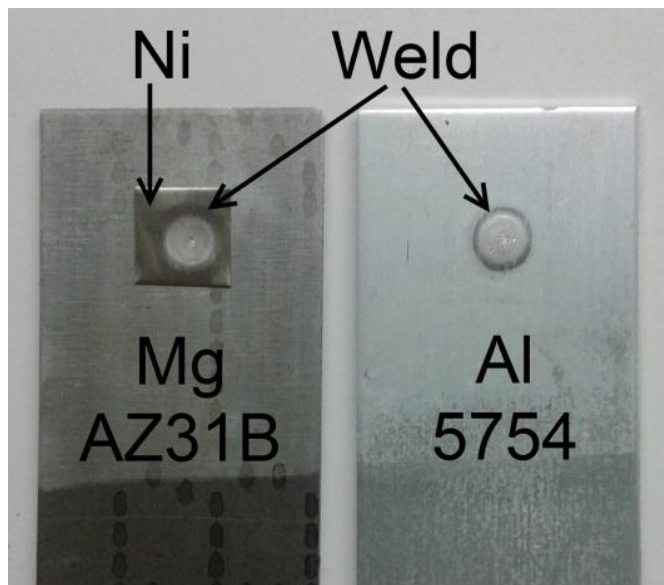


**Figure 4.1: Surface of the Al and Mg sheets after welding with bare Ni interlayer and 24 kA welding current**

Figure 4.2 shows relationship between melted zone size and welding current. The bulk of the Ni interlayer remained solid with only partial melting of the surface during the welding and therefore Al and Mg melted zone was measured separately. The melted zone size of both sides increased with welding current as typically observed in RSW. It was noted that the Mg alloy

sheet had a larger melted zone than that observed in the Al alloy side in all conditions examined.

The difference in the melted zone sizes observed in Figure 4.2 may be explained by variation in the contact resistance, since more heat always generated at the interface with higher contact resistance. In general, contact resistance follows the volume resistivity of the metals involved [2, 25]. Mg alloy AZ31B has greater electrical resistivity ( $92 \text{ n}\Omega\cdot\text{m}$ ) [60] than Al alloy 5754 ( $49 \text{ n}\Omega\cdot\text{m}$ ) [61], which would lead to increased heat generation and larger melted zone in the Mg sheet. In addition, greater heat losses will be expected in the Al sheet due to the higher thermal conductivity of Al 5754 alloy (which is  $147 \text{ W}\cdot\text{m}^{-1}\cdot\text{K}^{-1}$ ) [60] compared to Mg AZ31B alloy (reported to be  $96 \text{ W}\cdot\text{m}^{-1}\cdot\text{K}^{-1}$ ) [61].

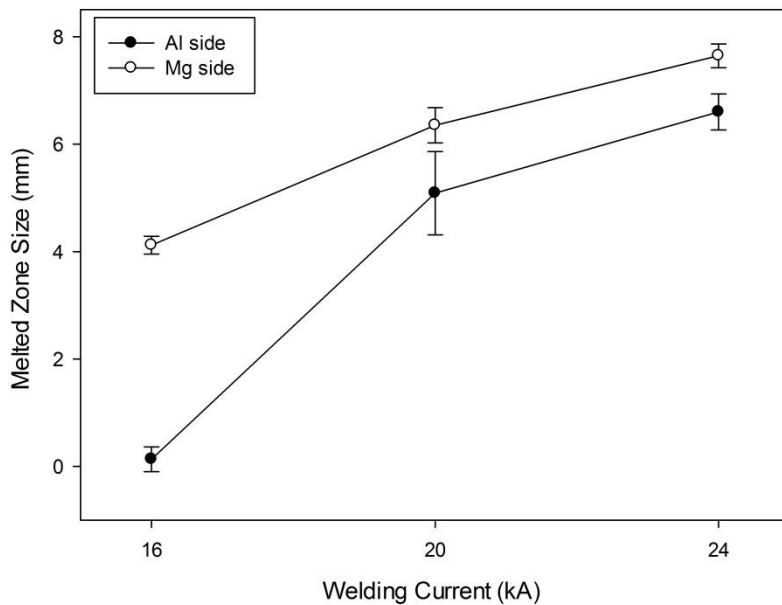


**Figure 4.2: Correlation between melted zone size on both Al and Mg side and welding current during RSW with bare Ni interlayer**

#### 4.1.2 Fracture Surface Examination

The fracture surface morphology was analysed on the sample made with 24 kA welding current. Figure 4.3 shows the fracture surface of the bare Ni interlayer at Al side. The results of EDX analysis of the different areas shown on the Figure 4.3 are summarised in Table 4.1. The evidence of molten Al which re-solidified on the surface of the Ni interlayer can only be observed in a narrow semicircle area at the periphery of the nugget (region A in Figure 4.3a). At

this region Al grains and dendrites (region 2 in Figure 4.3b) are observed growing from the Ni surface (region 1 in Figure 4.3b), and it appears this region did not contribute to the strength.

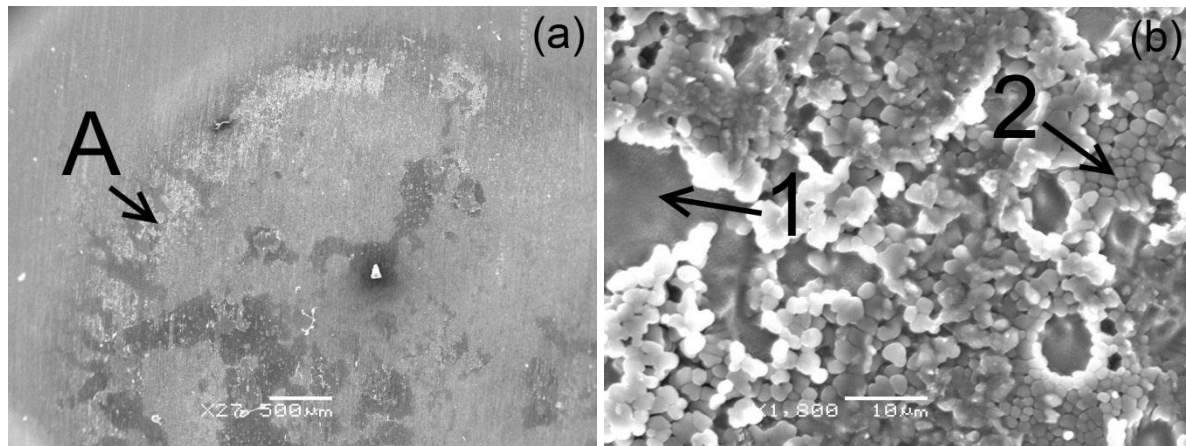


**Figure 4.3: Fracture surface of the bare Ni interlayer at Al side (produced in a weld made using 24 kA). a overview; b details of region A in a**

**Table 4.1: EDX quantification (in wt.%) of different areas in Figure 4.3b**

Area	Mg	Al	Ni
1	-	25.2	74.8
2	3.0	92.4	4.6

The absence of significant metallurgical reaction between Al and Ni is in contrast with other results when conducting RSW of Al to Ni without Mg sheet. It was found that the Al sheet and Ni foil employed in this study can be successfully spot welded producing strong joints then Mg sheet is not present. In this case the bulk of the Ni interlayer was not melted while the Al sheet was, similar to the welding of Al to Mg when Ni was present as an interlayer. However, reaction between Al and Ni can be observed along Al fusion zone/Ni interface when no Mg sheet was present. Figure 4.4a shows the SEM image of the Al/Ni interface of a weld made without Mg sheet. The composition of the reaction layer marked as B on Figure 4.4a (65.1 wt.% Ni and 34.9 wt.% Al), and a composition line scan made using EDX across the interface (Figure 4.4b) indicates that metallurgical bonding is possible between Al and Ni when only the two sheets are used. These observations suggest that more heat was generated in the Ni sheet compared to when the Mg sheet was present, since all the other conditions were kept the same.

The poor bonding observed in Figure 4.3 may be a result of lower heat generation caused by the spreading of the current, which also has a tendency to occur during RSW of three sheets Al assemblies [2].

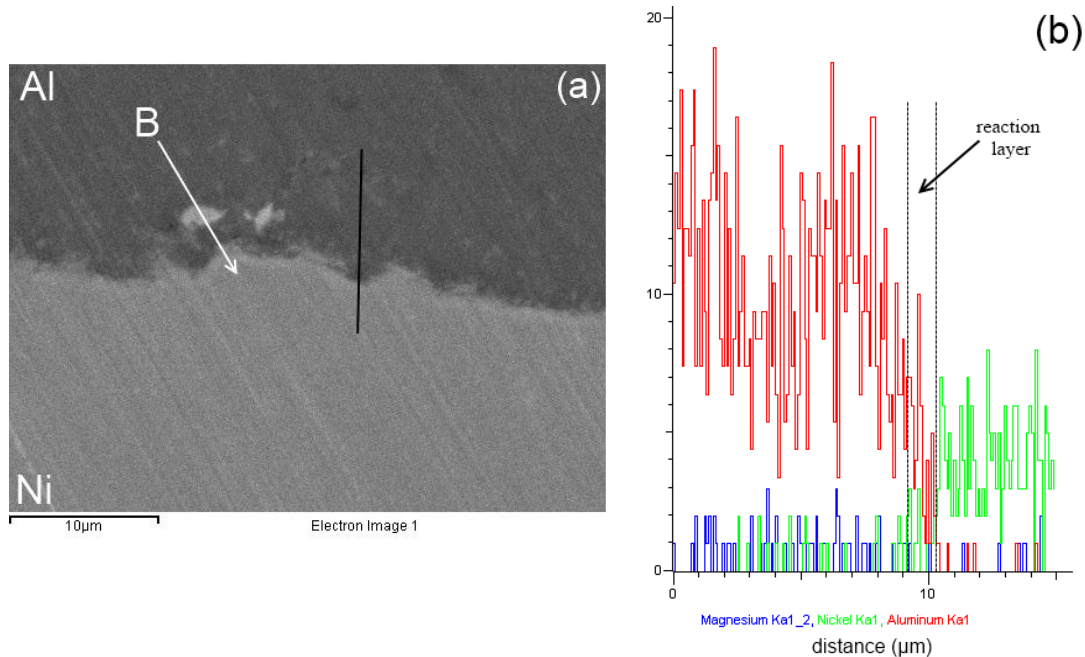


**Figure 4.4: Al/Ni weld (without Mg). *a* SEM micrograph; *b* EDX line scan across Al/Ni interface marked in *a***

The Ni interlayer stayed attached to the Mg surface, which suggests that some wetting and/or reaction between Mg and Ni occurred. A similar phenomenon was observed during diffusion bonding of Al to Mg with Ni interlayer [19], where reaction at Mg-Ni interface started much earlier than at Al/Ni interface.

X-Ray diffraction analysis was done on the fracture surface of bare Ni interlayer on both Al and Mg side (Figure 4.5). The sample made with 24 kA welding current was used for the analysis. Al sheet separated from Ni interlayer without applying force while Mg sheet was forced to separate from Ni. No intermetallic compounds were detected on the Ni surface on both Al and Mg side using XRD. Although Al-Ni phases were detected by EDX (Table 4.1), the small amount and fine thickness of those phases was beyond the resolution of XRD, making them difficult to identify.

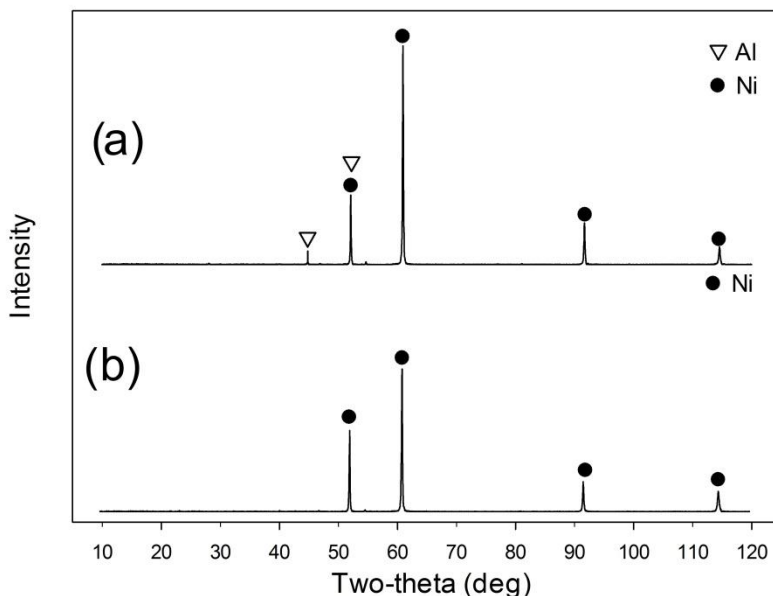


**Figure 4.5: XRD analysis of the bare Ni interlayer fracture surface on both Al and Mg side.  
a Al side; b Mg side**

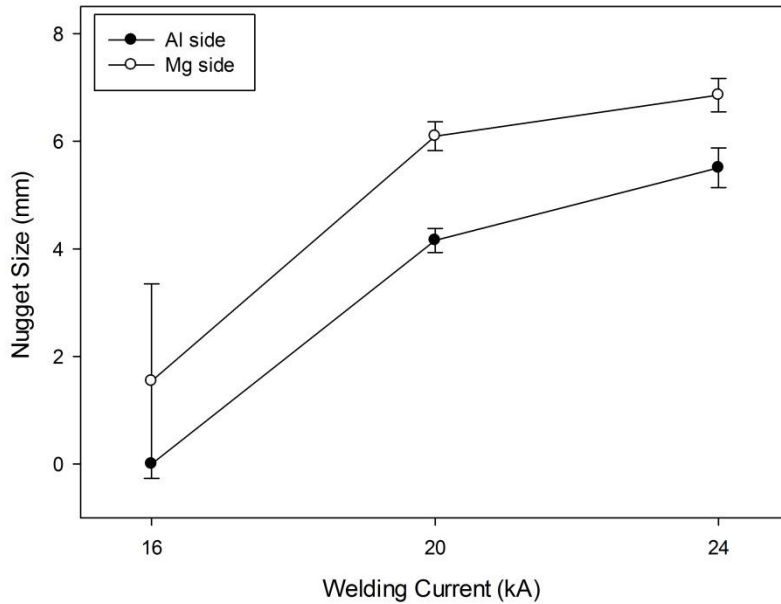
## 4.2 Experiments with Au-coated Ni Interlayer

Since no joints could be produced during RSW of Al to Mg with a bare Ni interlayer due to low heat generation in the Ni sheet, it was concluded that addition of very thin layer of a good braze material with melting point lower than that of Ni may improve metallurgical reaction at the Al/Ni and Mg/Ni interfaces. Since Au is known as a good braze metal, and it can be applied in very thin layers as commonly done by plating in microelectronics soldering, this may provide an alternative interlayer material. Literature also indicates that even solid-state bonds of Au coated Ni sheets might be stronger than the bare Ni joints with a fusion nugget [62]. Therefore, in order to improve metallurgical bonding and mechanical performance of Al/Mg dissimilar joints, experiments with Au-coated Ni were conducted. The same welding parameters as for bare Ni interlayer were used.

### 4.2.1 Mechanical Properties

The relationship between nugget size and welding current is shown on Figure 4.6. The nugget dimensions on the Mg side were always larger than that of the Al side as in case when a bare Ni interlayer was used (Figure 4.2). It was also noted that nuggets on both Al and Mg side

were smaller than in case with a bare Ni interlayer. Based on the samples made with 24kA welding current, the nugget on Al side was on average 1.1 mm (16%) smaller while nugget on Mg side was about 0.8 mm (10%) smaller than those obtained with a bare Ni interlayer. This decrease in nugget size was caused by the lack of an oxide on the Au surface and therefore lower contact resistance and heat generation at both Al/Ni and Mg/Ni interfaces.



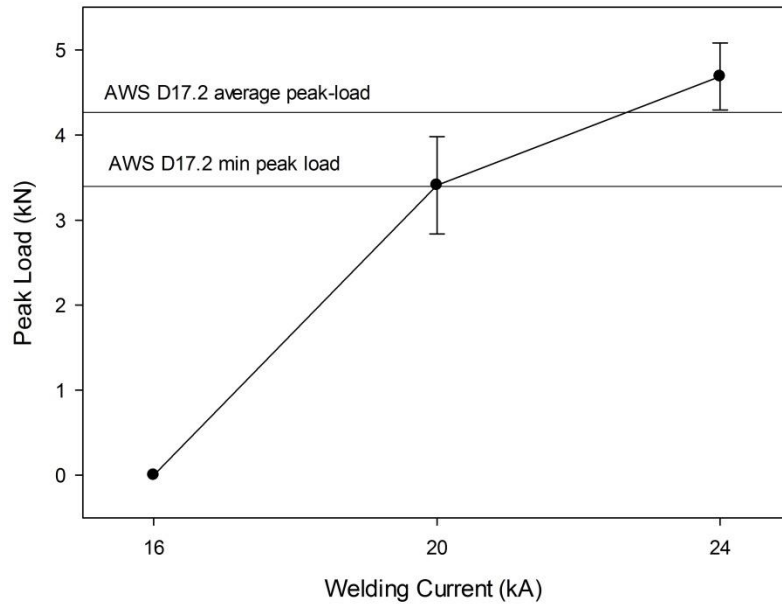
**Figure 4.6: Correlation between nugget size on both Al and Mg side and welding current during RSW with Au-coated Ni interlayer**

Figure 4.7 shows influence of welding current on peak load during tensile shear test, it can be seen that fracture loads increased with welding current. No joints were achieved with 16 kA welding current because insufficient amount of heat was generated, and joints were produced when the welding current increased to 20 or 24 kA. Although the fusion nugget was always smaller at Al side, welds made with 24 kA welding current (which was the optimal condition in the study), always failed at the Mg/Ni interface, suggesting that bonding at Al/Ni interface was stronger.

Welds made with 24 kA had an average peak load of 4.69 kN with a minimum of 4.34 kN while requirement of the AWS D17.2 standard is average of 4.27 kN with a minimum of 3.4 kN, hence the welds easily met requirement of the standard based on the ultimate strengths and sheet thickness of the base materials [20]. Furthermore the average fracture load was as high

as 90% of the strength of same size optimized AZ31B similar joints [63, 64] (based on the samples made with 24kA). Recently, Patel *et al.* [16] made an attempt to compare lap-shear strengths of Al/Mg dissimilar spot welds made by different welding techniques based on the data from the studies available in the literature [4, 16, 40, 43, 65]. The highest strength achieved was reported as 42 MPa by using an ultrasonic spot welding technique with a Sn interlayer [16]. Following the same calculation steps as employed by Patel *et al.* the lap shear strength of the welds achieved in the current study would reach 127 MPa (based on the samples made with 24kA). However as was mentioned by Patel *et al.* there was difference between studies in the thickness of the samples and in the types of Al and Mg alloys. In addition the nugget diameter for RSW and shoulder diameter for FSSW were used to calculate the respective areas for determination of lap-shear strength, which is not directly comparable.

Figure 4.8 shows the microhardness profile of Al/Mg weld made with Au-coated Ni interlayer and 24 kA welding current. It has been shown that Al-Mg intermetallic compounds have a microhardness of 200-300 HVN [4]. Since there was no apparent hardening observed at the fusion zones, it suggests that Al-Mg intermetallics did not form.



**Figure 4.7: Correlation between peak load and welding current during RSW of Al to Mg with Au-coated Ni interlayer**

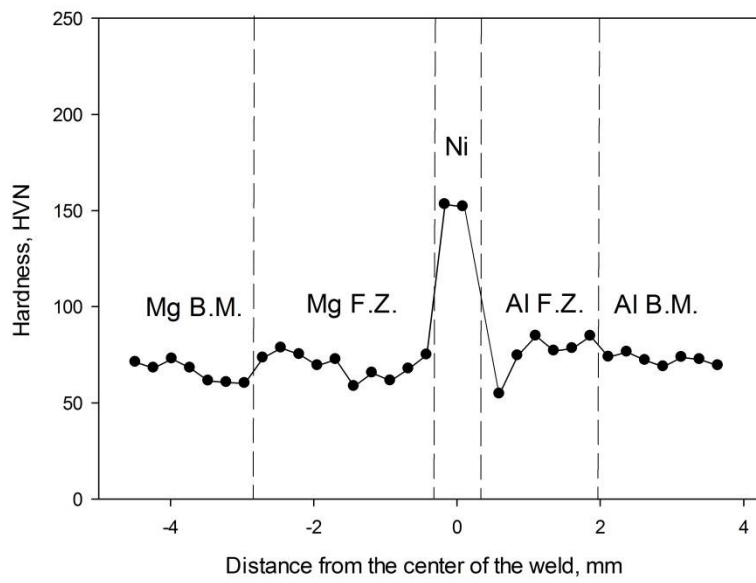


**Figure 4.8: Hardness distribution across Al/Mg weld made with Au-coated Ni interlayer and 24 kA welding current**

#### 4.2.2 Interfacial Microstructure Examination

Interfacial microstructure analysis was conducted on the samples made with 24 kA welding current. Figure 4.9 shows typical interfacial microstructure of Al/Mg joint made with Au-coated Ni interlayer. There are much more interfacial defects such as voids and pores at the Mg/Ni interface than at the Al/Ni interface. It also was noted that pores and cracks at Mg/Ni interface mostly concentrated in the center of a nugget, which is typical for RSW of Mg alloys [56, 66]. Porosity is a common defect in resistance spot welding of Mg alloys. Evaporation of Mg and hydrogen absorption are the primary mechanisms which lead to formation of the porosity [63, 67]. Some cracks are also might be observed in Al and Mg fusion zones. This was not unexpected, since solidification cracks are very common in RSW of both Al and Mg alloys [68-70]. The details of the interfacial microstructure of both interfaces are analysed in the following subsections.

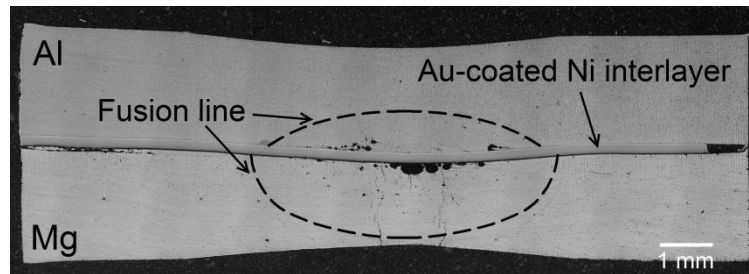


**Figure 4.9: Typical Al/Mg weld made with Au-coated Ni interlayer and 24kA welding current**

##### 4.2.2.1 Al/Ni Interface

There are three distinct zones in the Al/Ni interface such as shown on Figure 4.10. The center of the nugget was denoted as zone AI, edge of a nugget as zone AII and the region adjacent to the nugget as zone AIII. Details of the zone AI are shown on the Figure 4.11a. None of the Au coating can be found between Al and Ni in this zone (spectrum 3 in Table 4.2). As evident in Figure 4.11a, Au material was clearly dissolving into the bulk Al fusion zone and segregated along dendrite and grain boundaries (region 4 in Figure 4.11a). Microstructure of the zone AII and AIII is shown on the Figure 4.11b and Figure 4.11c respectively. In zones AII and AIII, Al was joined to the Ni by a Au-rich layer which acted as a filler metal. Microstructure of this Au rich filler metal is shown on Figure 4.11d, where the composition of this layer was roughly

the same in both zone AII and AIII – 21.3 wt.% Al, 78.7 wt.% Au. Microstructure and composition of this layer suggest that it was Au coating alloyed with Al. The only difference between zone AII and AIII is that zone AII located inside the fusion zone and zone AIII just beyond the fusion line. As can be seen on Figure 4.10, the thickness of the Au-rich layer is increasing from zone AII to the middle of zone AIII, which suggests that displacement of the Au-rich layer towards the outer diameter of the interface between Al and Ni occurred. The displacement of the Au-rich layer led to the formation of the direct contact between Al fusion zone and bare Ni surface in the center of a nugget (zone AI). In addition higher temperatures in the center of a nugget likely led to more intensive distribution of Au into the Al fusion zone in this region, which might have contributed to the depletion of Au coating in the center.

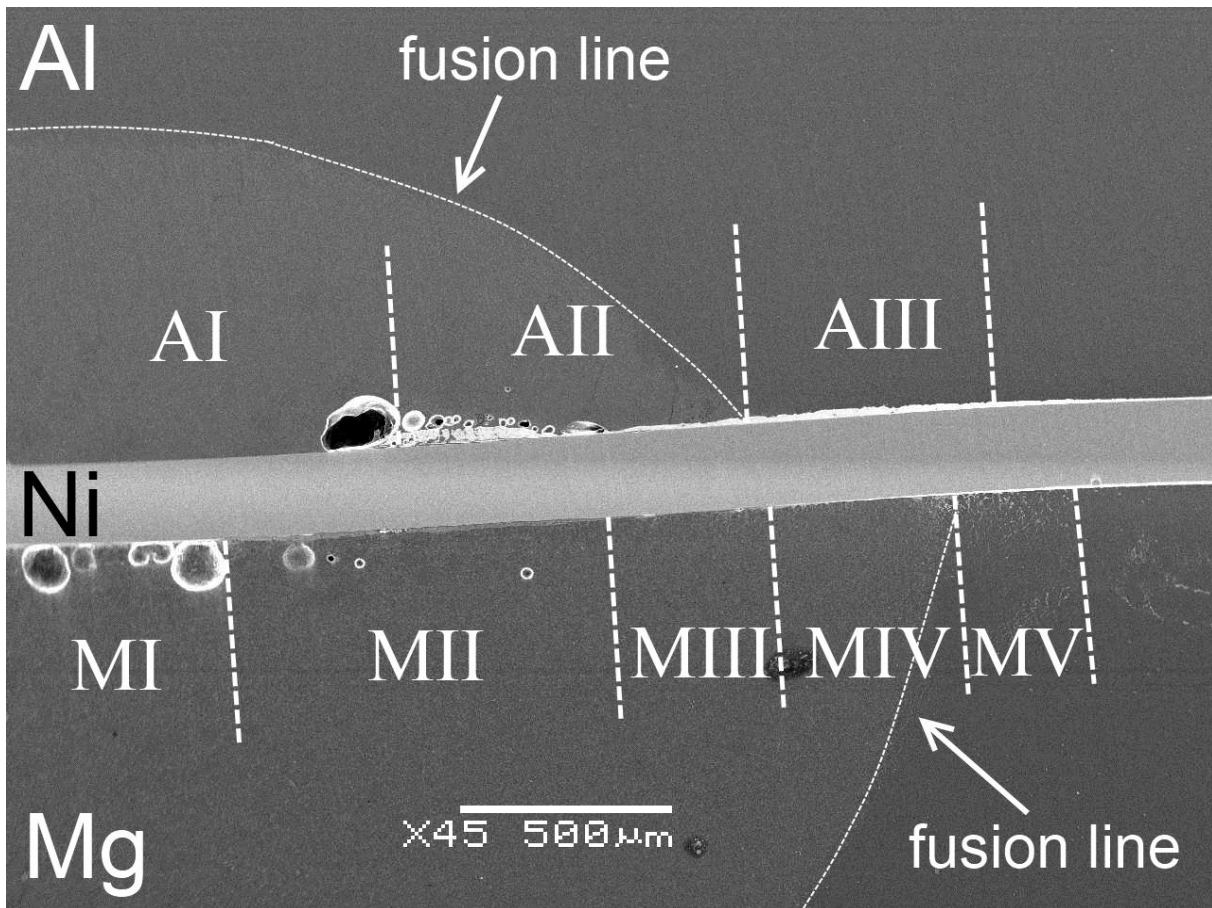


**Figure 4.10: Location of the zones which exhibit different interfacial microstructure in Al/Mg weld made with Au-coated Ni interlayer and 24kA welding current**

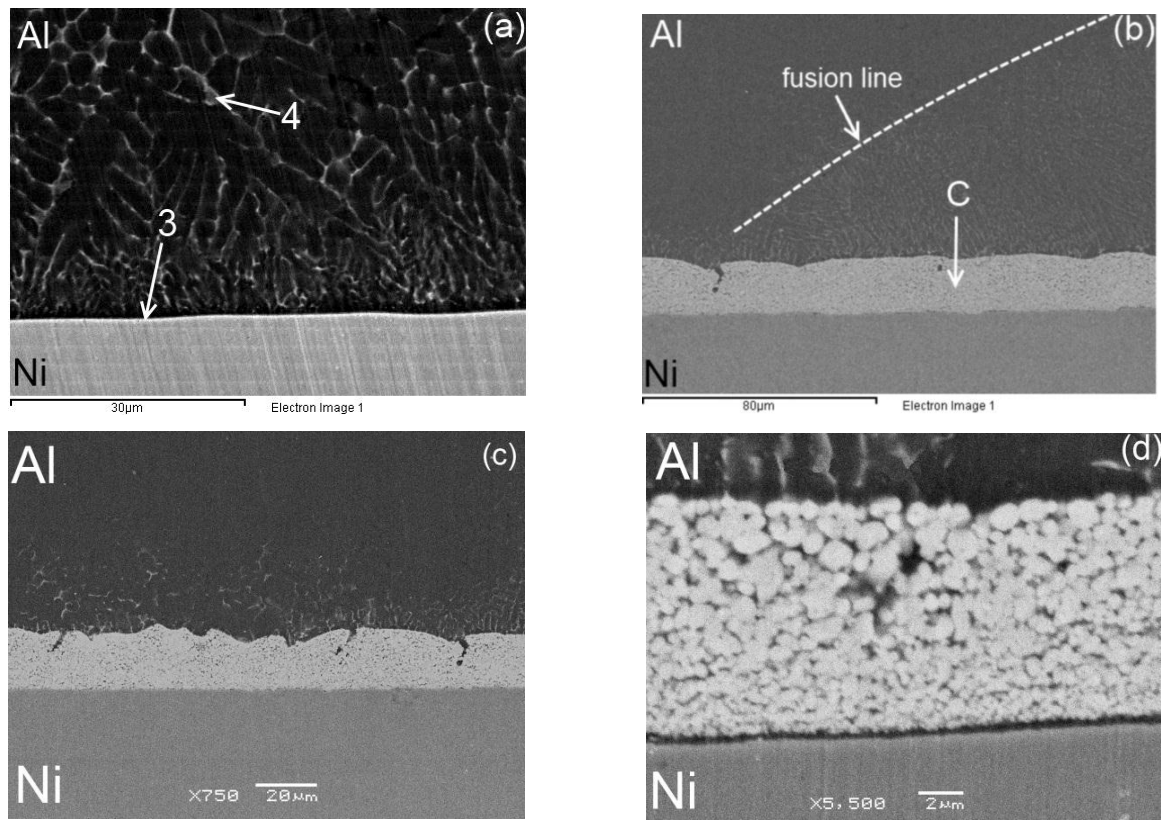


**Figure 4.11: Al/Ni interface of the weld made with Au-coated Ni interlayer and 24 kA welding current, which corresponds to interfaces noted in Figure 4.10. *a* zone Al; *b* zone All; *c* zone AlIII; *d* details of the region C from *b***

**Table 4.2: EDX quantification (in wt.%) of different areas in Figure 4.11**

Spectrum	Mg	Al	Ni	Au
3	-	20.6	79.4	-
4	3.8	82.4	-	13.8

#### 4.2.2.2 Mg/Ni Interface

Interfacial microstructure of the Mg/Ni interface is more complex than that of Al/Ni interface. Five distinct zones with different microstructure features can be observed at Mg/Ni interface. The zones were named MI, MII, MIII, MIV and MV from the center to the edge of a nugget respectively (Figure 4.10).

Microstructure of zone MI is shown on Figure 4.12a and b. Au was displaced/diffused into Mg fusion zone, in a similar manner to Al/Ni interface in the center (Figure 4.11a). However, unlike in the center of Al/Ni interface, Mg was not joined to the Ni directly. There are two different continuous and smooth Au rich layers between Mg and Ni in zone MI (region 5 and 6 in Figure 4.12a). Based on the EDX results (Table 4.3), the lighter layer (region 5 in Figure 4.12a) is the remnant of the original Au coating, while a darker and thinner Au rich layer (region 6 in Figure 4.12a), is Mg<sub>3</sub>Au intermetallic compound [42]. The formation of monolithic layer of Mg<sub>3</sub>Au intermetallic suppressed further distribution of Au coating into Mg fusion zone, and therefore significant amount of original Au coating remained undisturbed (region 5 in Figure 4.12a). Away from the continuous layer of Mg<sub>3</sub>Au compound is Mg fusion zone which was heavily enriched in Au (region 7 in Figure 4.12a). Based on the Au-Mg phase diagram (Figure 4.13), this region is likely Au-Mg eutectic structure, which consists of Mg<sub>3</sub>Au intermetallic compound and α-Mg. Numerous voids can also be found in zone MI (Figure 4.12b). The voids formed on the surface of the continuous Mg<sub>3</sub>Au layer, and likely slowed the diffusion of Au into Mg fusion zone.

In contrast with zone MI, no remnant of the Au coating layer (region 5 in Figure 4.12a) and no continuous Mg<sub>3</sub>Au layer (region 6 in Figure 4.12a) can be observed in zone MII (Figure 4.12c). Temperatures in this region were likely lower than in zone MI and therefore the Mg<sub>3</sub>Au compound did not form as continuous smooth layer leading to the more extensive diffusion of Au into Mg fusion zone. The absence of the interfacial defects also likely contributed to the intensive migration of Au into Mg. The Au-Mg eutectic structure similar to that in zone MI (region 7 in Figure 4.12a) is still present at the interface, indicating that molten Mg comes into little direct contact with Ni surface at the region.

The microstructure of the zone MIII is shown on the on Figure 4.10 and Figure 4.12d. It is similar to the zone MII, however there is much less Au in the Mg fusion zone near Ni surface and molten Mg contacts bare Ni surface in many locations.

Microstructures observed in zone MIV and MV are shown in Figure 4.12e. The remaining original Au coating appears in the beginning of zone MIV and its thickness increases approaching the nugget edge. The microstructure of the zone MIV is similar to that of zone MI, however no defects can be observed in this region, and it was not determined whether Mg<sub>3</sub>Au formed as a continuous layer as observed in zone MI (region 6 in Figure 4.12a). The amount of Mg fusion zone heavily enriched in Au in zone MIV (region 8 in Figure 4.12e) is much larger

than that in zone MIII, which suggests that squeezing of this phase from zone MIII to zone MIV may have occurred. The microstructure of zone MV is similar to that of zone MIV, however it is located beyond the fusion line. Surface melting of Au and partial melting of Mg likely occurred in the zone MV leading to microstructures similar to zone MIV.

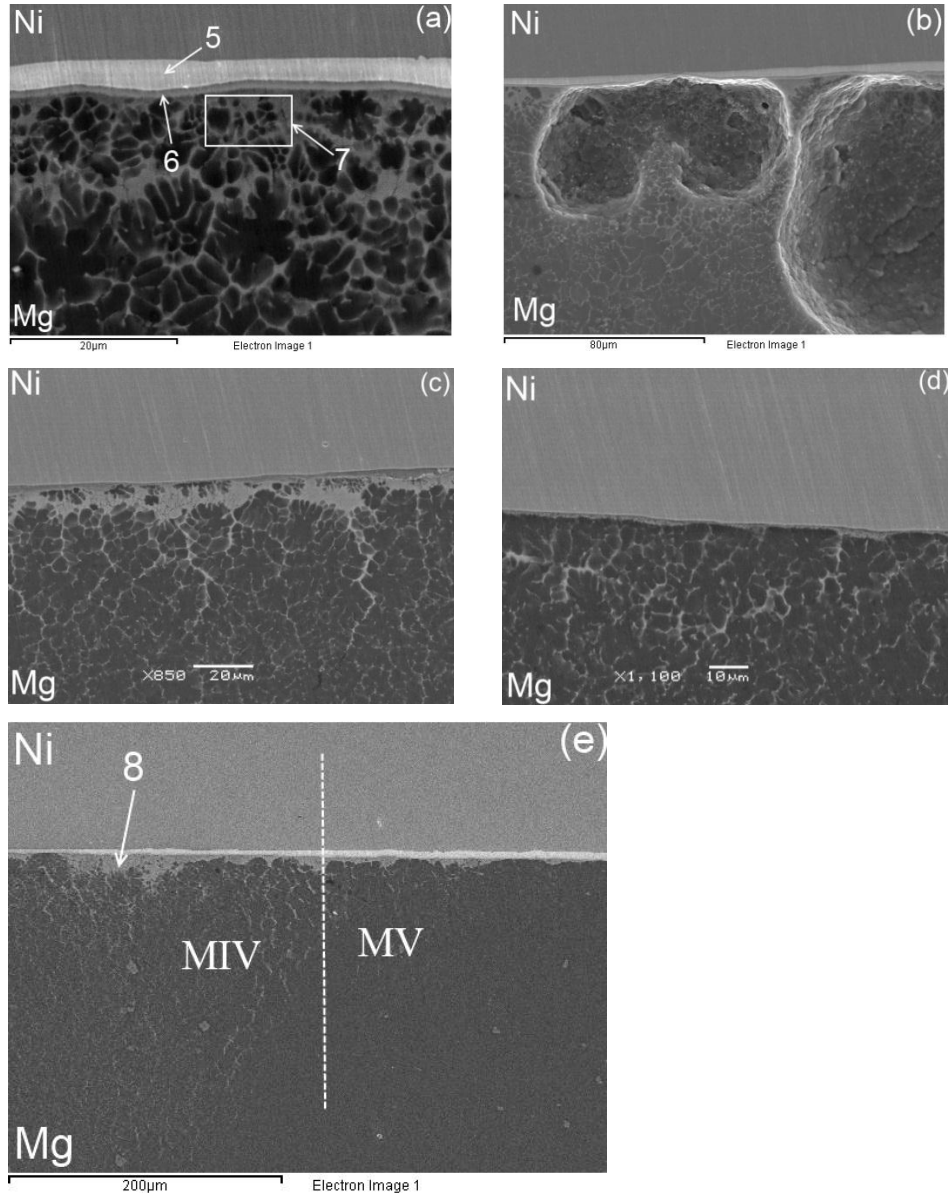


**Figure 4.12: Mg/Ni interfaces in the weld made with Au-coated Ni interlayer and 24 kA welding current, which corresponds to interfaces noted in Figure 4.10. a and b zone MI; c zone MII; d zone MIII; e zones MIV and MV**

**Table 4.3: EDX quantification (in wt.%) of different areas in Figure 4.12**

Spectrum	Mg	Al	Ni	Au
5	1.2	-	3.8	95.0
6	24.9	-	2.3	72.8
7	57.8	2.0	-	40.2
8	58.6	-	-	41.4

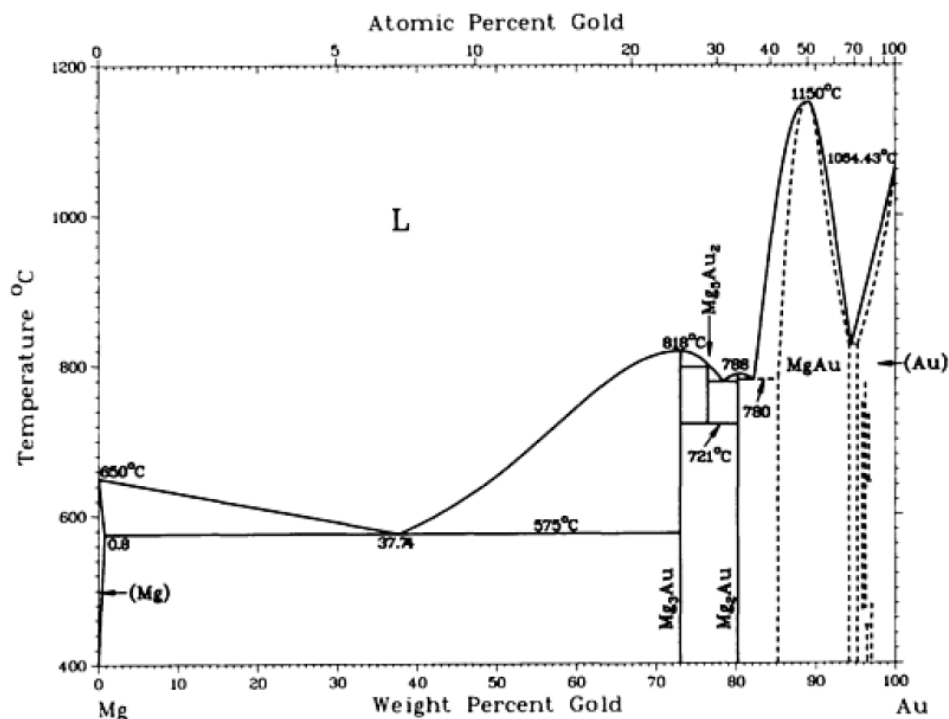


**Figure 4.13: Au-Mg binary phase diagram [42] (reprinted with permission of ASM International)**

#### 4.2.3 Fracture Surface Examination

The fracture surface morphology was analysed on the samples made with 24kA welding current, all the samples made with this conditions failed at Mg/Ni interface during the tensile shear test. The Au coated Ni interlayer was separated from Al sheet after the tensile shear test

in order to analyse fracture surface at Al side. Fracture surfaces at the Al and Mg sides were analysed separately and details of the analysis summarised in the following subsections.

#### 4.2.3.1 Al/Ni Interface

The fracture surface of the Au coated Ni interlayer at Al side is shown in Figure 4.14. Regions of the fracture surface which correspond to the interfacial microstructure zones AI, AII and AIII (Figure 4.10) are shown on Figure 4.14a.

Two regions with different morphologies and compositions can be found in zone AI, the regions marked as D and E on the Figure 4.14a. The composition (Table 4.4) and morphology of the region D (Figure 4.14b) suggests that in this region failure occurred within the Al fusion zone enriched in Au. Meanwhile in region E failure occurred at molten Al/Ni interface, since the region exhibits bare Ni surface (region 10 in Figure 4.14c) with only small amount of Al-rich particles attached to it (region 11 in Figure 4.14c). Chemical composition of the fracture surface in zone AII and AIII is 90.8 wt.% Au, 9.2 wt.% Al, which suggests that failure in this region occurred inside the Au rich phase which acted as a filler metal between Al and Ni.

Comparing these observations to the fracture morphology analysis of the sample made with bare Ni interlayer (Figure 4.3), it is clear that the addition of Au coating greatly improved metallurgical bonding at the Al/Ni interface. The major contribution of Au was that it acted as a filler metal at the edge of a nugget and at the region adjacent to a nugget (zone AII and AIII). In addition, in the center of a nugget (zone AI) failure partially occurred through Al fusion zone which suggests that this region also contributed to the strength. This can be explained by the fact that Ni surface was completely clean and oxide free under the Au coating, which promoted better wetting and bonding at the region. The same role played Zn coating during RSW of Mg to steel, where Zn was melted and squeezed to the periphery leaving clean steel surface for bonding in the center and acting as a filler metal at the periphery which led to the formation of higher strength welds [56].

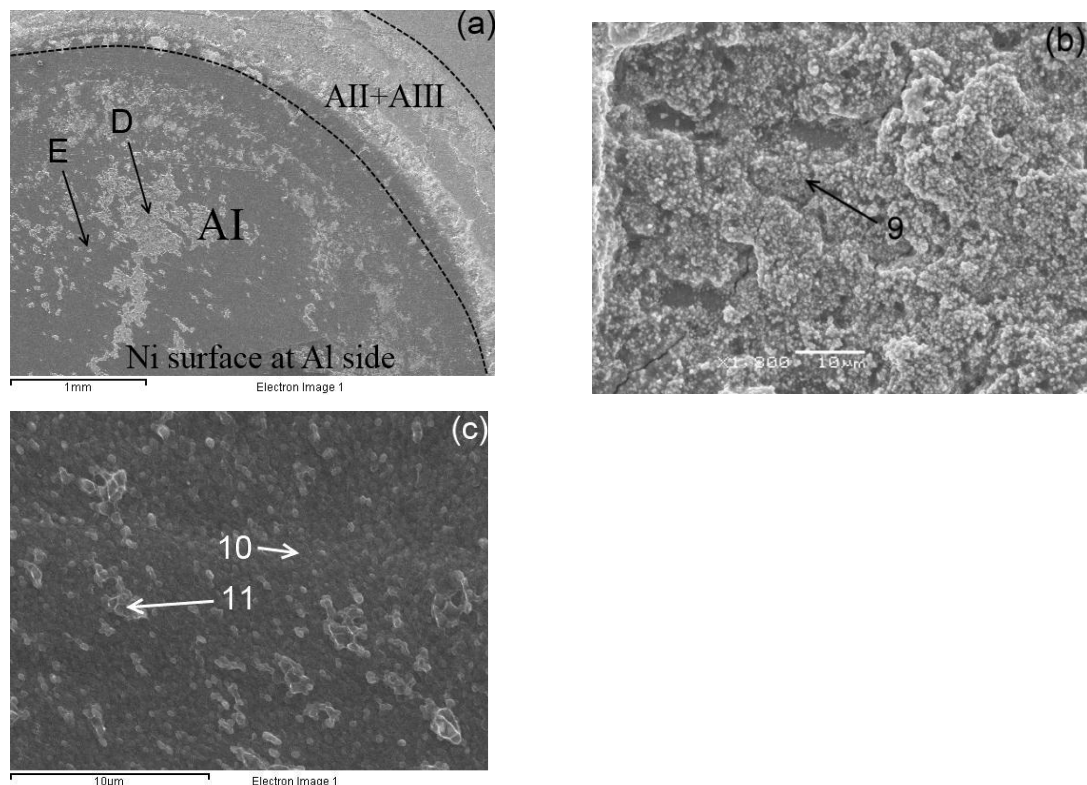


**Figure 4.14: Fracture surface of the Au coated Ni interlayer at Al side (produced in a weld made using 24 kA). a overview; b zone D from a; c details of the zone E from a**

**Table 4.4: EDX quantification (in wt.%) of different areas in Figure 4.14**

Spectrum	Al	Ni	Au
9	49.2	7.3	43.5
10	-	96.8	3.2
11	83.5	12.3	4.2

XRD analysis of the fracture surface of the Au coated Ni interlayer on Al side did not detect any Al-Ni intermetallics (Figure 4.15a). Similarly to the case with a bare Ni interlayer, possible Al-Ni intermetallics were detected by EDX (Table 4.4), however the size and amount of these phases were beyond the resolution of XRD.

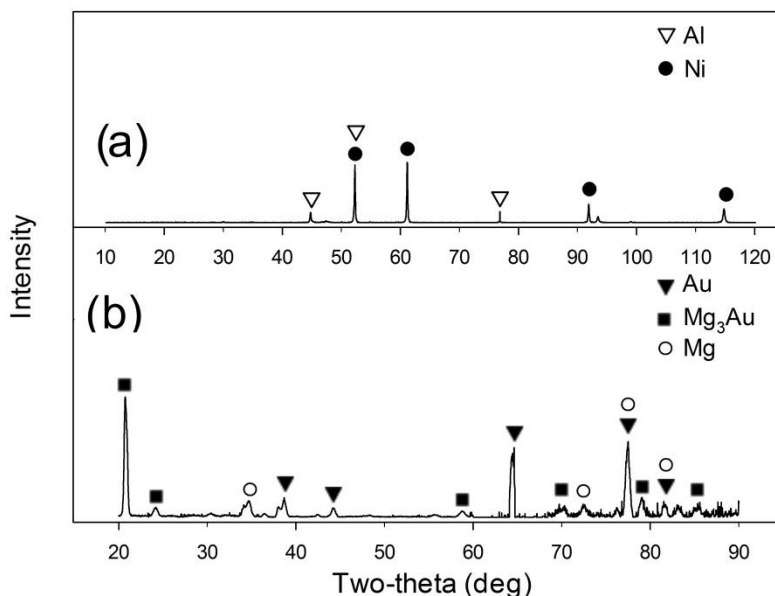


**Figure 4.15: XRD analysis of the Au-coated Ni interlayer fracture surface on both Al and Mg side. a Al side; b Mg side**

#### 4.2.3.2 Mg/Ni Interface

Figure 4.16 shows fracture surface morphology of the Au coated Ni interlayer at Mg side. Regions of the fracture surface which correspond to the interfacial microstructure zones MI - MV (Figure 4.10) are shown on the Figure 4.16a.

The morphology (Figure 4.16b) and chemical composition (Table 4.5) of zone MI suggests that failure in this region occurred inside Mg fusion zone very close to the continuous Mg<sub>3</sub>Au layer (Figure 4.12a), except locations where pores and voids were observed. A flat surface on the Mg<sub>3</sub>Au intermetallic layer can be found (region 13 in Figure 4.16b), under the voids (Figure 4.12b).

The fracture surface of zone MII exhibits a ductile morphology. Chemical composition (Table 4.5) of the region suggests that failure in this region occurred inside the Mg fusion zone at significant distance from the interface, since the amount of Au in this region (spectrum 14 in Table 4.5) is much lower than in Mg fusion zone near the interface.

The fracture morphology of zone MIII exhibits bare Ni surface (region 15 in Figure 4.16d) with Mg material only occasionally attached to it (region 16 in Figure 4.16d). This suggests that

bare Ni surface accommodated less molten Mg material than zones MI and MII where Au rich phases existed between the Ni surface and bulk of the Mg fusion zone.

Zones MIV and MV exhibited similar fracture morphologies. The composition and morphology of regions marked as MIV and MV on Figure 4.16a suggest that failure occurred along the surface of the residual Au coating which was partially melted (region 17 in Figure 4.16e).

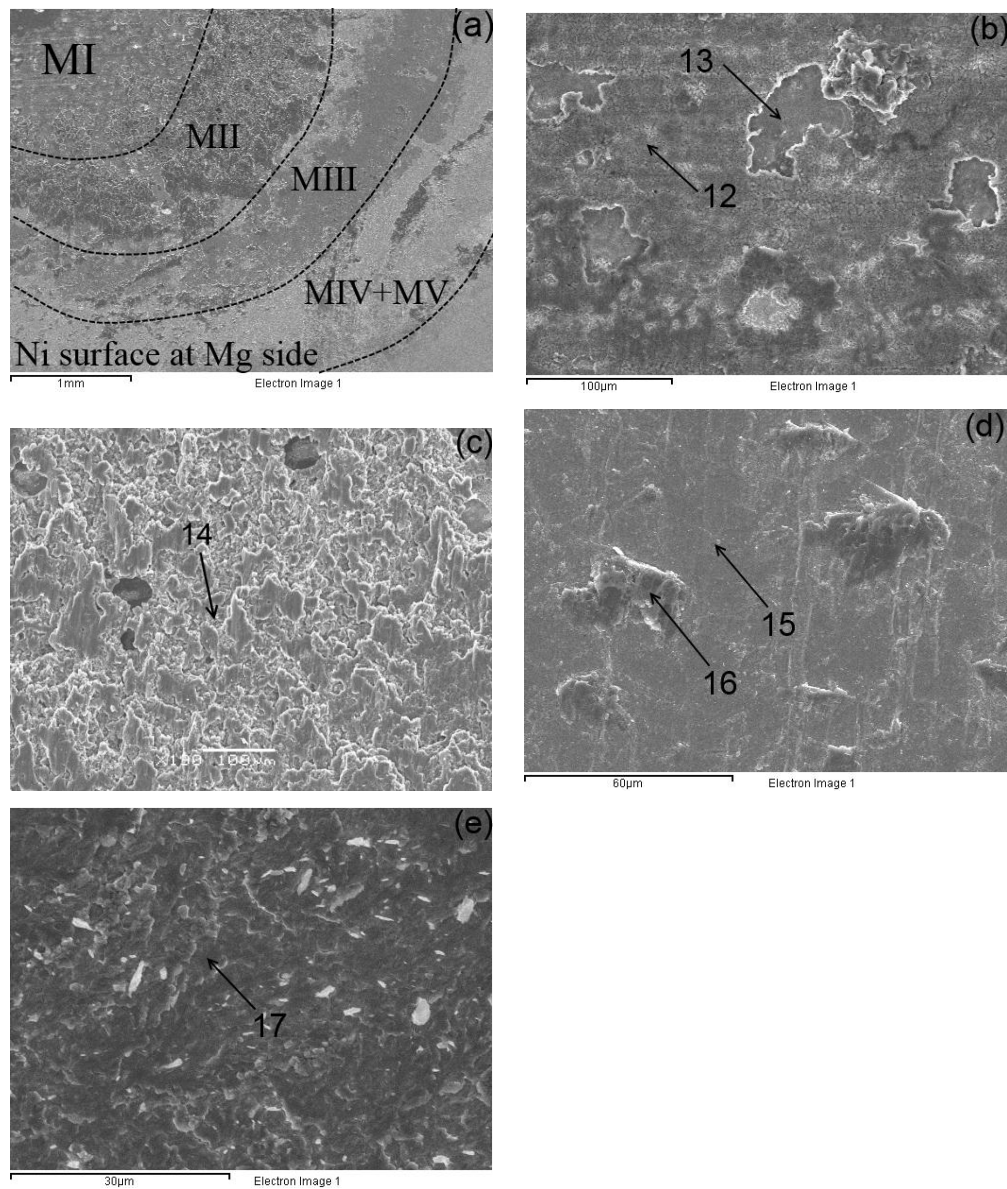


**Figure 4.16: Fracture surface of the Au coated Ni interlayer at Mg side (produced in a weld made using 24 kA). a overview; b details of zone MI from a; c details of zone MIII from a; d details of zone MIV+MV from a; e details of zones MIV and MV from a**

**Table 4.5: EDX quantification (in wt.%) of different areas in Figure 4.16**

Spectrum	Mg	Ni	Au
12	55.0	-	45.0
13	24.3	-	75.7
14	82.3	-	17.7
15	-	100.0	-
16	79.6	20.4	-
17	6.7	-	93.3

XRD analysis which was done on the fracture surfaces of the Au coated Ni interlayer at the Mg side (Figure 4.16a) indicated the presence of  $Mg_3Au$  intermetallic compound (Figure 4.16b), which supports the findings made regarding the interfacial microstructure and fracture surfaces using SEM and EDX techniques.

### 4.3 Summary

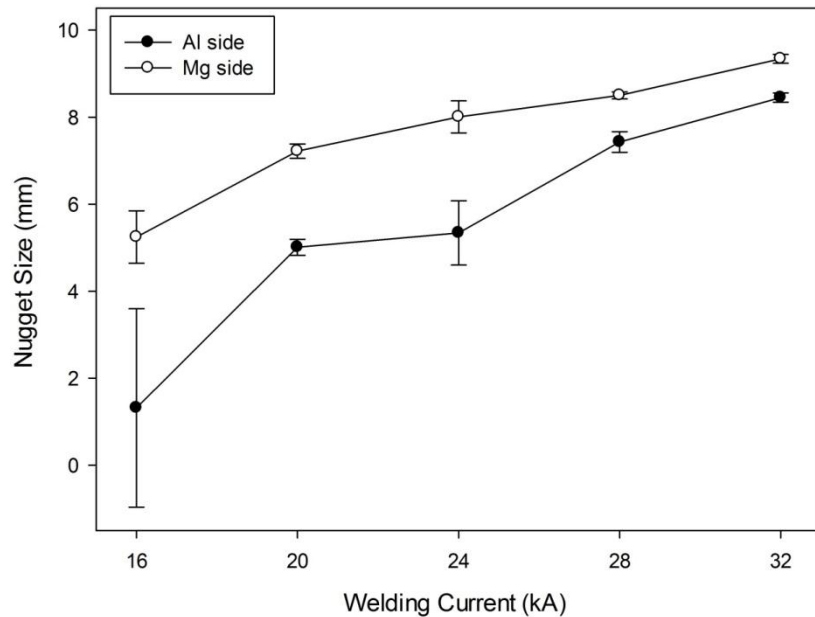
Mechanical and microstructural properties of the dissimilar Al/Mg resistance spot welds with bare and Au-coated Ni interlayers are investigated in this study. No joints were produced using a bare Ni interlayer. Therefore, experiments with Au-coated Ni interlayer were conducted. The bulk of the Ni interlayer remained intact during the welding which completely suppressed mixing of Al and Mg and formation of brittle intermetallics. Meanwhile, the addition of Au greatly improved metallurgical bonding at the interface and high strength welds were produced. A few different microstructural zones can be found at both Al and Mg side of the welds, which were characterized by differing microstructures and fractography.

## Chapter 5: Resistance Spot Welding of Al to Mg with Zn-coated Steel Interlayer

### 5.1 Experiments with Zn-coated Steel Interlayer

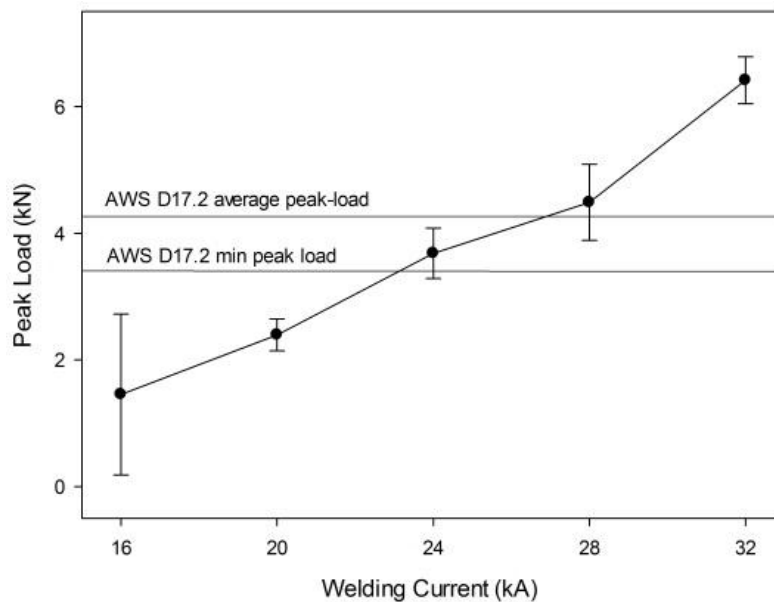
#### 5.1.1 Mechanical Properties

Figure 5.1 shows relationship between nugget size and welding current for welds made with Zn-coated steel interlayer. Nugget dimensions grew with welding current as expected during RSW. The steel interlayer was not melted during welding and nugget size was measured separately on both the Al and Mg side. It was noted that nugget on Mg side always was larger than that on Al side. Similarly to the case with Ni-based interlayers (Figure 4.2 and Figure 4.6) the decrease in nugget size was caused by lower electrical resistivity and higher thermal conductivity of Al alloy 5754 compared to Mg alloy AZ31B.



**Figure 5.1: Correlation between nugget size on both Al and Mg side and welding current during RSW with Zn-coated steel interlayer**

During tensile shear test samples made with all welding currents (16 to 32 kA) failed at Al/steel interface, suggesting that Mg/steel interface was stronger. Figure 5.2 shows relation between peak load and welding current. Welds made with welding current of 28 kA and higher easily met requirements of AWS D17.2 standard. The average peak load reached 74% of the strength of same size optimized AZ31B similar joints [63, 64]. Specific strength (peak load/nugget area) of the welds reached 94 MPa (based on the samples made with 28kA), which is lower than in the case of an Au-coated Ni interlayer (127 MPa) but still significantly higher than values calculated by Patel *et al.* [16] for Al/Mg spot welds made by different spot welding techniques [4, 16, 40, 43, 65]. Previously, 42 MPa was reported as the highest strength of Al/Mg spot welds [16]. However, as was mentioned in chapters 2.3.1 and 4.2.1, there was variation in thickness of the specimens and types of alloys employed in the studies. In addition, determination of specific strength (peak load/nugget area) is not common technique for comparison strength of the spot welds and therefore can be used only as reference.



**Figure 5.2: Correlation between peak load and welding current during RSW of Al to Mg with Zn-coated steel interlayer**

Figure 5.3 shows hardness distribution across Al/Mg weld made with Zn-coated steel interlayer and 28 kA welding current. It can be seen, that hardening did not occur neither in Mg nor in Al fusion zone, which suggests that formation of large amount of brittle intermetallics was

avoided. This was expected since steel interlayer remained solid and separated Al and Mg from mixing and intermetallic formation.

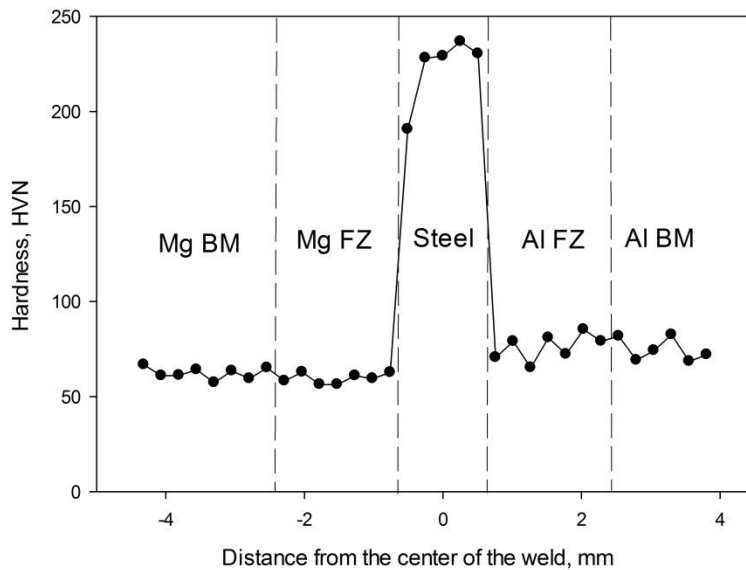


**Figure 5.3: Hardness distribution across Al/Mg weld made with Zn-coated steel interlayer and 28 kA welding current**

### 5.1.2 Interfacial Microstructure Examination

Interfacial microstructure of the welds made with 28 kA welding current was analysed in this study. Figure 5.4 shows an optical micrograph of a typical Al/Mg weld made with Zn-coated steel interlayer. It can be noted that there are much more interfacial defects such as voids and pores at Al/steel interface than at Mg/steel interface. This likely led to the failure of the welds at Al/steel interface. Details of each interface are analysed separately in the following subsections.

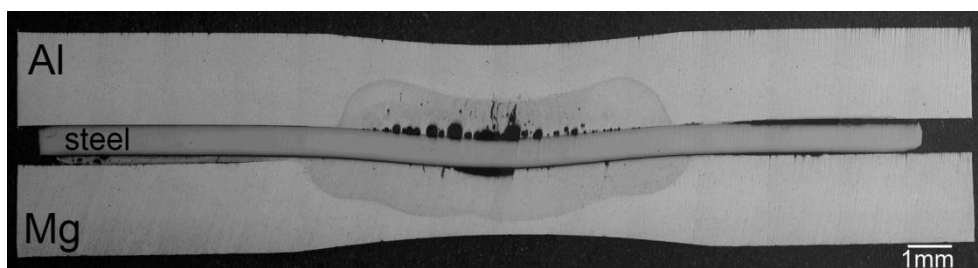


**Figure 5.4: Typical Al/Mg weld made with Zn-coated steel interlayer and 28 kA welding current**

### 5.1.2.1 Al/Steel Interface

There are three distinct zones in the Al/steel interface such as shown on the Figure 5.5. The interface inside fusion nugget was denoted as AS-I, the region adjacent to the nugget as AS-II, and region where bonding occurred through Zn-rich phase, as zone AS-III.

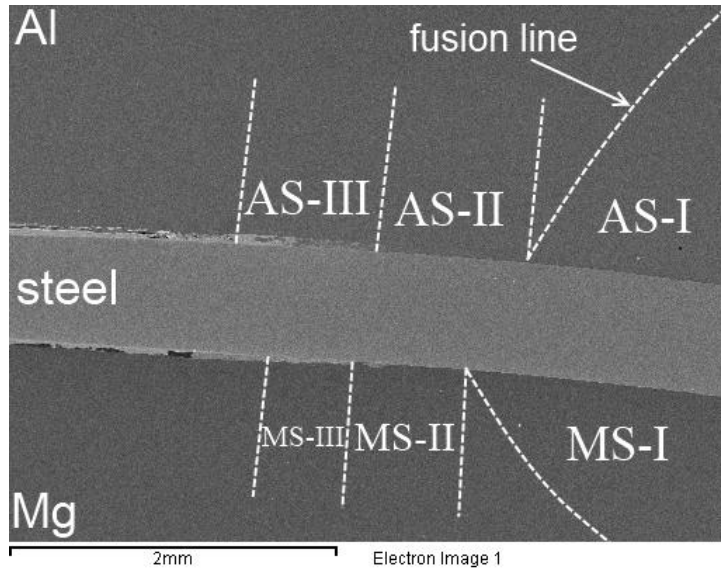


**Figure 5.5: Location of the zones which exhibit different interfacial microstructure in Al/Mg weld made with Zn-coated steel interlayer and 28 kA welding current**

Details of Al/steel interface at zone AS-I are shown on Figure 5.6. Figure 5.6a-c show center of a nugget while Figure 5.6d shows edge of zone AS-I close to the boundary with AS-II. None of the Zn coating can be found between Al and steel anywhere in the zone AS-I. Zn was likely melted and squeezed from the nugget due to low melting point of Zn ( $420^{\circ}\text{C}$ ) [60]. Microstructures of the interface at the center of the nugget and between voids (Figure 5.6b) exhibit a distinct Al-Fe reaction layer with an average thickness of  $1.3 \mu\text{m}$ . From Figure 5.6c it can be seen that voids located close to the Al-Fe reaction layer. Almost no voids were observed at the edge of a nugget, while the Al-Fe reaction layer still was present. However, the average thickness of the reaction layer at the edge of the fusion nugget was  $0.65 \mu\text{m}$  which is almost twice lower than that in the center. Therefore, it was concluded that thickness of this Fe-Al reaction layer was the highest at the center of the nugget and was gradually decreasing from

the center to the nugget's edge. Microstructural analysis suggests that the formation of Fe-Al reaction layer was the only mechanism which took place on entire area of AS-I zone.

Similar observations were made by other researchers [57-59, 71] regarding the microstructures and phases in dissimilar joints. Qiu *et al.* [57-59] also found that in dissimilar RSW of Al to steel, the thickness of the Al-Fe reaction layer (Figure 5.7c) is decreasing from the center to the edge of a nugget, such as shown on Figure 5.7b. That prior work also identified the intermetallics produced at the interface using TEM technique. Qiu *et al.* noted a 'tongue-like' morphology in the steel region side, which was identified as  $\text{Fe}_2\text{Al}_5$  intermetallic compound, while fine needle-like morphology at Al side was identified as  $\text{FeAl}_3$  as shown in Figure 5.7a. The same intermetallic compounds with similar shape were also observed by Bouche *et al.* [71] when studying the reaction layer between molten Al and solid Fe (Figure 5.8). Based on the distinct shape of  $\text{Fe}_2\text{Al}_5$  and  $\text{FeAl}_3$  intermetallic compounds and chemical composition analysis (Table 5.1), it was concluded that reaction layer observed in the current study also consists of  $\text{Fe}_2\text{Al}_5$  (region 18 in Figure 5.6b) and  $\text{FeAl}_3$  (region 19 in Figure 5.6b). The presence of such a reaction layer should not severely deteriorate the strength of the joints since cracks were not observed, and the maximum thickness of intermetallics did not exceed 1.3  $\mu\text{m}$ . It was reported by Qiu *et al.* [59] that only Al-Fe reaction layers thicker than 1.5  $\mu\text{m}$  can negatively influence the strength.

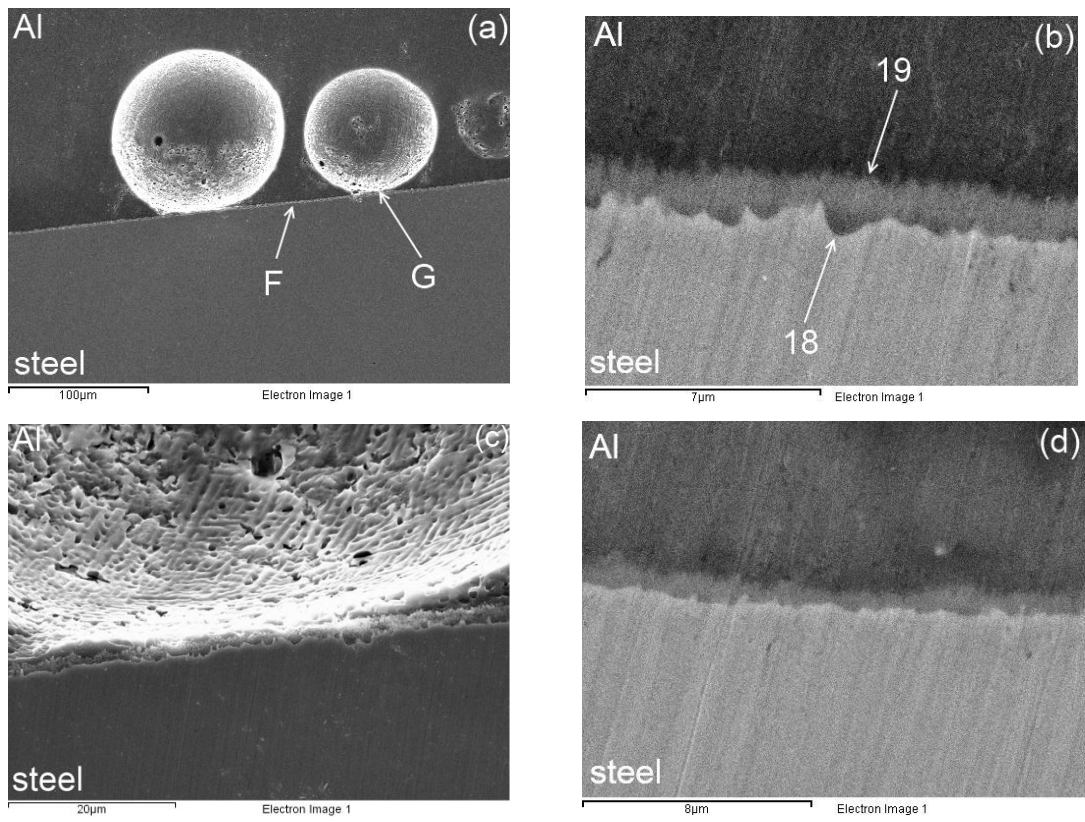


**Figure 5.6: Al/steel interface of zone AS-I from Figure 5.5. a center of AS-I; b details of F from a; c details of G from a; d zone AS-I close to the boundary with AS-II**

**Table 5.1: EDX quantification (in wt.%) of different areas in Figure 5.6**

Spectrum	Al	Fe	Mg	Zn
18	42.4	57.6	-	-
19	60.6	36.0	3.4	-

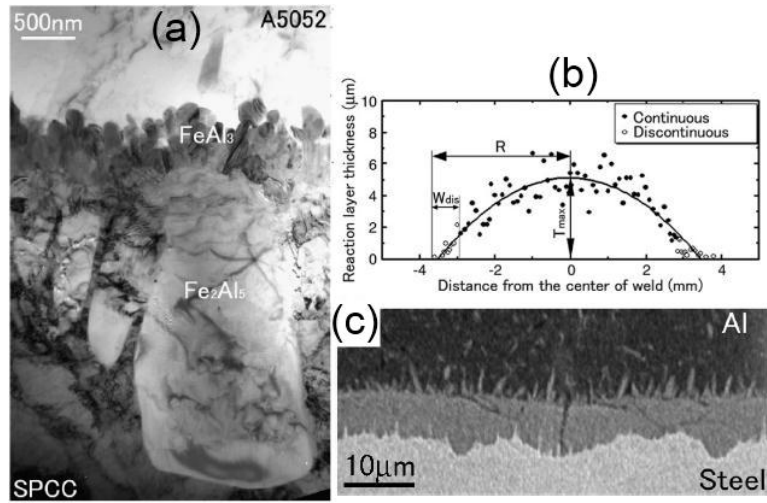


**Figure 5.7: Characterisation of interfacial microstructure of Al/steel RSW joint by Qiu et al. [57].** **a** bright field image of the reaction layer; **b** distribution chart of the reaction layer thickness at the welding interface; **c** SEM images of the weld cross section at the Al/steel interface

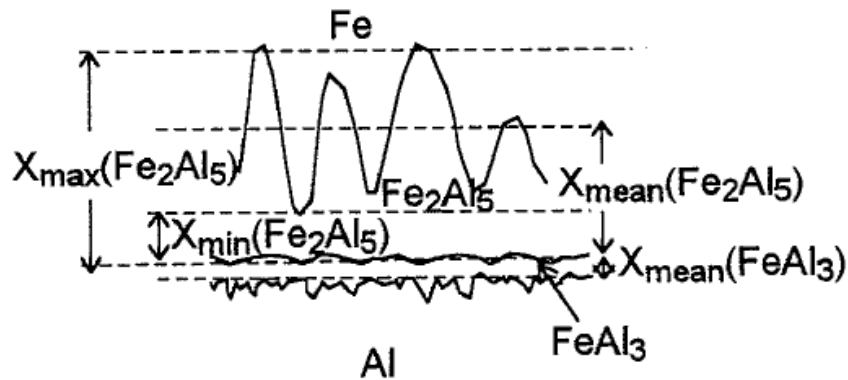


**Figure 5.8: Schematic representation of the phases formed at the interface between molten Al and solid Fe [71]**

Figure 5.9a shows the Al/steel interface at the region adjacent to the nugget (which was marked as AS-II in Figure 5.5). The region located outside the fusion zone (see Figure 5.5), indicated that some surface melting or partial melting of Al could occur in this region. Some discontinuous Al-Fe reaction products can be also observed at the interface. None of the Zn

coating layer can be found at this region, suggesting that Zn was squeezed further to zone AS-III and beyond.

Figure 5.9b shows Al/steel interface at the zone AS-III. It can be seen that a significant reaction occurred between Zn coating and Al sheet in the region. The Zn-Al reaction layer in the region was approximately 50  $\mu\text{m}$  thick which is 5 times larger than thickness of the original Zn coating. Zn likely was squeezed from the fusion nugget (zone AS-I) towards the outer nugget region (zone AS-II) and to the zone AS-III where it reacted with Al. Microstructure of the Zn-Al reaction layer suggests that it was formed by interdiffusion process. Bonding in the region occurred through this Zn-Al phase which acted as a filler metal.

Figure 5.9c shows region beyond zone AS-III. A thick layer of Zn-rich phase (labeled as region 22 in Figure 5.9c) was observed, and part of the original Zn coating was intact (region 23 in Figure 5.9c) in this zone. The Zn-rich phase observed in the region was likely squeezed from zones AS-I, AS-II and AS-III. The microstructure of this region suggests that temperatures were not high enough to let the Zn-rich phase bond to the original Zn-coating. Therefore, no bonding occurred in the region.

Overall, the interfacial microstructure of the Al/steel interface suggests that bonding occurred between Al and steel in zones AS-I, AS-II and AS-III marked on Figure 5.5, while no bonding occurred beyond zone AS-III. Similar observations were made by Liu *et al.* [56] during resistance spot welding of Mg to Zn-coated steel. They previously reported that Zn was melted and squeezed from the fusion nugget, leading to direct welding brazing in the fusion nugget area, solid state bonding at the region adjacent to the nugget and soldering through Zn-rich filler metal next to the solid state bonding region.

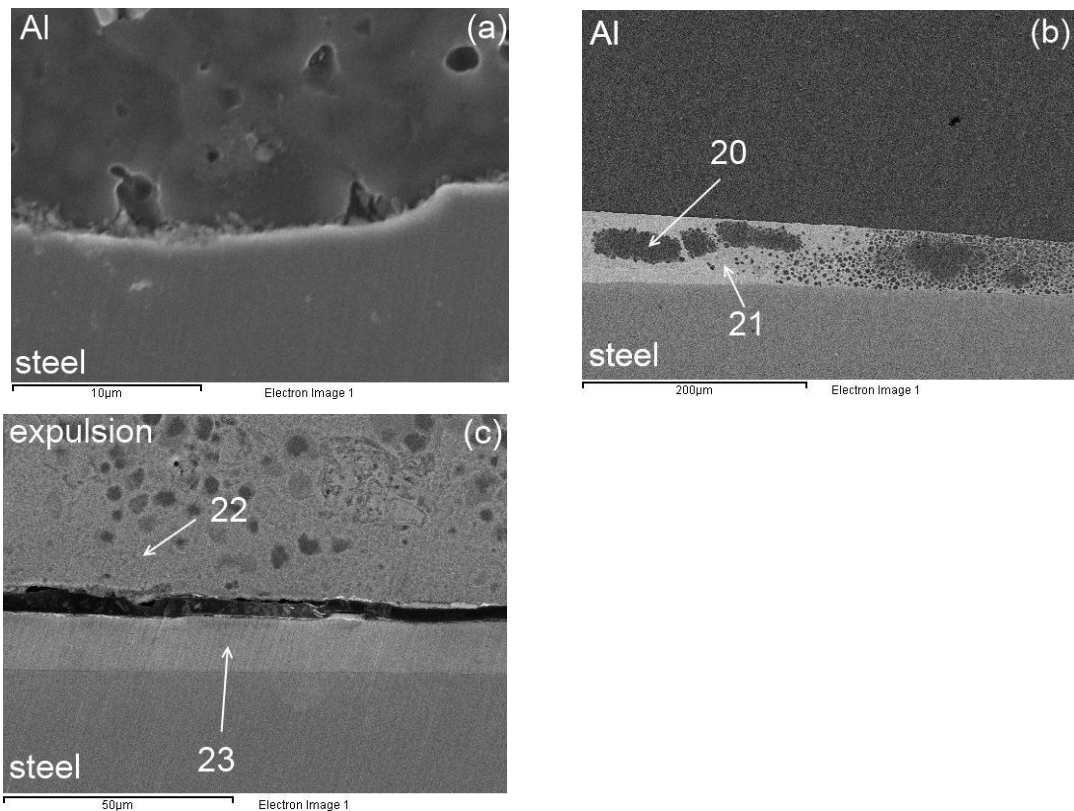


**Figure 5.9: Al/steel interface beyond the fusion nugget, which corresponds to interfaces noted in Figure 5.5. a zone AS-II; b zone AS-III; c region beyond AS-III**

**Table 5.2: EDX quantification (in wt.%) of different areas in Figure 5.9**

Spectrum	Al	Zn
20	100	-
21	25.5	74.5
22	25.8	74.3
23	-	100

#### 5.1.2.2 Mg/Steel Interface

There are three different microstructural zones in the Mg/steel interface. Similarly to Al/steel interface, region inside the fusion nugget was marked as MS-I, the region adjacent to

the nugget as MS-II, and region beyond MS-II where bonding occurred through Zn-rich phase, as zone MS-III. Figure 5.10 shows details of zone MS-I in the center, similar to the Al/steel interface where no Zn was found in the microstructure, suggesting that displacement of Zn to regions adjacent to the nugget occurred. From the element distribution map (Figure 5.10b), it can be seen that ultra-thin Fe-Al layer observed between Zn-coating and steel before welding (Figure 3.1) is still present at the interface. This observation corresponds to the findings made by Liu *et al.* [55] regarding RSW of Mg to Zn-coated steel. In experiments conducted by Liu *et al.* [55] the ultra-thin Fe-Al layer also remained intact during the welding. Author also found that this layer plays a crucial role in formation of the joint. It is known fact that Fe and Mg are virtually immiscible, however both elements can form high strength joint with nanoscale  $\text{Fe}_2\text{Al}_5$  layer due to edge to edge crystallographic planes matching. Since, similar ultra-thin layer of  $\text{Fe}_2\text{Al}_5$  compound exists in all hot-dip galvanised steels [52] it can be concluded that exactly the same or similar bonding mechanism as was observed by Liu *et al.* [55], took place in the current study. In addition Tan *et al.* [72, 73] reported that during laser welding brazing of Mg to Zn-coated steel, direct contact between molten AZ31B alloy and steel surface under Zn coating may result in growth of pre-existing layer of  $\text{Fe}_2\text{Al}_5$  due to diffusion of Al atoms from molten AZ31B alloy to the Fe-Al compound layer.

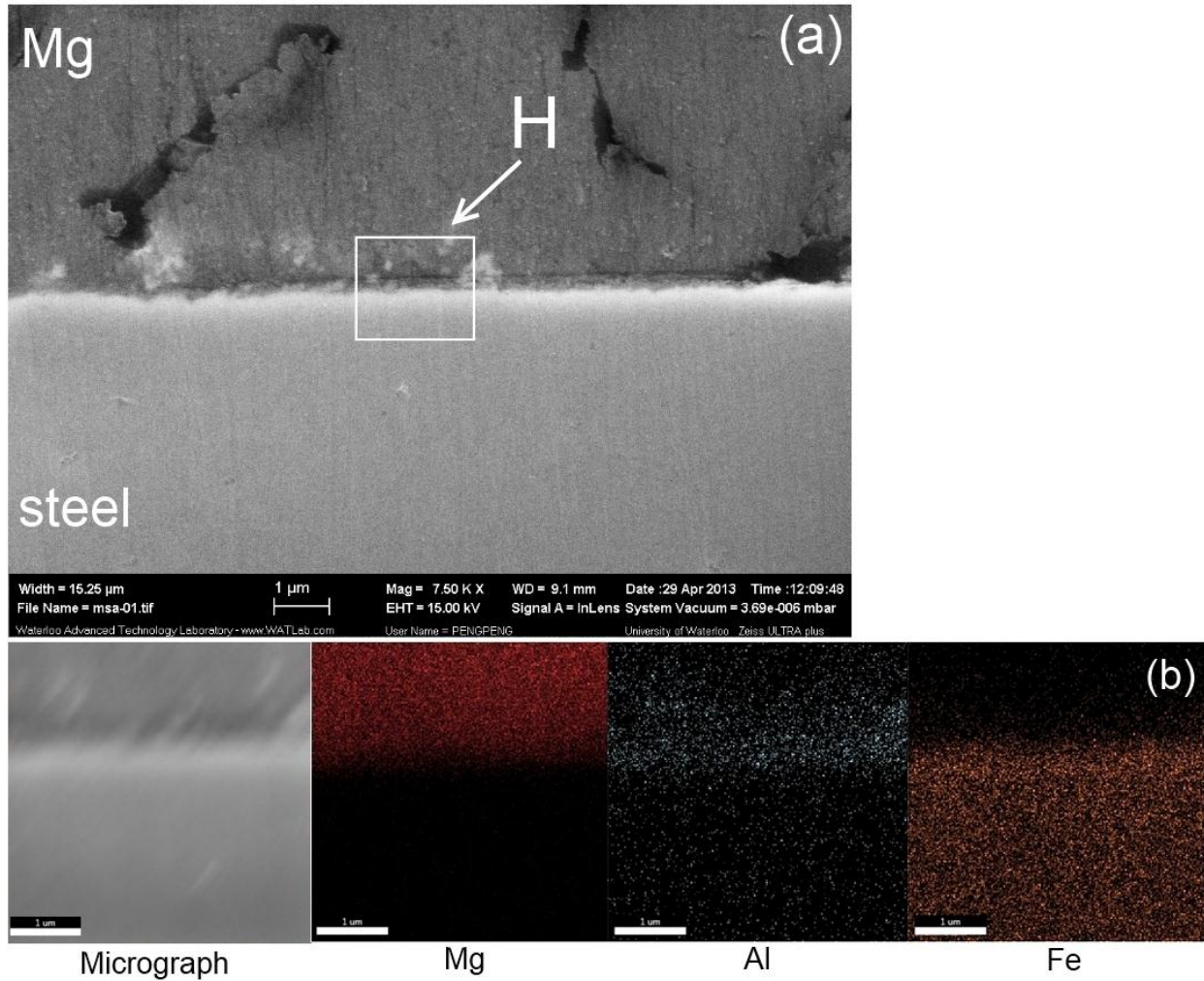


**Figure 5.10: Center of Mg/steel interface of the weld made with Zn-coated steel interlayer and 28 kA welding current. a SEM micrograph; b element distribution map of region H from a**

Figure 5.11 shows Mg/steel interface at the region adjacent to the fusion nugget. None of the Zn can be found at the zone MS-II close to the fusion nugget (Figure 5.11b), while some accumulations of Zn-rich phase can be found at the edge of zone MS-II close to the boundary with zone MS-III, such as shown on Figure 5.11a. Microstructure (Figure 5.11c) and chemical composition (spectrum 26 in Table 5.3) of these accumulations suggest that this is Mg-Zn

eutectic with a fine lamellar structure. The Zn also was dispersed into the Mg fusion zone in regions surrounding Zn accumulations in MS-II (Figure 5.11d). Despite the fact that zone MS-II located outside the fusion zone (Figure 5.5), it is possible that partial melting of Mg sheet still occurred at this region leading to formation of the Mg-Zn eutectic. The nanoscale  $\text{Fe}_2\text{Al}_5$  layer observed at the center of a nugget should also be present at the interface of zone MS-II. Only 5.3 wt.% Al was found at the interface between steel and Mg (spectrum 25 in Table 5.3), likely due to the limited resolution of EDX, since  $\text{Fe}_2\text{Al}_5$  intermetallic compound has about 55 wt.% Al. As was reported by Liu *et al.* [55, 56], even without melting, strong bonding between Mg and steel can occur in the region adjacent to the nugget due to an ultra-thin  $\text{Fe}_2\text{Al}_5$  layer. Formation of a similar Mg-Zn eutectic with fine lamellar structure also was observed during laser welding brazing of Mg to Zn-coated steel studied by Tan *et al.* [72, 73]. They reported that bonding between AZ31B Mg alloy and Fe-Al thin intermetallic layer can produce high strength joints while bonding between Mg-Zn eutectic structure and Fe-Al ultra-thin layer results in poorer bonding. Therefore, it is likely that regions where Mg-Zn eutectic was observed in zone MS-II (Figure 5.11c) in the current study will contribute to the strength less than rest of zone MS-II (Figure 5.11b).

Microstructures produced in zone MS-III can be seen on Figure 5.11a. In this region steel was bonded to Mg through Zn-rich filler metal, which marked 24 on Figure 5.11a. A Zn-rich phase which acted as a solder metal was squeezed to the zone MS-III from zones MS-I and MS-II. A similar phenomenon was observed by Liu *et al.* [56], during RSW of Mg to steel, where the Zn coating was melted and completely squeezed from the nugget towards surrounding regions where it played the role of a brazing material, which contributed to overall bonding area and increased fracture strength.

Figure 5.11e shows the Mg/steel interface beyond MS-III zone. A significant amount of squeezed Zn phase (region 28 in Figure 5.11) and intact original Zn-coating (region 29 in Figure 5.4) can be observed in the region. The presence of a high amount of Mg in the squeezed Zn-rich phase (spectrum 28 in Table 5.3) suggests that Zn first reacted with Mg and then was squeezed out of the nugget. It is likely some amount of this Zn-rich phase, was not completely squeezed which resulted in the formation of Mg-Zn eutectic in some areas in zone MS-II (Figure 5.11c). The microstructure suggests that no bonding occurred in the region, since the original Zn-coating remained intact.

Overall, interfacial microstructure suggests that some bonding occurred between Mg and steel in the zones MS-I, MS-II and MS-III marked on Figure 5.5, while no bonding occurred beyond zone MS-III. These observations are in a good agreement with studies conducted by Liu *et al.* [55, 56] on RSW of Mg to Zn-coated steel.

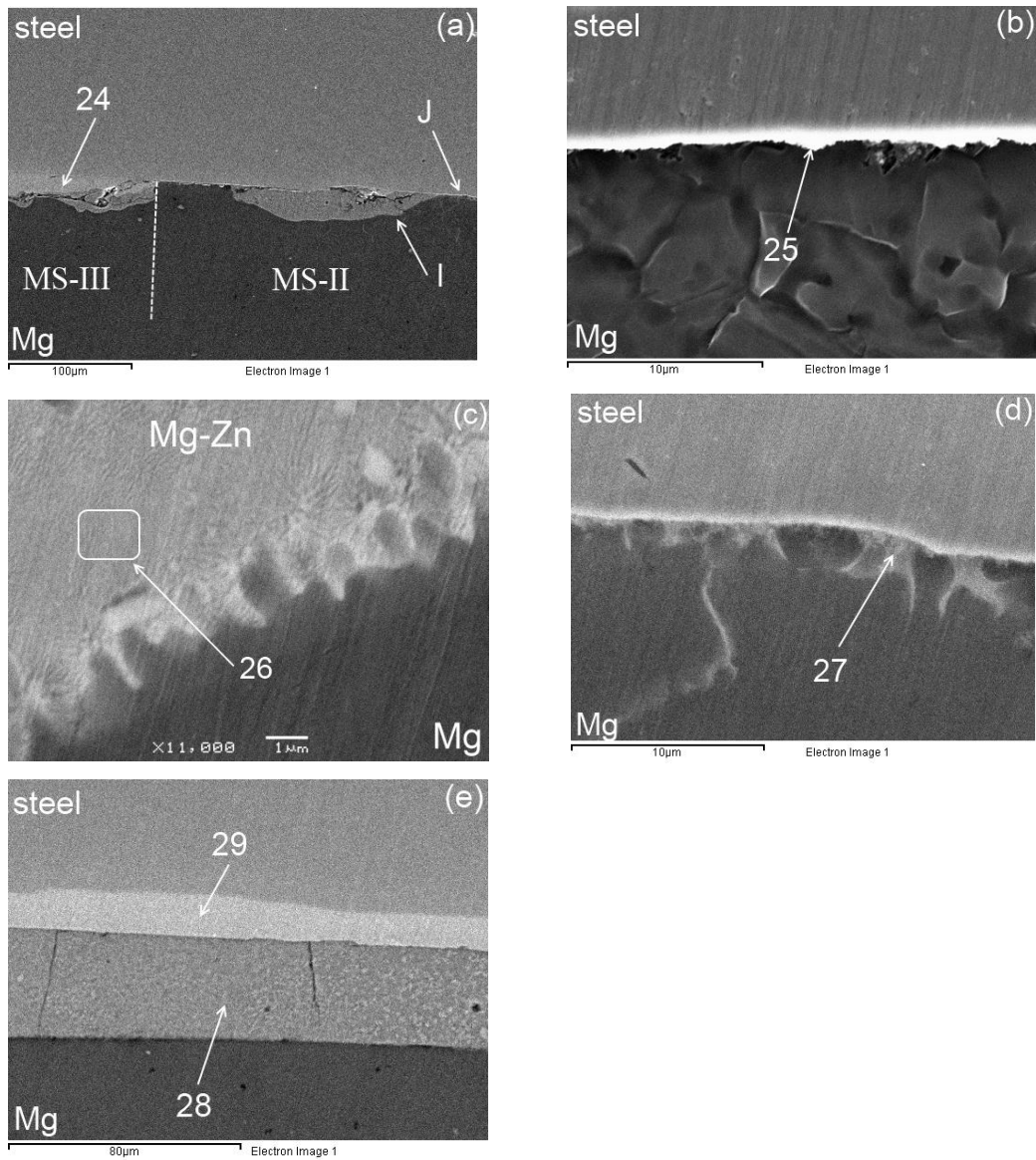


**Figure 5.11 – Mg/steel interface beyond the fusion zone. a zones MS-II and MS-III; b zone MS-II close to the fusion nugget; c details of I from a; d details of J from a; e region beyond zone MS-III**

**Table 5.3: EDX quantification (in wt.%) of different areas in Figure 5.11**

Spectrum	Al	Fe	Mg	Zn
24	-	-	17.3	82.7
25	5.3	52.6	42.1	-
26	-	-	45.4	54.6
27	-	8.4	65.5	26.1
28	-	-	45.2	54.8
29	-	-	-	100

### 5.1.3 Fracture Surface Examination

Aside from the interfacial microstructure, the fracture surface morphology of both Al/steel and Mg/steel interface was analysed on the samples made with 28kA welding current. As was mentioned in section 5.1.1, during tensile shear test all welds made with Zn-coated steel interlayer failed at Al/steel interface. Therefore, in order to analyse fracture surface on Mg side, steel interlayer was separated from Mg sheet after the tensile shear test. Fracture surfaces at the Al and Mg sides were analysed separately and details of the analysis summarised in the following subsections.

#### 5.1.3.1 Al/Steel Interface

Figure 5.12 shows the fracture surface of the Zn-coated steel interlayer at Al side. Regions of the fracture surface which correspond to the interfacial microstructure zones AS-I, AS-II and AS-III (Figure 5.5) are shown on Figure 5.12a.

It can be seen from Figure 5.12b that in the center of zone AS-I failure occurred inside Al fusion zone close to the interface since pores which concentrated near the interface can be observed on the fracture surface (region 30 in Figure 5.12b). An Fe-Al intermetallic compound layer with a flat surface can be found under the voids, and ductile fracture surfaces corresponding to the Al alloy fusion zone can be found between the voids (region 31 in Figure 5.12b), which suggest that porosity negatively influenced strength of the joints. Figure 5.12c shows edge of AS-I zone (region M in Figure 5.12a). The fracture morphology of this region is similar to that of the center of zone AS-I, but size of the voids at this region are considerably

smaller than in the center. A few river-like voids (region 32 in Figure 5.12c) can be observed in the region. Usually these river-like voids form as a result of accumulation of smaller voids [62], and this appears to be the same phenomenon in the current study.

The fracture morphology of zone AS-II shown in Figure 5.12d which was adjacent to the nugget, and appears to be where solid state bonding between Al and steel occurred (Figure 5.9a). The surface morphology of the region suggests that fracture occurred either at Al/steel interface (region 33 in Figure 5.12d) either inside Al sheet (region 34 in Figure 5.12d).

Figure 5.12e shows fracture surface of zone AS-III where Al-Zn reaction layer was observed (Figure 5.9b). The fracture morphology and chemical composition (Table 5.4) of the region suggest that failure occurred partially inside Al sheet (region 35 in Figure 5.12e) and partially inside Al-Zn reaction layer (region 36 in Figure 5.12e). Based on the fracture morphology and interfacial microstructure analysis (Figure 5.9b) it can be concluded that bonding in this region was promoted by the presence of Zn which contributed to the strength.

Figure 5.12f shows region adjacent to the zone AS-III, where significant expulsion of Zn-rich phase occurred. Composition of this region corresponds to the composition of the expulsion observed at the interfacial microstructure of the region (Figure 5.9c). This region exhibits a flat fracture morphology and therefore did not contribute to bonding in the region.

Overall the fracture surface morphology and interfacial microstructure of Al/steel interface suggests that zones AS-I, AS-II and AS-III contributed to the strength, while regions beyond AS-III (Figure 5.12f) did not. The joining occurred by direct welding brazing in zone AS-I, by solid state bonding in zone AS-II, by brazing through Zn filler metal in zone AS-III.

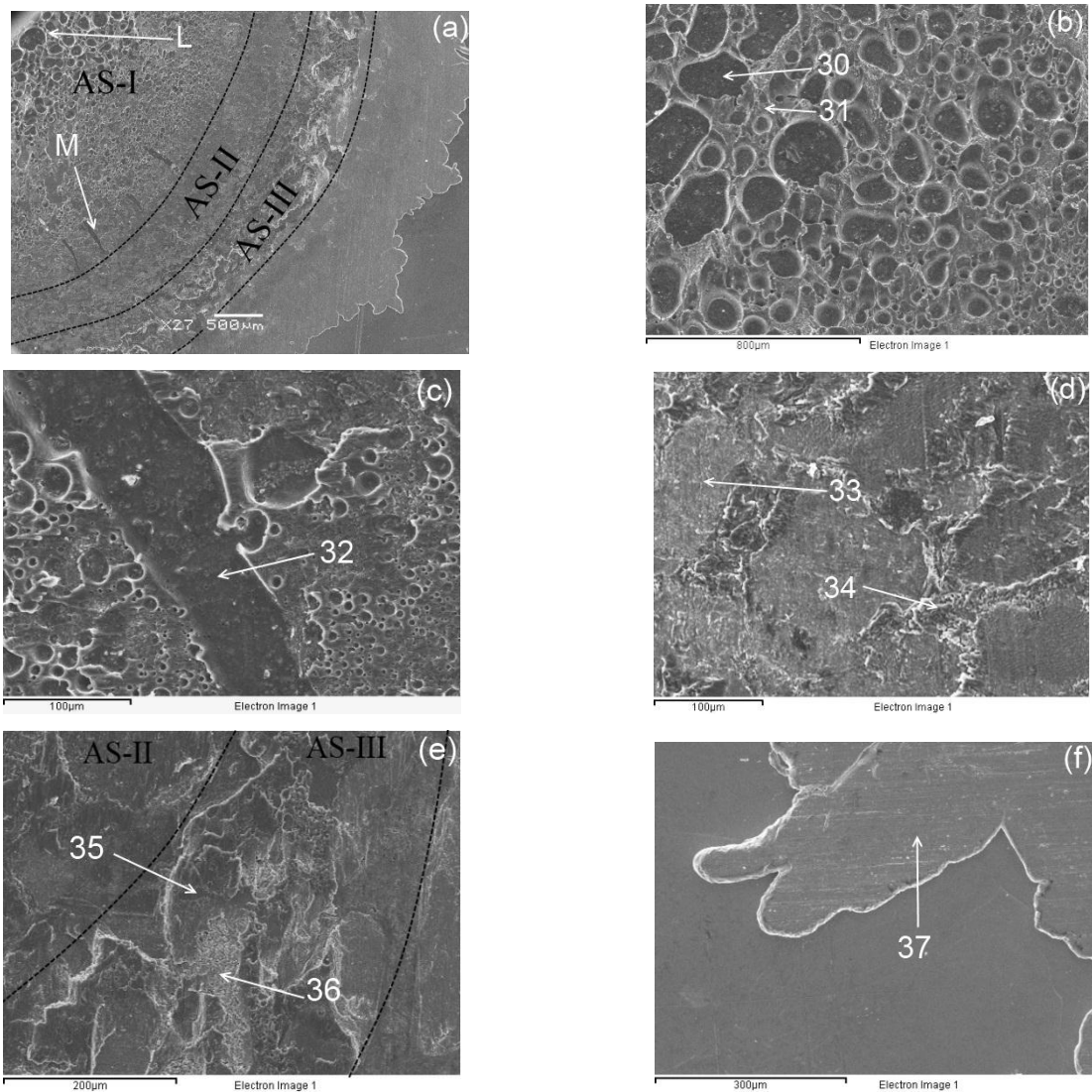


**Figure 5.12 - Fracture surface of the Zn-coated steel interlayer at Al side (produced in a weld made using 28 kA). a overview; b details of region L from a; c details of region M from a; d details of zone AS-II from a; e details of zone AS-III from a; f region beyond zone AS-III**

**Table 5.4: EDX quantification (in wt.%) of different areas in Figure 5.12**

Spectrum	Al	Fe	Mg	Zn
30	53.6	46.4	-	-
31	97.4	-	2.6	-
32	67.0	30.9	2.1	-
33	42.6	57.4	-	-
34	94.8	2.8	2.4	-
35	96.8	-	3.2	-
36	36.2	-	-	63.8
37	25.9	-	-	74.1

XRD analysis which was done on the fracture surfaces of the Zn coated steel interlayer at Al side (Figure 5.13) detected  $\text{Fe}_2\text{Al}_5\text{Zn}_{0.4}$  intermetallic compound. However, no phases which might correspond to  $\text{Fe}_2\text{Al}_5\text{Zn}_{0.4}$  were detected by SEM and EDX techniques during interfacial microstructure and fracture morphology analysis. This suggests that this compound likely did not play a crucial role in bonding of Al to steel.  $\text{Fe}_2\text{Al}_5$  and  $\text{FeAl}_3$  intermetallic compounds identified during interfacial microstructure analysis, based on EDX results, distinct shape and evidence from the literature, were not detected by XRD analysis, likely due to the fine thickness of these intermetallics.

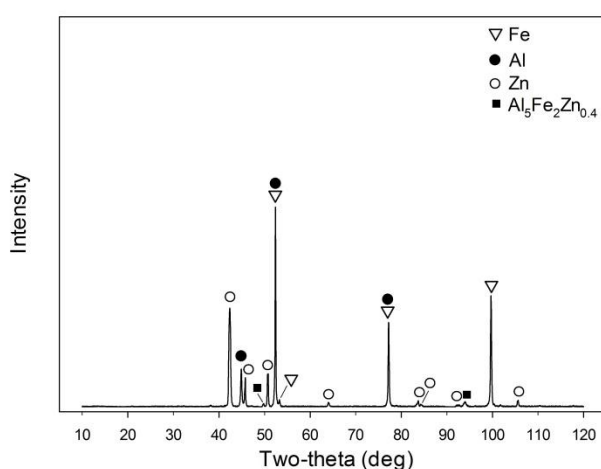


**Figure 5.13: XRD analysis of the Zn-coated steel interlayer fracture surface on Al side**

### 5.1.3.2 Mg/Steel Interface

Figure 5.14 shows fracture surface of the Zn-coated steel interlayer at Mg side. Regions of the fracture surface which correspond to the interfacial microstructure zones MS-I, MS-II and MS-III (Figure 5.5) are shown on Figure 5.14a.

It can be noted from Figure 5.14b and Table 5.5 that in the center of zone MS-I failure occurred inside Mg fusion zone. The ductile fracture morphology suggests that metallurgical bonding between molten Mg and steel interlayer occurred in this region. As discussed in section 5.1.2.2, bonding between Mg and steel was achieved due to the presence of an ultra-thin Fe-Al compound layer under Zn-coating (Figure 5.10). Figure 5.14c shows edge of MS-I zone. Fracture surfaces on the region show the steel surface under the Zn-coating (region 39 in Figure 5.14c) with a certain amount of Mg solidified on it (region 40 in Figure 5.14c). The morphology of the region suggests that edge of zone MS-I contributed to the strength less than the center, since a large area with ductile morphology was found in the center.

Figure 5.14d shows fracture morphology of zone MS-II, which corresponds to the region which was adjacent to the fusion nugget (Figure 5.5), and where solid state bonding between Mg and steel occurred. In this region, fracture occurred mainly within the Mg sheet close to the steel surface, since significant amount of Fe was detected on the fracture surface (Table 5.5). Regions where accumulations of Mg-Zn eutectic observed at the interfacial microstructure (Figure 5.11c), also can be found on the fracture surface (region 42 in Figure 5.14d). Fracture morphology of the region suggests that zone MS-II contributed to the strength.

In zone MS-III bonding between Mg and steel occurred through Zn-rich phase which acted as a filler metal (region 24 Figure 5.11a). Failure in the region occurred inside Zn-rich phase very close to the steel surface, since high amount of Fe was detected in the region (spectrum 43 in Table 5.5).

Expulsion observed during interfacial microstructure analysis can also be observed at the fracture surface (region 44 in Figure 5.14f). Fracture morphology and interfacial microstructure of this zone (Figure 5.11e) suggests that this region did not contribute to the strength.

Overall the fracture surface of Zn-coated steel at Mg side suggests that zones MS-I, MS-II and MS-III contributed to the strength while region beyond MS-III did not. Similarly to the case of the Al/steel interface, joining occurred in the Mg/steel interface by direct welding brazing in

zone MS-I, by solid state bonding in zone MS-II, by brazing through Zn-rich filler metal in zone MS-III. However much fewer voids were observed at Mg/steel interface and fracture surface, which likely led to the stronger bonding at Mg/steel interface and therefore welds failed at Al/steel interface.

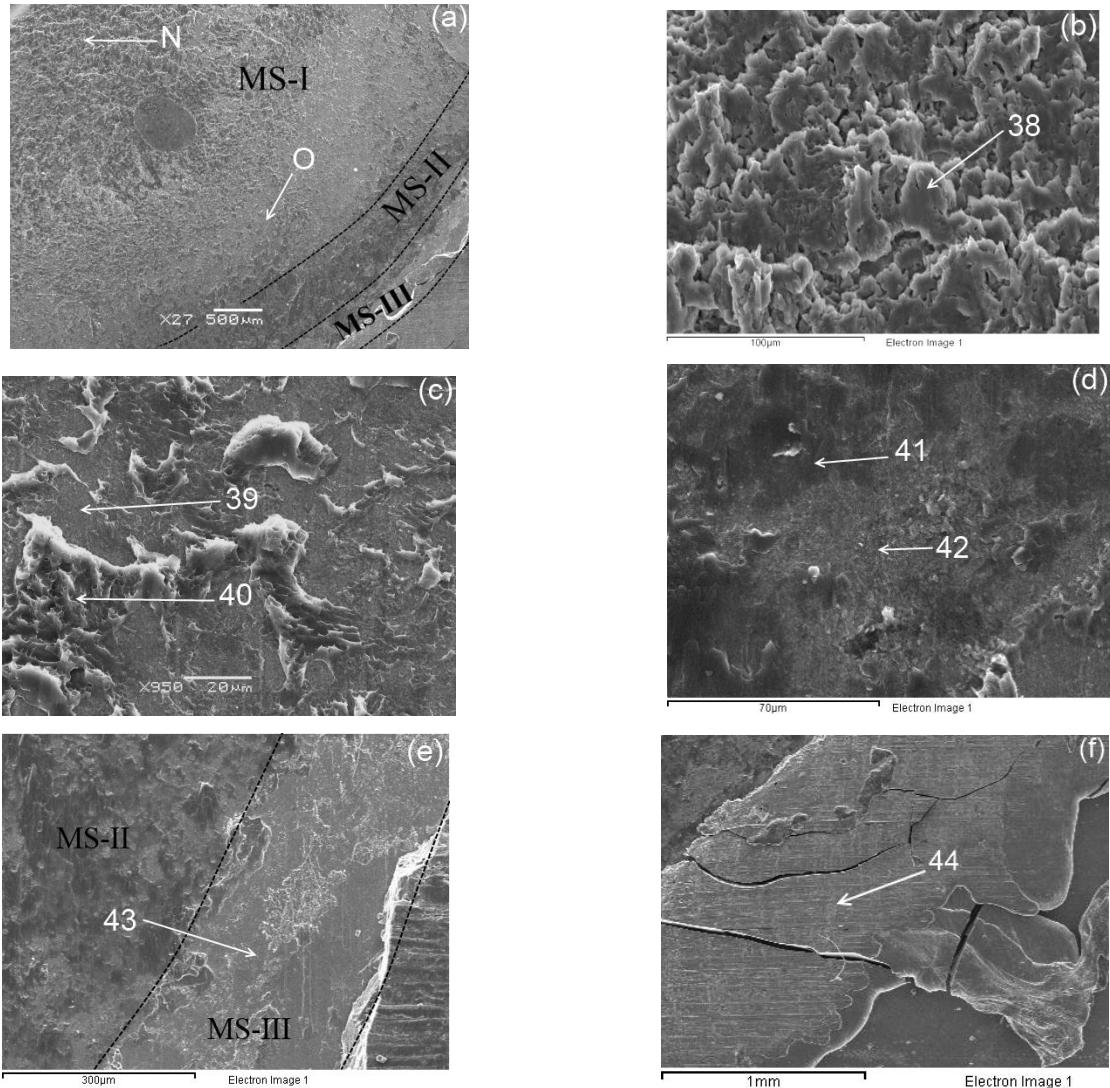


**Figure 5.14: Fracture surface morphology of the Mg/steel interface at steel side (produced in a weld made using 28 kA).** a overview; b details of region N from a; c details of region O from a; d details of zone MS-II from a; e details of zone MS-III from a; f region beyond MS-III zone

**Table 5.5: EDX quantification (in wt.%) of different areas in Figure 5.14**

Spectrum	Al	Fe	Mg	Zn
38	3.6	9.1	87.3	-
39	4.1	88.4	7.5	-
40	-	-	100	-
41	2.8	51.8	45.4	-
42	5.7	11.6	63.6	19.1
43	4.3	66.6	10.5	18.6
44	-	-	46.7	53.3

No intermetallic compounds were detected on the Zn-coated steel surface at Mg side using XRD (Figure 5.15). Although possible Mg-Zn phases were detected by SEM and EDX (Figure 5.11c), the small amount of these phases was likely beyond the resolution of XRD, making it is hard to observe.

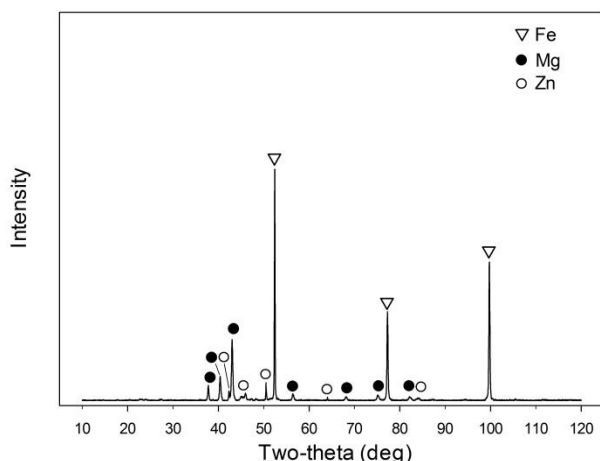


**Figure 5.15: XRD analysis of the Zn-coated steel interlayer fracture surface on Mg side**

## 5.2 Summary

In this chapter mechanical and microstructural properties of the dissimilar Al/Mg resistance spot welds made with Zn-coated steel interlayer were examined. Using standard lap-shear test, welding parameters which can produce acceptable quality welds were determined.

Interfacial microstructure and fracture surface of the high strength welds were analysed. Since, steel interlayer remained intact Al/steel and Mg/steel interface was analysed separately. The joint area on both Al and Mg sides can be divided into three different regions: direct welding brazing in the fusion nugget area, solid state bonding at the region adjacent to the nugget, and brazing through Zn based filler metal next to solid state region. Interfacial microstructure and fracture morphology of each zone analysed in details within the chapter.

## **Chapter 6: Conclusions**

### **6.1 RSW of Al to Mg with Ni-based Interlayers**

Mechanical and microstructural properties of the dissimilar Al/Mg resistance spot welds with bare and Au-coated Ni interlayers were investigated. The main conclusions can be summarised as following:

1. No joints were produced with bare Ni interlayer due to poor metallurgical bonding at Al/Ni interface.
2. Addition of Au coating improved metallurgical bonding at the interfaces and high strength welds were produced. The welds met fracture load requirements of the AWS D17.2 standard. Average failure load reached 90% of the similar AZ31B welds.
3. Different microstructures were observed at both Al/Ni and Mg/Ni interfaces. The Al alloy sheet was joined to Ni by direct welding-brazing in the center and by brazing through Au-based filler metal at the edge of a fusion nugget and at the region adjacent to the nugget. Mg was joined to Ni mostly through different Au rich phases, such as residual Au coating,  $Mg_3Au$  intermetallic compound layer, and Au-Mg eutectic structure.
4. Employing an interlayer with high melting point coated with good brazing material, such as Au-coated Ni clearly represents a promising approach in dissimilar resistance spot welding.

## **6.2 RSW of Al to Mg with Zn-coated Steel Interlayer**

Al/Mg resistance spot welds made with Zn-coated steel and different welding parameters were analysed. Mechanical properties and metallurgical features of the joints were examined in detail. The main findings include:

1. High strength Al/Mg welds were produced by RSW with Zn-coated steel interlayer. Failure load reached 74% of the similar AZ31B/AZ31B welds which was slightly lower than spot welds made with an Au-coated Ni interlayer. The welds also met requirements of the AWS D17.2 standard.
2. Similar bonding mechanisms took place at Al/steel and Mg/steel interfaces. The joint area on both Al and Mg side can be divided into three regions from the center to the edge: weld brazing of molten metal, solid state bonding, and soldering of Al (or Mg) to steel via the Zn-rich filler metal.
3. Zn coating played a crucial role in formation of the welds. Ultra-thin layer of Fe-Al compound prefabricated on steel surface during galvanizing process promoted bonding between Mg and steel, which are immiscible directly. The bulk of the Zn coating was melted and squeezed on significant distance from the nugget at both Al and Mg side. Squeezed Zn-rich phase acted as a solder metal which contributed to the bonding at Al/steel and Mg/steel interfaces.

## Appendix A: RSW of Al to Mg with Sn-coated Steel, Zn foil and Cu foil Interlayers

### A.1 RSW of Al to Mg with Sn-coated Steel Interlayer

#### A.1.1 Experimental

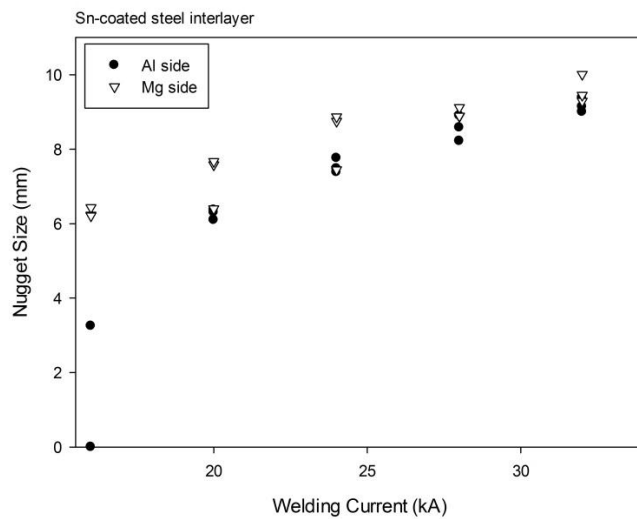
Electroplated Sn-coated steel was used to join Al and Mg. Overall thickness of the steel sheet was 0.6 mm, while Sn coating was approximately 10 µm. Composition of the steel is summarised in Table A-1. At least three samples per condition were made for tensile shear test and nugget size measurements. Experimental procedures used for experiments with Sn-coated steel interlayer were the same as for the other interlayers and described in Chapter 3 of this thesis.

**Table A-1: Chemical composition of the electroplated Sn-coated steel used as an interlayer (wt.%)**

C	Mn	P	S	Fe
0.01	0.5	0.01	0.005	Bal.

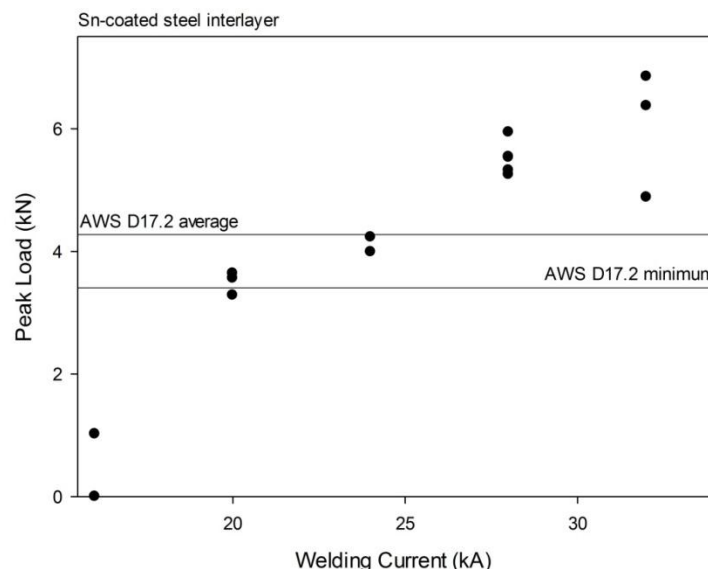
#### A.1.2 Mechanical Properties

Figure A-1 shows relationship between nugget size on Al and Mg sides and welding current. As typical in RSW, nugget size increased with welding current. Nugget dimensions on Mg side were always larger than on Al.



**Figure A-1: Correlation between nugget size on both Al and Mg side and welding current during RSW with Sn-coated steel interlayer**

Figure A-2 shows relationship between failure load and welding current. As typical in RSW, peak load increased with welding current. Welds made with welding current of 28 kA and higher met requirements of AWS D17.2 standard. As can be seen from Table A-2 welding coupons made with the same parameters often failed at different interfaces, suggesting that strength of Al/steel and Mg/steel interfaces was similar.



**Figure A-2: Correlation between peak load and welding current during RSW of Al to Mg with Sn-coated steel interlayer**

**Table A-2: Failure location of welds made with Sn-coated steel interlayer**

Welding Current and Sample #	Failure Location Side	Welding Current and Sample #	Failure Location Side	Welding Current and Sample #	Failure Location Side
16 kA – 1	Al	24 kA – 1	Mg	28 kA – 4	Al
16 kA – 2	Al	24 kA – 2	Al	32 kA – 1	Mg
16 kA – 3	Al	24 kA – 3	Al	32 kA – 2	Al
20 kA – 1	Mg	28 kA – 1	Mg	32 kA – 3	Mg
20 kA – 2	Al	28 kA – 2	Mg	32 kA – 4	Al
20 kA – 3	Al	28 kA – 3	Mg	32 kA – 5	Al

Figure A-3 shows microhardness profile of Al/Mg weld made with Sn-coated steel interlayer. No significant hardening was observed nor at Al fusion zone nor at Mg fusion zone, which suggests that Al-Mg brittle intermetallic compounds did not form.

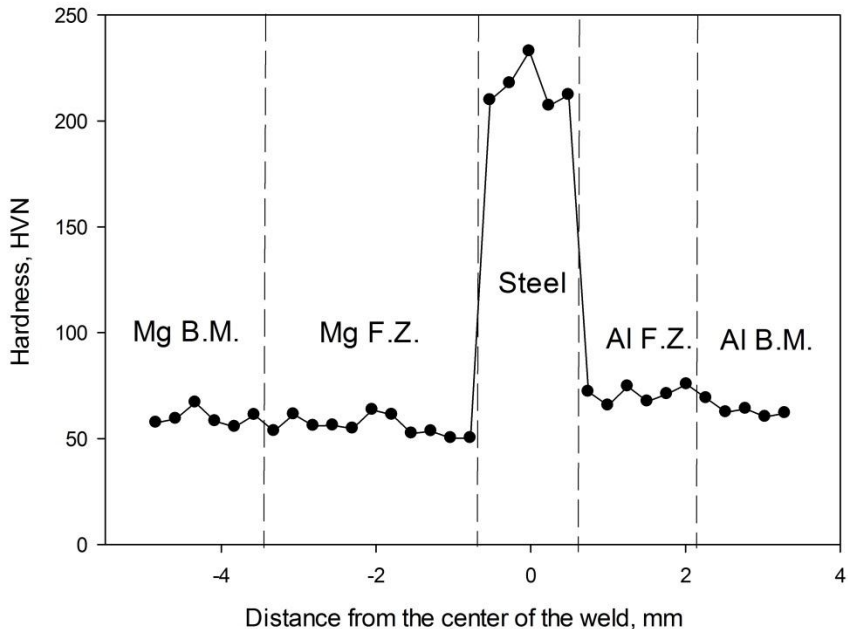


**Figure A-3: Hardness distribution across Al/Mg weld made with Sn-coated steel interlayer and 28 kA welding current**

#### A.1.3 Interfacial Microstructure

Figure A-4 shows typical Al/Mg resistance spot weld made with Sn-coated steel interlayer. Significant defects can be observed at both Al/steel and Mg/steel interfaces.

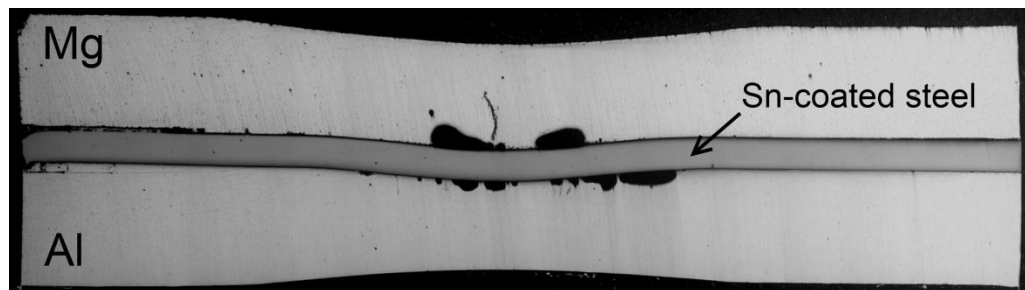


**Figure A-4: Typical Al/Mg weld made with Sn-coated steel interlayer and 28 kA welding current**

#### A.1.4 Fracture Surface Morphology

Figure A-5 shows fracture surface of the Sn-coated steel interlayer at Mg side. Center of a weld is shown on Figure A-5b. Fracture surface of the region exhibits steel surface with certain amount of Mg solidified on it, which suggests that some bonding occurred in this zone. Figure A-5c shows fracture surface of the outer region of the joint. Chemical composition of the region (Table A-3) suggests that failure in the region occurred through Mg fusion zone. It can be concluded that strong bonding occurred in the region, since there are areas which exhibit ductile fracture morphology.

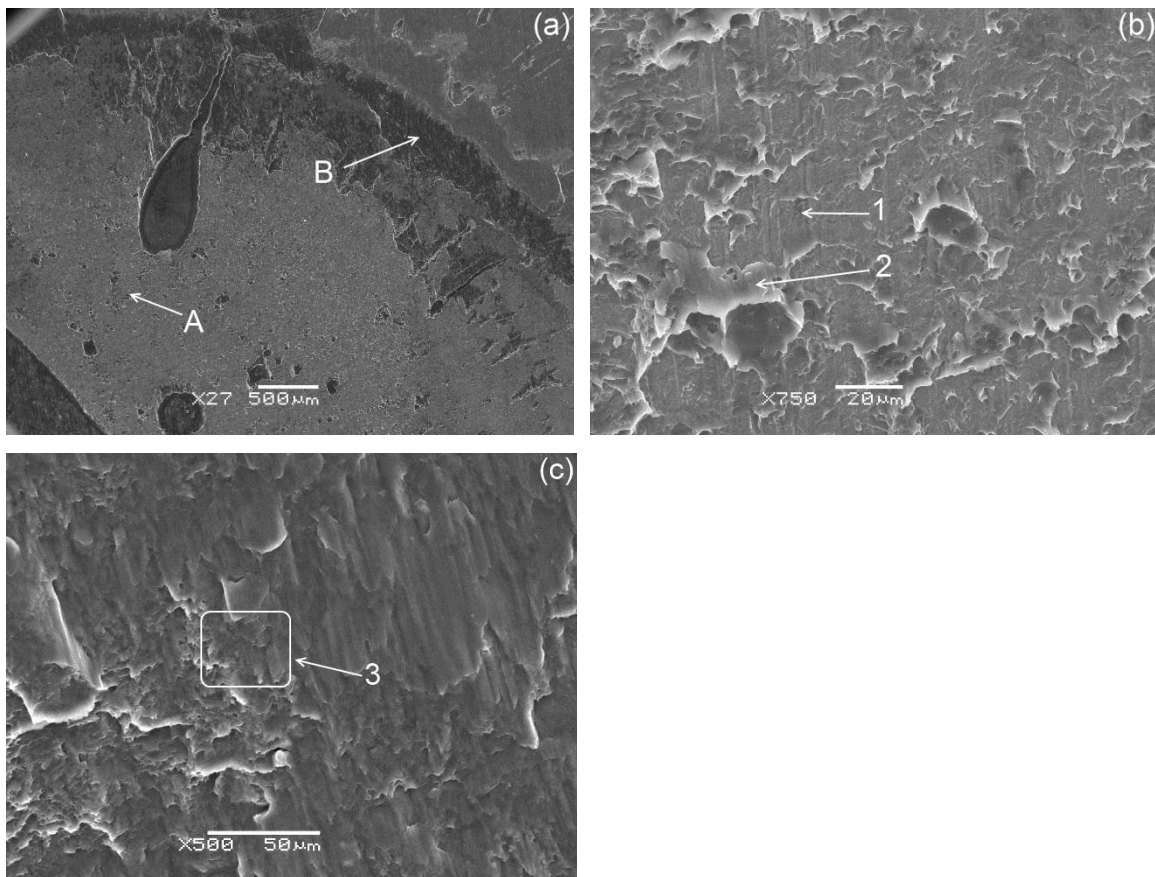


**Figure A-5: Fracture surface of the Sn-coated steel interlayer at Mg side (produced in a weld made using 28 kA). a overview; b details of region A from a; c details of region B from a**

**Table A-3: EDX quantification (in wt.%) of different areas in Figure A-5**

Spectrum	Mg	Al	Fe	Sn
1	27.7	-	72.3	-
2	96.2	3.8	-	-
3	100	-	-	-
4	97.1	-	-	2.9

### A.1.5 Conclusions

Experiments conducted with Sn-coated steel interlayer suggest that it might be a suitable candidate to the interlayer for dissimilar Al/Mg RSW. Mechanical properties achieved with this interlayer are similar to those achieved with Zn-coated steel interlayer. Bulk of the steel interlayer remained intact during the welding which prevented formation of brittle Al-Mg intermetallics.

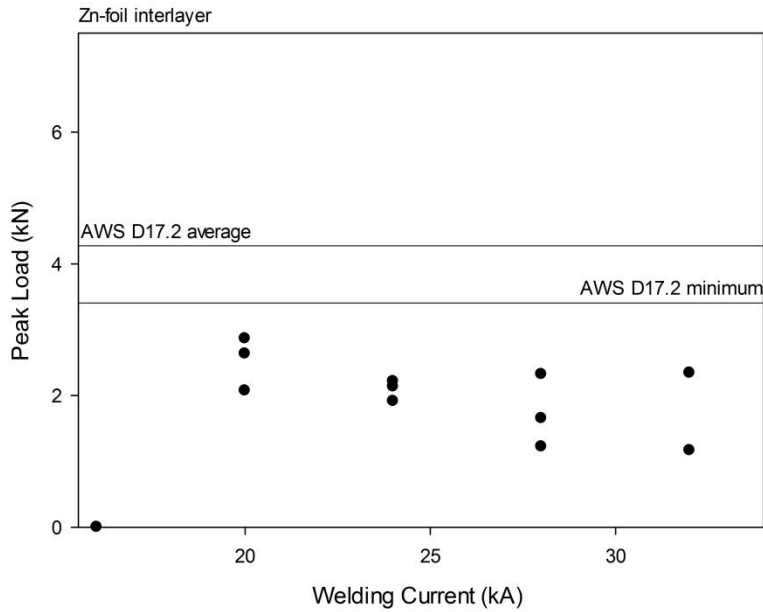
## A.2 RSW of Al to Mg with Zn foil Interlayer

### A.2.1 Experimental

Commercially pure Zn foil with thickness of 0.254 mm (1/10") was used as an interlayer to join Al and Mg by RSW process. Zn foil was ultrasonically cleaned in acetone for 10 minutes prior the welding. Experimental procedures used for experiments with Sn-coated steel interlayer were the same as for the other interlayers and described in Chapter 3 of this thesis.

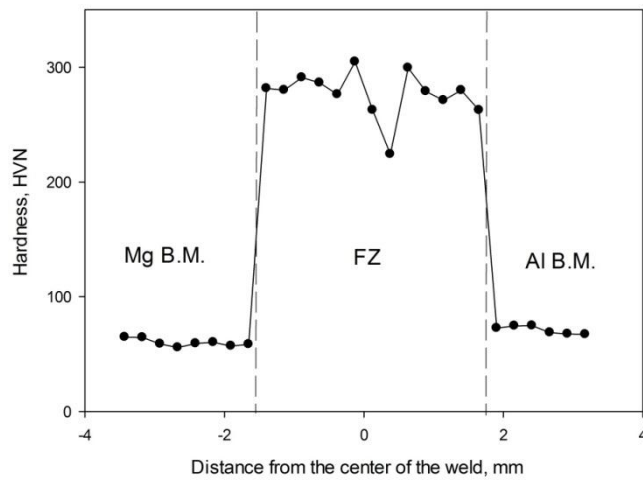
### A.2.2 Mechanical Properties

Figure A-6 shows relationship between peak load and welding current for welds made with Zn foil interlayer. It can be seen that none of the welds were strong enough to meet requirements of AWS D17.2 standard. It was observed that welds made with higher heat input not necessarily produced higher strength welds. All the samples failed through the fusion zone.



**Figure A-6: Correlation between peak load and welding current during RSW of Al to Mg with Zn foil interlayer**

Figure A-7 shows microhardness profile of Al/Mg weld made with Zn foil interlayer. Microhardness of the fusion zone ranged from 224 to 304 HVN, which is much higher than hardness of AZ31 (about 50 HVN), Al 5754 (about 60 HVN) or Zn (35 HVN) prior welding.



**Figure A-7: Hardness distribution across Al/Mg weld made with Zn foil interlayer and 28 kA welding current**

### A.2.3 Interfacial Microstructure

Figure A-8 shows interfacial microstructure of a weld made with Zn foil interlayer. Zn foil was completely melted due to low melting point of Zn ( $420^{\circ}\text{C}$ ) which resulted in formation of common Mg-Al-Zn fusion zone. It can be seen that greater part of the fusion nugget located at Mg sheet side, which suggests that more Mg material was melted than Al. Microstructure of the fusion nugget (Figure A-8b) consists of two phases. Both phases are mixtures of Al, Mg and Zn. Darker matrix phase is Mg rich while lighter secondary phase with dendritic arms shape is Zn rich. Only 10 to 16 wt.% Al present in microstructure of the fusion zone due to limited melting of Al sheet.

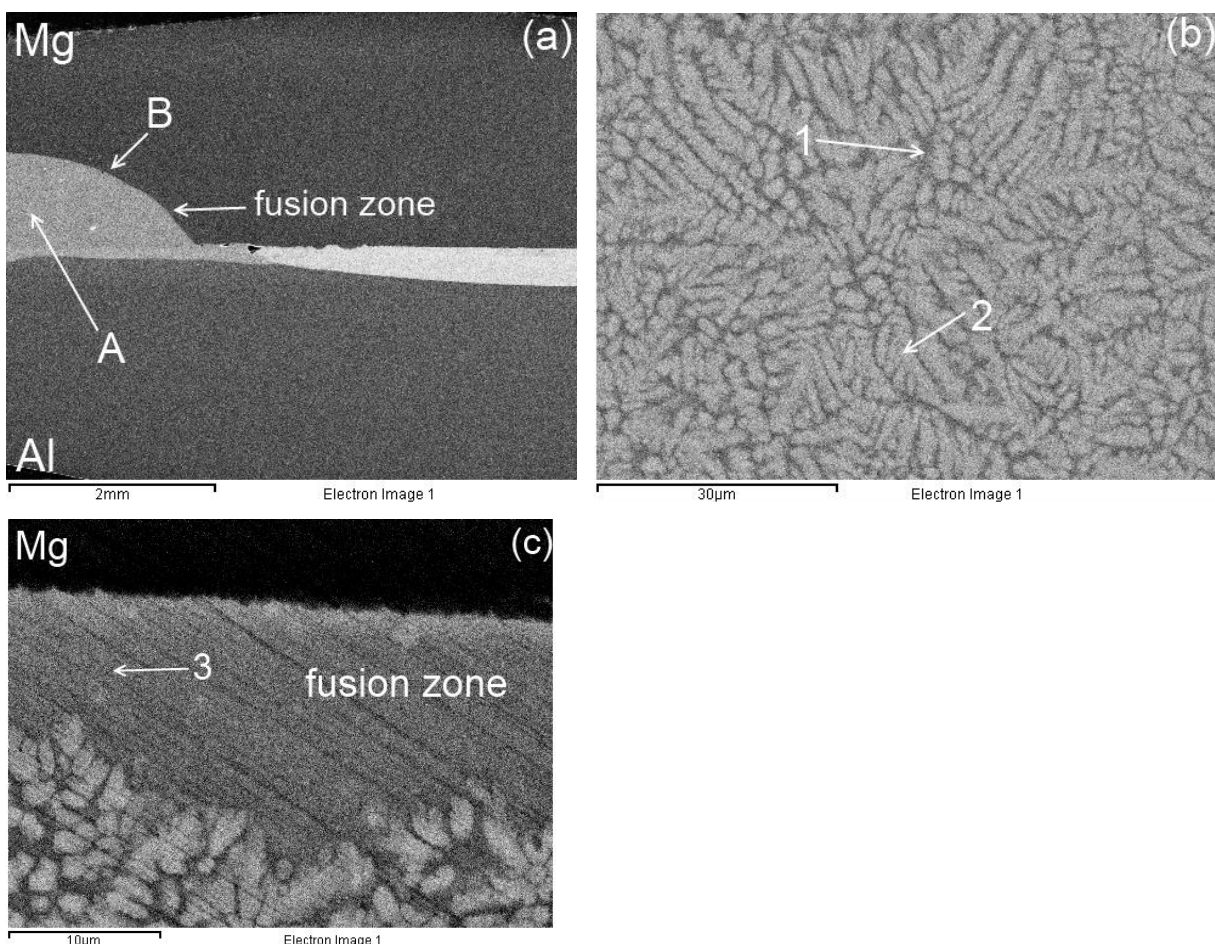


**Figure A-8: Interfacial microstructure of Al/Mg weld made with Zn foil interlayer and 28 kA welding current . a overview; b details of region A from a; c details of region B from a**

**Table A-4: EDX quantification (in wt.%) of different areas in Figure A-8**

Spectrum	Mg	Al	Zn
1	48.5	13.3	38.2
2	30.8	16.0	53.2
3	49.9	10.9	39.2

#### A.2.4 Fracture Surface

Figure A-9 shows fracture surface of Al/Mg weld made by RSW with Zn foil interlayer at Mg side. Brittle fracture morphology can be found on entire nugget area which corresponds with microhardness profile and poor mechanical performance of the welds. Fracture morphology and chemical composition of the region adjacent to the nugget (Figure A-9d) suggests that bonding through Zn-rich filler metal occurred in the region.

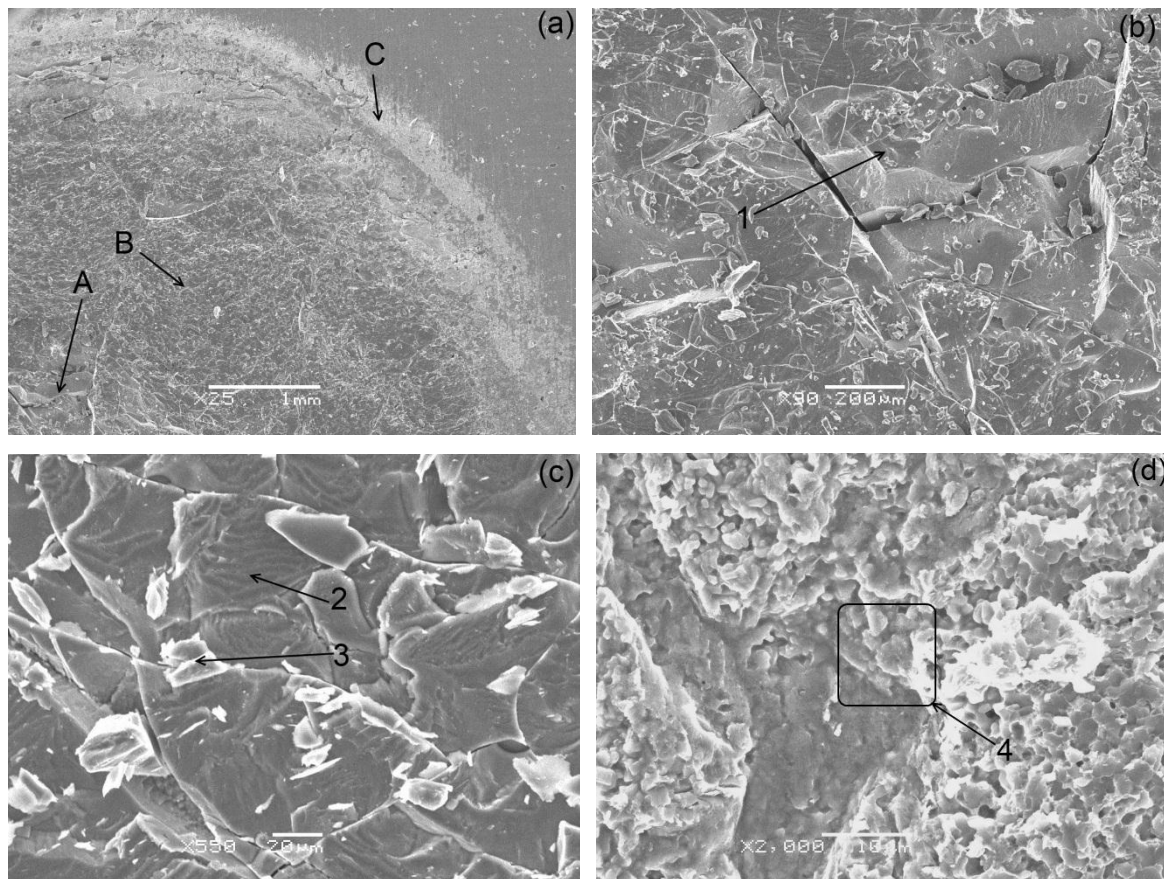


**Figure A-9: Fracture surface of Al/Mg weld made by RSW with Zn foil interlayer at Mg side (produced in a weld made using 28 kA). a overview; b details of region A from a; c details of region B from a; d details of region C from a**

**Table A-5: EDX quantification (in wt.%) of different areas in Figure A-9**

Spectrum	Mg	Al	Zn
1	37.1	11.5	51.4
2	27.2	45.9	26.9
3	30.5	36.7	32.8
4	16.4	4.3	79.3

#### A.2.5 Conclusions

Experiments conducted with Zn foil interlayer suggest that it is likely not a suitable material for dissimilar Al/Mg RSW. Zn has low melting temperature which results in its melting

and mixing with Al and Mg. It was found that formed Al-Mg-Zn phases are hard, brittle and perform poorly during tensile-shear test.

### A.3 RSW of Al to Mg with Cu Interlayer

#### A.3.1 Experimental

Commercially pure Cu foil with thickness of 0.127 mm was used as an interlayer to join Al and Mg by RSW process. Al and Mg alloys and experimental procedures used for experiments with Cu foil interlayer are described in Chapter 3 of this thesis.

#### A.3.2 Mechanical Properties

Table A-6 and Figure A-10 show relationship between peak load and welding current for welds made with Cu foil interlayer. It can be seen that none of the welds was strong enough to meet requirements of AWS D17.2 standard.

**Table A-6: Tensile-shear test data for welds made with Cu foil interlayer**

Welding Current and Sample #	Peak Load, kN	Extension, mm	Average Peak Load, kN
28 kA – 1	0.98	0.1	1.45
28 kA – 2	1.91	0.3	
32 kA – 1	2.34	0.4	2.42
32 kA – 2	2.49	0.3	

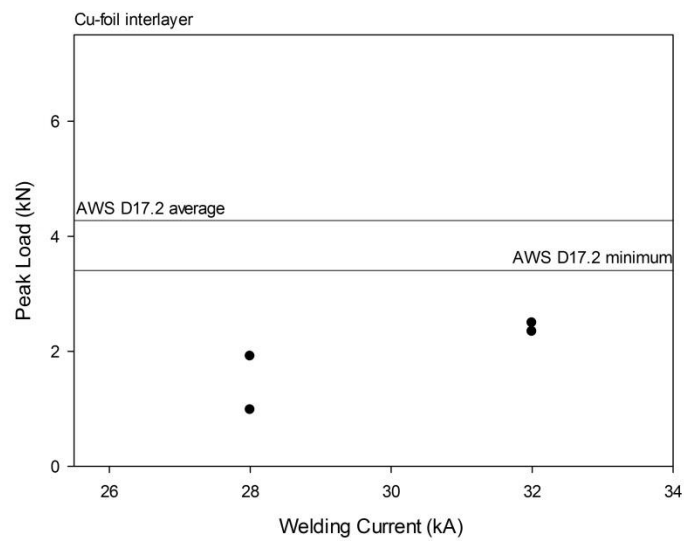


**Figure A-10: Correlation between peak load and welding current during RSW of Al to Mg with Cu foil interlayer**

## Appendix B: Direct RSW, Weld Bonding and Adhesive Bonding of Al to Mg

### B.1 Comparison of RSW, Weld Bonding and Adhesive Bonding of Mg alloy AZ31B to Al alloy 5754

#### B.1.1 Experimental

Dimensions of the 5754 and AZ31B alloy welding coupons were 100 mm x 25 mm x 2 mm. Surface of all coupons was treated according to the procedure described in Chapter 3 of this thesis. Terokal 5087-02P adhesive was applied for Weld Bonding (WB) and Adhesive Bonding (AB) and then cured at temperature of 180°C for 30 min. Welding parameters for RSW were: welding current in range from 16 to 20 kA, welding time 8 cycles, electrode force 4 kN. Welding parameters for WB were selected to be 8 kA for 3 cycles plus 28 or 32 kA for 8 cycles, electrode force in case of WB was 8 kN. During WB process following order of operations was used: application of adhesive, welding, curing joints in the furnace. Lap-shear and mechanised peel test were used to evaluate strength of the joints. Peel test set-up and coupon geometry are shown on Figure B-1. Nugget diameter was measured from fracture surface of Al sheet.

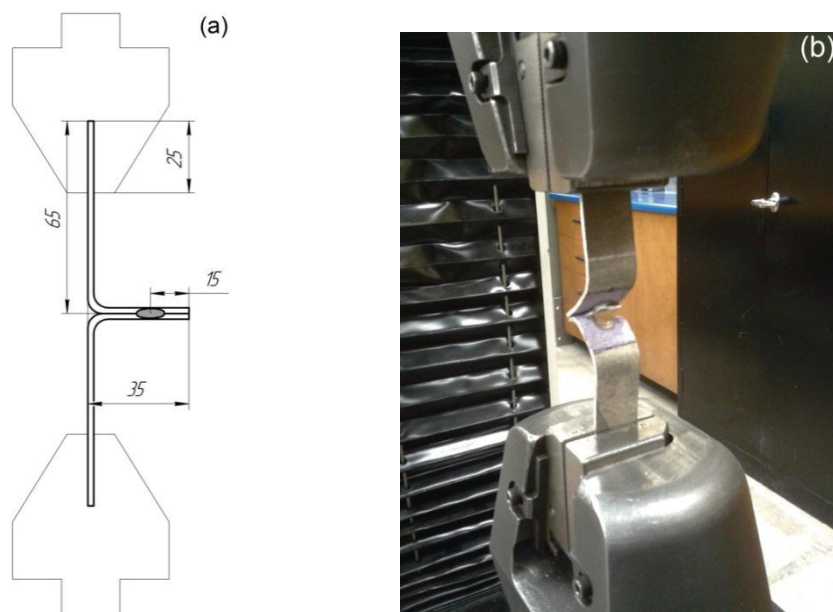


Figure B-1: Mechanised peel test. **a** test set-up and coupon geometry; **b** joint made by weld bonding at the last stage of the peel test

## B1.2 Mechanical Properties

Table B-1 and Table B-2 show results of mechanised peel and lap-shear tensile tests respectively. It can be seen that AB produced strongest joints, while weakest joints were produced by RSW. Strength of the joints made by WB was higher than that of resistance spot welds, but lower than that of AB joints. This suggests that fusion nugget provided much lower bonding strength than adhesive.

**Table B-1: Mechanised peel test data for AZ31B/5754 joints made by RSW, weld bonding and adhesive bonding**

Welding Current and Sample #	Peak Load, kN	Average Peak Load, kN	Extension, mm	Average Extension, mm	Diameter, mm	Average Diameter, mm
Adhesive Bonding						
Sample - 1	0.38	0.40	11.7	9.6	not applicable	not applicable
Sample - 2	0.41		7.5		not applicable	
Weld Bonding (RSW+ Adhesive)						
28 kA – 1	0.33	0.3	11.2	9.55	8.23	8.17
28 kA – 2	0.27		7.9		8.12	
32 kA – 1	0.25	0.25	10.7	6.45	8.61	9.42
32 kA – 2	0.24		2.2		9.43	
Resistance Spot Welding						
16 kA – 1	0.09	0.07	0.5	0.45	9.42	9.38
16 kA – 2	0.04		0.4		9.34	
20 kA – 1	0.06	0.03	0.8	0.40	9.94	9.8
20 kA – 2	0.00		0		9.66	

**Table B-2: Tensile-shear test data for AZ31B/5754 joints made by RSW, weld bonding and adhesive bonding**

Welding Current and Sample #	Peak Load, kN	Average Peak Load, kN	Extension, mm	Average Extension, mm	Diameter, mm	Average Diameter, mm
Adhesive Bonding						
Sample - 1	7.07	8.21	2.4	4.35	not applicable	not applicable
Sample - 2	9.35		6.3		not applicable	
Weld Bonding (RSW+ Adhesive)						
28 kA – 1	5.90	4.87	1.2	0.9	8.36	8.3
28 kA – 2	3.84		0.6		8.25	
32 kA – 1	7.81	5.95	3.5	2.1	9.11	8.95
32 kA – 2	4.09		0.7		8.80	
Resistance Spot Welding						
16 kA – 1	2.71	2.48	0.4	0.35	9.68	9.46
16 kA – 2	2.25		0.3		9.62	
20 kA – 1	1.83	1.51	0.3	0.2	9.45	9.65
20 kA – 2	1.19		0.10		9.47	

## B.2 RSW of Mg alloy AM60 to Al alloy 5754

### B.2.1 Experimental

Sheets of AM60 Mg alloy with thickness of 2.0 mm and sheets of Al alloy 5754 with thickness of 2.0 mm and 3.0 mm were used. The welding parameters were: welding current in range from 24 to 34 kA; welding time 8 cycles; electrode force 4 kN. Surface treatment, tensile test and other procedures were performed according to Chapter 3 of this thesis.

### B2.2 Mechanical Properties

Table B-3 shows results of lap-shear tensile test of spot welded AM60 and 5754 equal thickness sheets (2.0 mm). While, Table B-4 shows tensile test data for dissimilar thickness joints between 2.0 mm thick AM60 alloy and 3.0 mm 5754 alloy. It can be seen that strength of

the welds made with thicker Al sheet was higher than that of equal thickness joints. However, even then 3.0 mm thick Al sheets were employed, none of the welds met requirements of AWS D17.2 standard. All welds failed in interfacial mode.

**Table B-3: Tensile-shear test data for spot welded AM60 (2.0 mm) and 5754 (2.0 mm) sheets**

Welding Current and Sample #	Peak Load, kN	Extension, mm	Average Peak Load, kN
24 kA – 1	2.23	0.4	2.65
24 kA – 2	3.07	0.5	
26 kA – 1	2.83	0.5	2.59
26 kA – 2	2.35	0.4	
30 kA – 1	2.79	0.5	2.56
30 kA – 2	2.33	0.4	

**Table B-4: Tensile-shear test data for spot welded AM60 (2.0 mm) and 5754 (3.0 mm) sheets**

Welding Current and Sample #	Peak Load, kN	Extension, mm	Average Peak Load, kN
24 kA – 1	3.08	0.5	3.08
26 kA – 1	2.63	0.4	2.81
26 kA – 2	2.99	0.4	
30 kA – 1	3.49	0.6	3.27
30 kA – 2	3.05	0.5	
34 kA – 1	2.46	0.3	1.9
34 kA – 2	1.33	0.2	

## Appendix C: RSW of Mg to Steel

### C.1 Experimental

Welding specimens used for test of RSW of Mg to steel, were commercially available sheets of Mg alloy AM60 and Zn-coated HSLA steel. Dimensions of the Mg and steel welding coupons were 100 mm x 25 mm x 2 mm and 100 mm x 25 mm x 1.8 mm respectively. The welding parameters were: welding current in range from 16 to 24 kA; welding time 8 cycles; electrode force 4 kN. One set of the welds was made with FF25 domed electrode cups on both Mg and steel side and second set of the welds was prepared using a flat-face electrode cup at the steel side. The surface of the Mg sheets was treated with solution of 2.5 g chromic oxide and 100 mL water prior to welding, and the steel coupons were ultrasonically cleaned in acetone. Tensile test and other procedures, which are not mentioned in this section, were performed as described in Chapter 3 of this thesis.

### C.2 Mechanical Properties

Table C-1 shows Tensile-shear test data for AM60/steel welds made with domed electrode cups at both sides. While, Table C-2 shows tensile test data for AM60/steel welds made with a flat-face electrode at steel side and domed electrode at Mg side. It can be seen that in both cases, with similar and dissimilar electrode cups, welds made with welding current of 20 kA or higher met strength requirements of AWS D17.2 standard (4.27 kN).

**Table C-1: Tensile-shear test data for AM60/steel welds made with domed electrodes at both sides**

Welding Current and Sample #	Peak Load, kN	Extension, mm	Average Peak Load, kN
16 kA – 1	2.48	0.3	3.4
16 kA – 2	4.32	0.7	
20 kA – 1	5.26	1.2	5.4
20 kA – 2	5.54	1.1	

**Table C-2: Tensile-shear test data for AM60/steel welds made with a flat-face electrode at steel side**

Welding Current and Sample #	Peak Load, kN	Extension, mm	Average Peak Load, kN
16 kA – 1	2.97	0.3	3.26
16 kA – 2	3.55	0.7	
20 kA – 1	4.42	1.2	4.43
20 kA – 2	4.43	1.1	
24 kA – 1	6.35	1.4	6.63
24 kA – 2	6.9	1.4	

## Appendix D: RSW of Mg Alloys

### D.1 RSW of AM60 to ZEK100

Table D-1 summarises tensile test data for welds made between sheets of AM60 and ZEK100 Mg alloys. Welding coupons size was 100 mm x 25 mm x 2 mm for AM60 sheets and 100 mm x 25 mm x 1.6 mm for ZEK 100 sheets. Welds failed in interfacial mode.

**Table D-1: Tensile-shear test data for AM60/ZEK100 welds**

Welding Parameters and Sample #	Peak Load, kN	Extension, mm	Average Peak Load, kN
22 kA–8cycles–1	2.78	0.7	2.88
22 kA–8cycles–2	2.97	0.7	
26 kA–8cycles–1	3.82	0.9	3.73
26 kA–8cycles–2	3.63	1	
30 kA–8cycles–1	4.84	1.6	4.81
30 kA–8cycles–2	4.77	1.6	

### D.2 RSW of AM60 to AZ31

Table D-2 shows results of the tensile test of AM60/AZ31 welds. Welding coupons geometry for both alloys was: 100 mm x 25 mm x 2 mm. Nugget size was measured from the fracture surface using optical microscope. All the other procedures were executed according to Chapter 3 of this thesis. It was noted that in case of pull-out button failure mode, fracture always propagated through AM60 side.

**Table D-2: Tensile-shear test data for AM60/AZ31 welds**

Welding Parameters and Sample #	Peak Load, kN	Extension, mm	Diameter, mm	Failure Mode	Average Peak Load, kN
16 kA–8cycles–1	1.6	0.4	7.38	interface	1.87
16 kA–8cycles–2	2.16	0.5	7.48	interface	
16 kA–8cycles–3	1.85	0.3	7.26	interface	
20 kA–8cycles–1	4.61	0.9	8.64	interface	4.5
20 kA–8cycles–2	4.18	1.1	8.58	interface	
20 kA–8cycles–3	4.7	1	8.74	interface	
24 kA–8cycles–1	5.29	1.3	9.66	pull-out	5.15
24 kA–8cycles–2	5.19	1.3	9.79	pull-out	
24 kA–8cycles–3	4.98	1.3	9.35	pull-out	
28 kA–8cycles–1	6.68	1.7	10.85	pull-out	6.11
28 kA–8cycles–2	5.71	1.6	10.96	pull-out	
28 kA–8cycles–3	5.94	1.8	10.75	pull-out	

### D.3 RSW of AM60 Cast to AZ31

Table D-3 shows results of the tensile test of AM60(cast)/AZ31 welds. Exactly the same experimental procedures as for study of RSW of AM60(sheet) to AZ31 (Appendix D.2) were used. In pull-out failure mode, fracture always propagated through AM60 side.

**Table D-3: Tensile-shear test data for AM60(cast)/AZ31 welds**

Welding Parameters and Sample #	Peak Load, kN	Extension, mm	Diameter, mm	Failure Mode	Average Peak Load, kN
24 kA–8cycles–1	5.01	1.3	9.19	interface	4.99
24 kA–8cycles–2	5.25	1.4	9.26	interface	
24 kA–8cycles–3	4.71	1.2	9.35	interface	
28 kA–8cycles–1	5.72	1.6	9.80	pull-out	5.34
28 kA–8cycles–2	4.49	2.3	9.86	pull-out	
28 kA–8cycles–3	5.5	1.6	9.32	pull-out	

**D.4 RSW of AM60 Cast to AZ80**

Table D-4 summarises tensile test data for welds made between AM60 cast and AZ80 wrought Mg alloys. Welding coupons size was 100 mm x 25 mm x 2 mm. All the welds failed in pull-out button mode. Fracture always propagated through the sheet of AZ80 alloy.

**Table D-4: Tensile-shear test data for AM60(cast)/AZ31 welds**

Welding Parameters and Sample #	Peak Load, kN	Extension, mm	Diameter, mm	Failure Mode	Average Peak Load, kN
20 kA–8cycles–1	3.43	1.2	9.21	pull-out	3.68
20 kA–8cycles–2	3.92	1.3	9.2	pull-out	
24 kA–8cycles–1	3.87	1.4	9.9	pull-out	4.04
24 kA–8cycles–1	4.2	1.6	10.16	pull-out	
28 kA–8cycles–2	4.15	1.6	10.66	pull-out	4.23
28 kA–8cycles–3	4.3	2.8	10.23	pull-out	

## D.5 RSW of AM60 Cast and AM60 Wrought Alloys

Similar resistance spot welding of AM60 cast and AM60 wrought was compared. Table D-5 shows tensile test results. It can be seen that spot welds of wrought AM60 alloy had higher strength. Figure D-1 shows microstructure of base metal of AM60 cast and wrought alloys.

**Table D-5: Tensile-shear test data for resistance spot welds of AM60(cast)/AM60(cast) and AM60(wrought)/AM60(wrought) combinations**

Welding Parameters and Sample #	Peak Load, kN	Extension, mm	Diameter, mm	Failure mode	Average Peak Load, kN
RSW of AM60(cast) to AM60(cast)					
26 kA–8cycles–1	4.31	1.5	12.00	pull-out	4.05
26 kA–8cycles–2	3.59	2.7	11.86	through thickness	
26 kA–8cycles–1	4.24	1.5	12.01	pull-out	
RSW of AM60(wrought) to AM60(wrought)					
26 kA–8cycles–1	4.63	1.4	10.85	pull-out	5.18
26 kA–8cycles–2	5.48	1.7	10.86	pull-out	
26 kA–8cycles–3	5.43	2.4	10.63	through thickness	

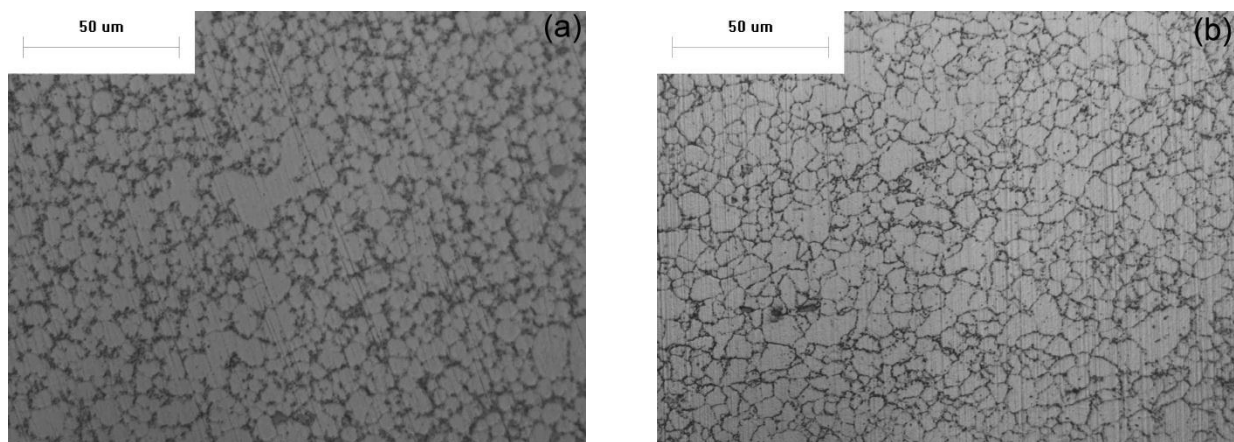


**Figure D-1: Microstructure of AM60 Mg alloy base metal. a cast; b wrought**

## Appendix E: RSW of Unequal Thickness AZ31B Sheets

AZ31B Mg alloy sheets with thickness of 1.6 and 2.0 mm were successfully joined by RSW. Results of tensile-shear test are summarised in Table E-1. Experimental procedure for testing of this material combination is described in Chapter 3. Welds made with welding current of 20 kA or higher easily met strength requirements of AWS D17.2 standard (3.18 kN) for this materials combination.

**Table E-1: Tensile-shear test data for AM60(cast)/AZ31 welds**

Welding Parameters and Sample #	Peak Load, kN	Average Peak Load, kN	Welding Parameters and Sample #	Peak Load, kN	Average Peak Load, kN
17 kA–8cycles–1	1.85	1.95	26 kA–8cycles–1	4.46	5.21
17 kA–8cycles–2	2.05		26 kA–8cycles–2	4.32	
17 kA–8cycles–3	1.97		26 kA–8cycles–3	4.07	
20 kA–8cycles–1	3.44	3.38	30 kA–8cycles–1	5.16	6.34
20 kA–8cycles–2	3.36		30 kA–8cycles–2	5.51	
20 kA–8cycles–3	3.36		30 kA–8cycles–3	4.98	

## References

- [1] T. J. Lienert, S. S. Babu, T. A. Siewert and V. L. Acoff, *ASM Handbook, Volume 6A - Welding Fundamentals and Processes*. ASM International, 2011.
- [2] RWMA, Ed., *Resistance Welding Manual*. Philadelphia, PA: R.W.M.A., 2003.
- [3] American Welding Society, A. O'Brien and C. Guzman, *Welding Handbook: Welding Processes, Part 2*. American Welding Society, 2004.
- [4] F. Hayat, "The effects of the welding current on heat input, nugget geometry, and the mechanical and fractural properties of resistance spot welding on Mg/Al dissimilar materials," *Mater Des*, vol. 32, pp. 2476-2484, 2011.
- [5] N. Jeal, "High-performance magnesium," *Adv Mater Processes*, vol. 163, pp. 65-67, 2005.
- [6] R. Borrisutthekul, Y. Miyashita and Y. Mutoh, "Dissimilar material laser welding between magnesium alloy AZ31B and aluminum alloy A5052-O," *Science and Technology of Advanced Materials*, vol. 6, pp. 199-204, 2005.
- [7] L. Liu and H. Wang, "Microstructure and Properties Analysis of Laser Welding and Laser Weld Bonding Mg to Al Joints," *Metallurgical and Materials Transactions A*, vol. 42, pp. 1044-1050, 2011.
- [8] G. Mahendran, V. Balasubramanian and T. Senthilvelan, "Developing diffusion bonding windows for joining AZ31B magnesium-AA2024 aluminium alloys," *Mater Des*, vol. 30, pp. 1240-1244, 2009.
- [9] Y. Li, P. Liu, J. Wang and H. Ma, "XRD and SEM analysis near the diffusion bonding interface of Mg/Al dissimilar materials," *Vacuum*, vol. 82, pp. 15-19, 2007.
- [10] R. Zettler, da Silva, A Augusto Monarco, S. Rodrigues, A. Blanco and J. F. dos Santos, "Dissimilar Al to Mg alloy friction stir welds," *Advanced Engineering Materials*, vol. 8, pp. 415-421, 2006.
- [11] Z. Liang, K. Chen, X. Wang, J. Yao, Q. Yang, L. Zhang and A. Shan, "Effect of Tool Offset and Tool Rotational Speed on Enhancing Mechanical Property of Al/Mg Dissimilar FSW Joints," *Metall. Mater. Trans. A*, vol. 44A, pp. 3721-3731, 2013.
- [12] W. Chang, S. Rajesh, C. Chun and H. Kim, "Microstructure and mechanical properties of hybrid laser-friction stir welding between AA6061-T6 Al alloy and AZ31 Mg alloy," *Journal of Materials Science & Technology*, vol. 27, pp. 199-204, 2011.

- [13] L. Zhao and Z. Zhang, "Effect of Zn alloy interlayer on interface microstructure and strength of diffusion-bonded Mg-Al joints," *Scr. Mater.*, vol. 58, pp. 283-286, 2008.
- [14] L. Liu, X. Liu and S. Liu, "Microstructure of laser-TIG hybrid welds of dissimilar Mg alloy and Al alloy with Ce as interlayer," *Scr. Mater.*, vol. 55, pp. 383-386, 2006.
- [15] Y. Wang, G. Luo, J. Zhang, Q. Shen and L. Zhang, "Microstructure and mechanical properties of diffusion-bonded Mg-Al joints using silver film as interlayer," *Materials Science and Engineering: A*, vol. 559, pp. 868-874, 2013.
- [16] V. Patel, S. Bhole and D. Chen, "Improving weld strength of magnesium to aluminium dissimilar joints via tin interlayer during ultrasonic spot welding," *Science and Technology of Welding & Joining*, vol. 17, pp. 342-347, 2012.
- [17] M. Gao, S. Mei, X. Li and X. Zeng, "Characterization and formation mechanism of laser welded Mg and Al alloys using Ti interlayer," *Scr. Mater.*, vol. 67, pp. 193-196, 2012.
- [18] J. Shang, K. Wang, Q. Zhou, D. Zhang, J. Huang and G. Li, "Microstructure characteristics and mechanical properties of cold metal transfer welding Mg/Al dissimilar metals," *Mater Des*, vol. 34, pp. 559-565, 2012.
- [19] J. Zhang, G. Luo, Y. Wang, Q. Shen and L. Zhang, "An investigation on diffusion bonding of aluminum and magnesium using a Ni interlayer," *Mater Lett*, vol. 83, pp. 189-191, 2012.
- [20] American Welding Society, *AWS D17.2/D17.2M Specification for Resistance Welding for Aerospace Applications*. Miami, FL, USA: AWS, 2007.
- [21] P. Penner, L. Liu, A. Gerlich and Y. Zhou, "Feasibility study of resistance spot welding of dissimilar Al/Mg combinations with Ni based interlayers," 2013  
DOI:10.1179/1362171813Y.0000000129 ([www.maneypublishing.com/journals/stw](http://www.maneypublishing.com/journals/stw); [www.ingentaconnect.com/content/maney/stwj](http://www.ingentaconnect.com/content/maney/stwj)).
- [22] American Welding Society, *ANSI/AWS D8. 9-97, Recommended Practices for Test Methods for Evaluating the Resistance Spot Welding Behavior of Automotive Sheet Steel Materials*. Miami, FL, USA: AWS, 1997.
- [23] Ruukki's, *Resistance Welding Manual*. Rautaruukki Corporation, Helsinki, Finland, 2009.
- [24] D. W. Dickinson, "Welding in the automotive industry," Tech. Rep. AISI Report SG81-5, August, 1981.
- [25] W. Tan, S. Lawson and Y. Zhou, "Effects of Au plating on dynamic resistance during small-scale resistance spot welding of thin Ni sheets," *Metallurgical and Materials Transactions A*, vol. 36, pp. 1901-1910, 2005.

- [26] G. E. Totten and D. S. MacKenzie, *Handbook of Aluminum Volume 1: Physical Metallurgy and Processes*. Marcel Dekker, Inc., New York, NY, 2003.
- [27] M. K. Kulekci, "Magnesium and its alloys applications in automotive industry," *The International Journal of Advanced Manufacturing Technology*, vol. 39, pp. 851-865, 2008.
- [28] A. Musfirah and A. Jaharah, "Magnesium and Aluminum Alloys in Automotive Industry," *Journal of Applied Sciences Research*, vol. 8, pp. 4865-4875, 2012.
- [29] R. A. Schultz and A. K. Abraham, "Metallic material trends for north american light vehicles," in *Great Designs in Steel Seminar, American Iron and Steel Institute, Southfield, Mich*, 2007, .
- [30] G. Cole, "Magnesium vision 2020-a north american automotive strategic vision for magnesium," in *IMA-PROCEEDINGS-*, 2007, pp. 13.
- [31] G. Mahendran, S. Babu and V. Balasubramanian, "Analyzing the Effect of Diffusion Bonding Process Parameters on Bond Characteristics of Mg-Al Dissimilar Joints," *Journal of Materials Engineering and Performance*, vol. 19, pp. 657-665, 2010.
- [32] M. Joseph Fernandus, T. Senthilkumar and V. Balasubramanian, "Developing Temperature–Time and Pressure–Time diagrams for diffusion bonding AZ80 magnesium and AA6061 aluminium alloys," *Mater Des*, vol. 32, pp. 1651-1656, 2011.
- [33] V. Balasubramanian, M. J. Fernandus and T. Senthilkumar, "Development of processing windows for diffusion bonding of aluminium/magnesium dissimilar materials," *Weld. World*, vol. 57, pp. 523-539, 2013.
- [34] M. Joseph Fernandus, T. Senthilkumar, V. Balasubramanian and S. Rajakumar, "Optimizing Diffusion Bonding Parameters to Maximize the Strength of AA6061 Aluminum and AZ61A Magnesium Alloy Joints." *Exp Tech*, vol. DOI: 10.1111/j.1747-1567.2012.00815.x, 2012.
- [35] Y. Yan, Z. Zhang, W. Shen, J. Wang, L. Zhang and B. Chin, "Microstructure and properties of magnesium AZ31B–aluminum 7075 explosively welded composite plate," *Materials Science and Engineering: A*, vol. 527, pp. 2241-2245, 2010.
- [36] R. Borrisutthekul, Y. Miyashita and Y. Mutoh, "Dissimilar material laser welding between magnesium alloy AZ31B and aluminum alloy A5052-O," *Science and Technology of Advanced Materials*, vol. 6, pp. 199-204, 2005.
- [37] X. Qi and L. Liu, "Fusion welding of Fe-added lap joints between AZ31B magnesium alloy and 6061 aluminum alloy by hybrid laser–tungsten inert gas welding technique," *Mater Des*, vol. 33, pp. 436-443, 2012.

- [38] S. Kore, J. Imbert, M. Worswick and Y. Zhou, "Electromagnetic impact welding of Mg to Al sheets," *Science and Technology of Welding & Joining*, vol. 14, pp. 549-553, 2009.
- [39] Y. C. Chen and K. Nakata, "Friction stir lap joining aluminum and magnesium alloys," *Scr. Mater.*, vol. 58, pp. 433-436, 3, 2008.
- [40] Y. Sato, A. Shiota, H. Kokawa, K. Okamoto, Q. Yang and C. Kim, "Effect of interfacial microstructure on lap shear strength of friction stir spot weld of aluminium alloy to magnesium alloy," *Science and Technology of Welding & Joining*, vol. 15, pp. 319-324, 2010.
- [41] L. Liu, X. Liu and S. Liu, "Microstructure of laser-TIG hybrid welds of dissimilar Mg alloy and Al alloy with Ce as interlayer," *Scr. Mater.*, vol. 55, pp. 383-386, 2006.
- [42] H. Baker and H. Okamoto, *ASM Handbook, Volume 3 - Alloy Phase Diagrams*. ASM international, 1992.
- [43] D. H. Choi, B. W. Ahn, C. Y. Lee, Y. M. Yeon, K. Song and S. B. Jung, "Formation of intermetallic compounds in Al and Mg alloy interface during friction stir spot welding," *Intermetallics*, vol. 19, pp. 125-130, 2011.
- [44] V. Firouzdor and S. Kou, "Al-to-Mg Friction Stir Welding: Effect of Positions of Al and Mg with Respect to the Welding Tool," *Welding Journal*, vol. 88, pp. 213-224, 2009.
- [45] P. Venkateswaran and A. Reynolds, "Factors affecting the properties of Friction Stir Welds between aluminum and magnesium alloys," *Materials Science and Engineering: A*, vol. 545, pp. 26-37, 2012.
- [46] L. Liu, L. Zhao and Z. Wu, "Influence of holding time on microstructure and shear strength of Mg-Al alloys joint diffusion bonded with Zn-5Al interlayer," *Materials Science and Technology*, vol. 27, pp. 1372-1376, 2011.
- [47] X. Liu, R. Huang, H. Wang and S. Liu, "Improvement of TIG lap weldability of dissimilar metals of Al and Mg," *Science and Technology of Welding & Joining*, vol. 12, pp. 258-260, 2007.
- [48] L. Liu, L. Zhao and R. Xu, "Effect of interlayer composition on the microstructure and strength of diffusion bonded Mg/Al joint," *Mater Des*, vol. 30, pp. 4548-4551, 2009.
- [49] F. Scherm, J. Bezold and U. Glatzel, "Laser welding of Mg alloy MgAl<sub>3</sub>Zn<sub>1</sub> (AZ31) to Al alloy AlMg<sub>3</sub> (AA5754) using ZnAl filler material," *Science and Technology of Welding & Joining*, vol. 17, pp. 364-367, 2012.
- [50] H. Zhang and J. Song, "Microstructural evolution of aluminum/magnesium lap joints welded using MIG process with zinc foil as an interlayer," *Mater Lett*, vol. 65, pp. 3292-3294, 2011.

- [51] D. Shi, B. Wen, R. Melnik, S. Yao and T. Li, "First-principles studies of Al–Ni intermetallic compounds," *Journal of Solid State Chemistry*, vol. 182, pp. 2664-2669, 2009.
- [52] ILZRO - GalvInfo Center, "GalvInfoNote #10 The Role of Aluminum in Continuous Hot-Dip Galvanizing," 2003.
- [53] J. Culcasi, P. Sere, C. Elsner and A. Di Sarli, "Control of the growth of zinc–iron phases in the hot-dip galvanizing process," *Surface and Coatings Technology*, vol. 122, pp. 21-23, 1999.
- [54] H. Lee and J. Kim, "Effect of Ni addition in zinc bath on formation of inhibition layer during galvannealing of hot-dip galvanized sheet steels," *J. Mater. Sci. Lett.*, vol. 20, pp. 955-957, 2001.
- [55] L. Liu, L. Xiao, J. Feng, L. Li, S. Esmaeili and Y. Zhou, "Bonding of immiscible Mg and Fe via a nanoscale Fe<sub>2</sub>Al<sub>5</sub> transition layer," *Scr. Mater.*, vol. 65, pp. 982-985, 2011.
- [56] L. Liu, L. Xiao, J. Feng, Y. Tian, S. Zhou and Y. Zhou, "The mechanisms of resistance spot welding of magnesium to steel," *Metallurgical and Materials Transactions A*, vol. 41, pp. 2651-2661, 2010.
- [57] R. Qiu, H. Shi, K. Zhang, Y. Tu, C. Iwamoto and S. Satonaka, "Interfacial characterization of joint between mild steel and aluminum alloy welded by resistance spot welding," *Mater Charact*, vol. 61, pp. 684-688, 2010.
- [58] R. Qiu, C. Iwamoto and S. Satonaka, "Interfacial microstructure and strength of steel/aluminum alloy joints welded by resistance spot welding with cover plate," *J. Mater. Process. Technol.*, vol. 209, pp. 4186-4193, 2009.
- [59] R. Qiu, C. Iwamoto and S. Satonaka, "The influence of reaction layer on the strength of aluminum/steel joint welded by resistance spot welding," *Mater Charact*, vol. 60, pp. 156-159, 2009.
- [60] A. Handbook, *ASM Handbook, Volume 2 - Properties and Selection: Nonferrous Alloys and Special-Purpose Materials*. ASM International, 1990.
- [61] Aalco metals, "Aluminium Alloys - Aluminium 5754 Properties, Fabrication and Applications, Supplier Data by Aalco," 2005.
- [62] W. Tan, Y. Zhou and H. Kerr, "Effects of Au plating on small-scale resistance spot welding of thin-sheet nickel," *Metallurgical and Materials Transactions A*, vol. 33, pp. 2667-2676, 2002.
- [63] L. Liu, S. Zhou, Y. Tian, J. Feng, J. Jung and Y. Zhou, "Effects of surface conditions on resistance spot welding of Mg alloy AZ31," *Science and Technology of Welding & Joining*, vol. 14, pp. 356-361, 2009.

- [64] L. Liu, L. Xiao, J. Feng, Y. Tian, S. Zhou and Y. Zhou, "Resistance Spot Welded AZ31 Magnesium Alloys, Part II: Effects of Welding Current on Microstructure and Mechanical Properties," *Metallurgical and Materials Transactions A*, vol. 41, pp. 2642-2650, 2010.
- [65] A. Panteli, Y. Chen, D. Strong, X. Zhang and P. Prangnell, "Optimization of aluminium to magnesium ultrasonic spot welding," in *Proc. TMS Conf., JOM*, San Diego, CA, USA, 2011, .
- [66] R. Qiu, H. Shi, H. Yu, K. Zhang, Y. Tu and S. Satonaka, "Effects of electrode force on the characteristic of magnesium alloy joint welded by resistance spot welding with cover plates," *Mater. Manuf. Process.*, vol. 25, pp. 1304-1308, 2010.
- [67] H. Zhao and T. DebRoy, "Pore formation during laser beam welding of die-cast magnesium alloy AM60B-mechanism and remedy," *Welding Journal*, vol. 80, pp. 204-210, 2001.
- [68] R. Florea, D. Bammann, A. Yeldell, K. Solanki and Y. Hammi, "Welding Parameters Influence on Fatigue Life and Microstructure in Resistance Spot Welding of 6061-T6 Aluminum Alloy," *Mater Des*, vol. 45, pp. 456-465, 2012.
- [69] D. Sun, B. Lang, D. Sun and J. Li, "Microstructures and mechanical properties of resistance spot welded magnesium alloy joints," *Materials Science and Engineering: A*, vol. 460, pp. 494-498, 2007.
- [70] N. K. Babu, S. Brauser, M. Rethmeier and C. Cross, "Characterization of microstructure and deformation behaviour of resistance spot welded AZ31 magnesium alloy," *Materials Science and Engineering: A*, vol. 549, pp. 149-156, 2012.
- [71] K. Bouché, F. Barbier, A. Coulet, K. Bouché, F. Barbier and A. Coulet, "Intermetallic compound layer growth between solid iron and molten aluminium," *Materials Science & Engineering A*, vol. 249, pp. 167-175, .
- [72] C. Tan, L. Li, Y. Chen, C. Mei and W. Guo, "Interfacial microstructure and fracture behavior of laser welded–brazed Mg alloys to Zn-coated steel." *Int J Adv Manuf Technol*, vol. DOI10.1007/s00170-013-4910-4, 2013.
- [73] L. Li, C. Tan, Y. Chen, W. Guo and X. Hu, "Influence of Zn Coating on Interfacial Reactions and Mechanical Properties During Laser Welding-Brazing of Mg to Steel," *Metallurgical and Materials Transactions A*, vol. 43, pp. 4740-4754, 2012.